Roles for the adhesion molecule Contactin2 in the development and function of neural circuits in zebrafish

---

A Dissertation

presented to

the Faculty of the Graduate School

at the University of Missouri-Columbia

In Partial Fulfillment

of the Requirements for the Degree

Doctor of Philosophy

---

by

Suman Gurung

Dr. Anand Chandrasekhar, Dissertation Supervisor

May 2018

The undersigned, appointed by the dean of the Graduate School, have examined the dissertation entitled

Roles for the adhesion molecule Contactin2 in the development and function of neural circuits in zebrafish

presented by Suman Gurung,

a candidate for the degree of Doctor of Philosophy,

and hereby certify that, in their opinion, it is worthy of acceptance.

Dr. Anand Chandrasekhar

Dr. Andrew McClellan

Dr. Dawn Cornelison

Dr. Mark Hannink

ACKNOWLEDGEMENTS

First, I would like to thank the two most important women in my life, my mother Goma Gurung and wife-to-be Priya Bariya. My mother was always there to hear my journey through graduate school, whether it be my failed experiments, my hectic academic schedule with teaching and research or eureka moments as I've worked on my thesis. I thank Priya, whose unconditional love is the source of my strength and happiness. I would also like to thank other members of my family for their love and support.

I cannot thank enough my advisor, Anand Chandrasekhar, for his guidance in my pursuit of this journey. By his example, he has shown me what a good scientist, teacher, and advisor should be. I would also like to thank my dissertation committee members, Dawn Cornelison, Andrew McClellan, and Mark Hannink who have provided me with excellent scientific suggestions as well as professional guidance.

My journey wouldn't be possible without the help and support of previous lab members: Vinoth Sittaramane, Xiufang Pan, Priyanka Singh, and Whitney Bryant. I owe much of my progress to them. I thank graduate students Emilia Asante and Devynn Hummel for making the lab a fun place to be even during the weekends. I appreciate all the hard work of Moe Baccam for keeping our zebrafish healthy and happy. I would like to thank all past and present undergraduates in the lab. Thanks to members from the Cornelison lab,

especially Laura Arnold for her help with lab reagents and advice, in both academics and life.

Thank you to the zebrafish committee at Washington University at St. Louis for their suggestions and guidance in my project. Four hours of driving to and from Washington University was no match for the valuable suggestions provided by the committee.

I thank all my Nepalese friends here in Columbia for making this place home away from home and making me realize that there is life outside of lab and school. May the force be with them.

TABLE OF CONTENTS

LIST OF FIGURES

LIST OF TABLES

ABSTRACT

Neuronal migration and axon guidance are critical developmental processes that are essential for establishing functional neural circuits underlying complex cognitive and motor functions. Precise neuronal migration and axon guidance are dependent upon cell-cell and cell-substrate interactions, which are mediated by several membrane-associated molecules. The relatively concise segmental organization of the hindbrain and the simple scaffold of axon tracts in the zebrafish brain provides an ideal model to study how different molecules collaborate to guide migrating neurons and growing axons to their final location. In this thesis, I examine the roles of membrane molecules during neuron migration and axon guidance in zebrafish. In Chapter 3, I show the generation of *Contactin2 (Cntn2)* null mutant using CRISPR/Cas9 and characterize *cntn2* mutant. I demonstrate a role for *cntn2* in facial branchiomotor (FBM) neuron migration and fasciculation of medial longitudinal fascicle (MLF) axons. In addition, using touch-evoked escape response and swimming assays, I show sensorimotor deficits in *cntn2* mutants. Collectively, these data demonstrate distinct developmental roles for zebrafish *cntn2* in neuronal migration and axon fasciculation, and in the function of sensorimotor circuits. In Chapter 4, I examine pairwise genetic interactions between several PCP and non-PCP genes for FBM neuron migration. I show that *vangl2* is rather unique in exhibiting genetic interactions with several PCP and non-PCP genes. These data suggest that

vangl2 might be playing a central role in regulating the function of many PCP and non-PCP genes for FBM neuron migration. In Chapter 6, I describe a novel genetic approach which utilizes the human CD59 receptor (hCD59) and the bacterial toxin intermedilysin (ILY) for rapid cell ablation in zebrafish.

CHAPTER 1: INTRODUCTION

A major challenge in neuroscience is to generate a full understanding of the cellular and molecular mechanisms underlying the formation of functional networks in the central nervous system. Establishment of functional neuronal circuits depends on the ability of specific populations of neurons to form appropriate synaptic connections with target neurons or non-neuronal cells. During the development of the nervous system these connections are formed through a series of consecutive events. First, the process of neural induction and differentiation give rise to different classes of neurons from progenitor cells (Jessell, 2000). Following neuronal differentiation, immature neurons migrate from their birthplace to their final positions (Hatten, 2002). Upon reaching to their final location, neurons extend axons, which navigate through the developing brain by responding to various cellular and extracellular (diffusible) cues to reach to their specific targets (Tessier-Lavigne and Goodman, 1996), and establish synapses. Finally, synaptic refinement takes place which involves the reorganization of synapses and connections. These events are important for the establishment of functional neural circuits that govern complex motor and cognitive functions.

In this chapter, I will briefly review molecular mechanisms regulating neuronal migration and axon guidance. Next, I will review three topics that figure prominently in my studies: 1) the migration of facial branchiomotor (FBM) neurons in the hindbrain, 2) the outgrowth and organization of axons of the nucleus of the medial longitudinal fasciculus (nucMLF) and Rohon-Beard (RB) neurons in the midbrain and spinal cord, respectively, and 3) the fasciculation of retinal ganglion cell (RGC) axons.

1.1 NEURONAL MIGRATION DURING DEVELOPMENT

The function of a neural circuit depends on the precise connections made by neurons with their targets. Neuronal migration is a ubiquitous feature of nervous system development that brings neurons into appropriate spatial relationships with each other and non-neuronal tissue. During development of the nervous system, newborn neurons migrate away from the germinal layer to locations where they form functional neural circuits. A migratory neuron must make several decisions: whether to migrate, what direction to migrate in, and when to terminate migration. Neuronal migration is largely dependent on the ability of the migrating neurons to interact with neighboring cells and with their extracellular environment to sense and respond to different migration signals.

In the developing neural tube, neuronal precursors move in the plane of the neuroepithelium called the ventricular zone (VZ). Neuroepithelial cells after being specified as neurons, begin to differentiate and migrate away from the VZ along distinct radial and tangential pathways to their final destinations (Hatten, 1999; Parnavelas et al., 2002). Neuronal migration can be classified into radial and tangential modes based on the direction in which the neurons migrate relative to the surface of the CNS.

1.1.1 Radial Migration

During radial migration, neurons translocate from the VZ to the more superficial layers in the brain through the radial glial fibers (Hatten, 1999). Radial migration is the most extensively studied form of neuronal migration in the CNS. Radially migrating

neurons are closely associated with the radial glial processes, which are the substrate upon which these neurons migrate (Rakic, 1974). Radially migrating neurons exhibit a bipolar morphology and move along the processes of glial cells in three repetitive steps. They first extend a leading process in the direction of migration (Rivas and Hatten, 1995) which is followed by nucleokinesis, or nuclear translocation. Nucleokinesis begins with the forward movement of the centrosome into the leading process. The final step involves retraction of the trailing process at the rear of the cell (Horwitz and Parsons, 1999) (Fig. 1.1).

1.1.2 Tangential migration

While most neurons migrate radially to reach to their final destinations, a significant number of cortical and other neurons also migrate, but independently of radial glia (Chandrasekhar, 2004; Hatten, 1999; Lois et al., 1996; Marin and Rubenstein, 2003; Pearlman et al., 1998). This glia-independent migration, which occurs along axes orthogonal to the direction of radial migration, is called tangential migration. In contrast to radial migration, which generates distinct neuronal layers or clusters, tangential migration generates neuronal diversity within a given brain region (Marin and Rubenstein, 2003). The molecular and cellular mechanisms governing the tangential migration are less well understood when compared to radial migration.

Due to their conserved organization as well as the stereotypic migration, the facial branchiomotor (FBM) neurons have become an excellent model to study neuronal

migration in the vertebrate embryo (Chandrasekhar, 2004; Song, 2007). Branchiomotor neurons are generated in specific rhombomeres in the hindbrain and innervate muscles that arise in the pharyngeal arches (Chandrasekhar et al., 1997).

1.1.3 FACIAL BRANCHIOMOTOR (FBM) NEURONS

The FBM neurons are a subset of cranial motor neurons found in the vertebrate brainstem (Chandrasekhar, 2004; Gilland and Baker, 2005). In mammals, the facial motor neurons innervate muscles of facial expression, and of the middle ear and upper neck. In all vertebrates investigated, except chicken, FBM neurons undergo a complex and stereotyped tangential migration in the hindbrain along the rostral-caudal axis from rhombomere 4 (r4) to r6 and r7 (Chandrasekhar, 2004) (Fig. 1.2A). Stable transgenic lines, such as the *Tg(isl1:GFP)* strain that labels all branchiomotor neurons (Higashijima et al., 2000), allow for the visualization of distinct cell populations in live embryos (Fig. 1.2B).

1.1.4 Mechanisms regulating tangential migration of facial branchiomotor (FBM) neurons

Tangential migration of FBM neurons is highly dependent on environmental cues as well as cell-intrinsic mechanisms. Several factors have been shown to cell-autonomously regulate the ability of the motor neurons to respond to environmental cues, including transcription factors like r4-expressed Hoxb1 and FBM neuron-

expressed Ebf, Nkx6.1, Hdac1 and Tbx20 (Garel et al., 2000; Muller et al., 2003; Nambiar et al., 2007; Pocock et al., 2008; Song, 2007). Conversely, loss of rhombomere identity in *Krox20* (expressed in r3 and r5) and *Kreisler/valentino/MafB* (expressed in r5 and r6) mutants leads to defective FBM neuron migration, likely a non-cell autonomous effect due to the loss of environmental cues (Chandrasekhar et al., 1997; Garel et al., 2000). Studies in zebrafish have identified several genes necessary for FBM neuron migration from r4 to r6 and r7. Chromatin regulatory proteins Hdac1 (Nambiar et al., 2007) and REST (Mapp et al., 2011), elongation factor Foggy/Spt5 (Cooper et al., 2005), stromal cell-derived factor Sdf1a/Cxcl1a its receptor CxcR4 and CxcR7 (Cubedo et al., 2009), the autism susceptibility protein Met and its Hgf ligand (Elsen et al., 2009), adhesion GPCR gpr125 (Li et al., 2013), the cell adhesion molecule Cntn2 (Sittaramane et al., 2009) and ECM molecules, Lamininα1 and γ1 (Grant and Moens, 2010; Sittaramane et al., 2009), are necessary for FBM neuron migration.

1.1.4.1 Cell adhesion molecules with potential roles in FBM neuron migration

During migration, neurons interact with signals found on neighboring cells and the extracellular matrix (ECM). Laminins are heterotrimeric protein complexes and can modulate a neuron's response to extracellular guidance molecules. In zebrafish, Lamininα1 *(lama1)*, a broadly expressed ECM molecule, plays a role in FBM neuron migration (Paulus and Halloran, 2006; Sittaramane et al., 2009). Consistent with this,

morpholino-based analyses have identified *itga6a* and *itgb1*, which respectively encode IntegrinA6 and IntegrinB1 subunits of a Laminin-binding receptor, as potential regulators of FBM neuron migration (V. Sittaramane, S. Gurung, and A. Chandrasekhar, unpublished data). Mutations in *celsr2*, which encodes an atypical Cadherin, cause severe defects in FBM neuron migration (Wada et al., 2006). Similarly, disruption of neural cell adhesion molecule Cdh2 expression or function generated migration defects where most of the FBM neurons failed to migrate out of r4 (Rebman et al., 2016; Stockinger et al., 2011). We previously showed that the cell adhesion molecule Contactin-2 (Cntn2)/ Transient Axonal Glycoprotein (Tag1) is necessary for the migration of the FBM neurons in the zebrafish (Sittaramane et al., 2009). Together, these studies highlight the importance of cell-cell and cell-substrate interactions during FBM neuron migration. However, some of these data, including the *cntn2* results, were obtained using antisense morpholinos, with possibilities of off-target effects and toxicity (Eisen and Smith, 2008). *Therefore, we generated loss-of-function mutations in cntn2 using CRISPR/Cas9 to address potential concerns with the MO knockdown studies and to investigate roles for zebrafish Cntn2 at later developmental stages in* ***Chapter 3***.

1.1.4.2 The non-canonical Wnt/Planar cell polarity (PCP) pathway and FBM neuron migration

Wnts are secreted glycoproteins that bind to Frizzled (Fz), a seven-pass transmembrane receptor. Binding of Wnts to Fz activates one of two signaling

pathways, a canonical pathway that allows β-catenin to mediate transcriptional changes (Logan and Nusse, 2004), and a non-canonical pathway that activates downstream ROCK and Jun kinases altering cytoskeleton arrangements or cell polarity. Planar Cell Polarity (PCP) signaling has been primarily studied in the context of the polarization of epithelial tissues. The non-canonical Wnt pathway has been shown to regulate both cell polarity and movements of dorsal mesodermal cells during convergent extension and also later during neural tube closure (Veeman et al., 2003). In zebrafish, Wnt/PCP signaling regulates convergence and extension during movements during vertebrate gastrulation (Roszko et al., 2009) and aids in establishing the polarity of neural progenitors (Ciruna et al., 2006). The importance of PCP signaling in regulating FBM neuron migration has been well demonstrated. Mutation in Wnt/PCP components like Van gogh-like 2 (Vangl2) (Bingham et al., 2002; Glasco et al., 2012; Jessen et al., 2002; Vivancos et al., 2009), Prickle1a (Pk1a) (Carreira-Barbosa et al., 2003), Prickle1b (Pk1b) (Rohrschneider et al., 2007), Scribble1 (Scrib1) (Wada et al., 2005), Frizzled3a and Celsrs 1-3 (Qu et al., 2010; Wada et al., 2006) leads to FBM neuron migration defects in zebrafish and mouse. However, other components of PCP pathway do not appear to play roles in FBM neuron migration. (Disheveled, Wnts, Rho Kinase)

1.1.4.3 Role of *vangl2* in tangential migration of FBM neurons

The *trilobite* locus encodes Van gogh-like 2 (Vangl2) (Jessen et al., 2002), a core component of Wnt/PCP pathway (Veeman et al., 2003). Vangl2 is a four-pass membrane-spanning protein with the N-terminal and C-terminal domains located in the

cytosol, with a PDZ domain-binding motif (PBM) at the C-terminus (Darken et al., 2002; Katoh, 2005; Park and Moon, 2002). The tangential migration of FBM neurons from r4 to r6 and r7 is eliminated in *vangl2-/-* mutants (Bingham et al., 2002; Jessen et al., 2002). *vangl2* is expressed broadly in the hindbrain, and largely functions non-autonomously for FBM neuron migration (Jessen et al., 2002). During my graduate work, I contributed to two projects involving the 1) identification of cell-type where Vangl2 functions and 2) examination of the roles of Vangl2 domains in FBM neuron migration. I have briefly summarized the papers below.

1.1.4.1.1 Identification of cell-type where Vangl2 functions (Sittaramane et al., 2013)

Vangl2 is broadly expressed in zebrafish hindbrain, and it functions largely non-cell autonomously to regulate FBM neuron migration (Jessen et al., 2002). However, the cell-type within which Vangl2 acts is unknown. Using targeted transplantations and cell type-specific transgene expression, we demonstrated that *vangl2* functions primarily in floor plate cells in r4 to regulate migration. Importantly, we ruled out a role for *vangl2* in FBM neurons for mediating motor neuron-motor neuron interactions (collective migration). FBM neurons frequently contact floor plate cells in r4, and a biologically active GFP-Vangl2 fusion protein is enriched on floor plate cell membranes. These observations suggest that Vangl2 present on floor plate membranes facilitates signaling necessary for initiating FBM neuron migration

1.1.4.1.2 Roles of Vangl2 domains in FBM neuron migration (Pan et al., 2014)

In vertebrates, Vangl2 is necessary for developmental and physiological processes including convergence and extension (CE) movements during gastrulation (Marlow et al., 1998), wound repair (Caddy et al., 2010), tumor cell migration (Cantrell and Jessen, 2010), and orientation of cilia in many tissues and organs (Borovina et al., 2010; May-Simera et al., 2010; Song et al., 2010). However, despite its broad roles in development and disease, the roles of various domains of Vangl2 in specific cellular behaviors such as FBM neuron migration have not been studied. We, therefore, wanted to examine the roles of specific Vangl2 domains in the context of FBM neuron migration. To do this, we generated various myc-tagged Vangl2 variants lacking specific domains and asked whether these Vangl2 variants could rescue FBM neuron migration defects of *vangl2-/-* mutants by RNA injection. However, this strategy was not feasible because RNA injection of several constructs generated CE defects. To bypass CE defects induced by RNA injection, we generated transgenic lines for heat shock-inducible expression of the Vangl2 variants. Surprisingly, migration of FBM neurons was strongly inhibited in heat-shocked transgenic embryos, a dominant-negative phenotype not observed following RNA injection. This unexpected dominant negative effect of Vangl2 overexpression precluded an analysis of the various Vangl2 domains to rescue FBM neuron migration in *vangl2-/-* mutants. Therefore, instead of testing whether the Vangl2

variants could rescue FBM neuron migration in *vangl2-/-* mutants, we tested their abilities to generate the dominant-negative phenotype. We found that membrane associated functions of the N-terminal and C-terminal domains of Vangl2 are involved in regulating FBM neuron migration. Importantly, using temperature shifts, we determined that Vangl2 function is required between 15-20 hpf, coinciding with the onset of migration, and suggesting that Vangl2 is required for the initiation of FBM neuron migration in r4.

1.2 Genetic interaction between *vangl2* and other PCP and non-PCP molecules for FBM neuron migration

Previous studies have shown that *vangl2* functions with *knypek (glypican4/6)*, *pipetail (wnt5a)*, *silberblick (wnt11)* and *disheveled (Dsh)* to regulate convergence and extension movements in Wnt/PCP pathway (Jessen et al., 2002; Park and Moon, 2002). However, there are multiple lines of evidence suggesting that the role of *vangl2* in FBM neuron migration is independent of its function in the Wnt/PCP pathway. 1) Several *trilobite* alleles only generate mild CE defects but exhibit severe FBM neuron migration defects. 2) *vangl2* functions cell autonomously for CE movements and non-cell autonomously for FBM neuron migration (Jessen et al., 2002). (3) Mutations in other PCP molecules such as *knypek (glypican4/6)*, *pipetail (wnt5a)* and *silberblick (wnt11)* produce CE defects, but do not affect FBMN migration (Jessen et al., 2002; Park and Moon, 2002). These observations suggest strongly that *vangl2* may function through the

novel, Wnt/PCP-independent cellular and molecular mechanisms to mediate FBM neuron migration. Interestingly, we showed previously that *cntn2* (a non-PCP gene) and *vangl2* genetically interact during FBM neuron migration since injection of a suboptimal dose of *cntn2* MO enhances the weak FBM neuron migration phenotype of *vangl2* heterozygotes (Sittaramane et al., 2009). This result suggests that Cntn2 and Vangl2 participate in a common mechanism to regulate FBM neuron migration. Similarly, *vangl2* has also been shown to genetically interact with *gpr125* (a non-PCP gene) for FBM neuron migration (Li et al., 2013). Together, these data suggest that *vangl2* may interact with other non-PCP molecules expressed in the FBM neurons or in the environment to regulate FBM neuron migration. However, these genetic interaction data were obtained from morpholino studies with possibilities of off-target effects and toxicity (Eisen and Smith, 2008). We, therefore, aimed to validate the genetic interaction between *vangl2* and *cntn2*, and *vangl2* and *gpr125* using genetic mutants in chapter 3 and 4. We also tested for genetic interaction between *vangl2* and other PCP and non-PCP genes for FBM neuron migration.

1.3 AXON GUIDANCE DURING DEVELOPMENT

During development of the nervous system, axons follow very precise pathways to reach their destination. Axons reach their target by integrating many external signals. The correct wiring of the nervous system depends on the ability of axons to locate and recognize their appropriate synaptic partners. Axons are equipped with motile and

highly sensitive structures called growth cones to help navigate their way. Growth cones sense guidance cues, both attractive and repulsive, in the environment by extending fingerlike projections called filopodia. These structures use guidance cues as their “road signs” to reach their appropriate targets. Growth cone extension, retraction, or turning occurs from the rearrangement of the growth cone’s cytoskeleton and the modulation of growth cone-substrate adhesivity. Neighboring cells, as well as axons, provide guidance cues to growing axons. Together, two intimately associated processes: 1) axon guidance and 2) axon growth help to establish appropriate synaptic connections, generate topographic maps and define receptive fields during the critical periods. Misregulation in this process could cause synaptic dysfunctions and lead to impaired cognitive and mental abilities seen in many developmental as well as psychiatric disorders (Engle, 2010).

1.3.1 Cellular and molecular mechanisms involved in axon guidance

Proper assembly of functional neural circuits requires tight regulation of axon growth and guidance. With the technological advances in molecular genetics, high-resolution imaging, and neuronal culture, tremendous progress has been made in elucidating the molecular and cellular mechanisms underlying pathway selection and target recognition. Over the past years, a plethora of molecules has been identified that regulate axon growth and guidance during the development of the nervous system.

1.3.1a Guidance molecules

Guidance cues include molecules from several gene families that are conserved across many species. These molecules are either expressed in the environment for long-range communication or on the cell surface for short-range communication between surrounding cells and growth cones. Four families of guidance cues were originally identified that mediate axons guidance.

1.3.1a1 Netrins

Netrin (Net) proteins are a family of evolutionarily conserved laminin-related diffusible proteins that are secreted by the floor plate to attract commissural axons to cross the midline (Kaprielian et al., 2001; Serafini et al., 1994). Vertebrate Netrins were first identified in the Chick, where they function to promote commissural axons outgrowth and guidance toward the floor plate (Serafini et al., 1996). Netrins have been shown to regulate axon guidance in many organisms, from nematodes and insects to higher mammals (Kaprielian et al., 2001). Commissural axons exhibit pathfinding defects and fail to reach the floor plate in mice lacking functional netrin (Serafini et al., 1996). UNC-5 and DCC (Deleted in Colorectal Carcinoma) have been identified as receptors for netrins through biochemical and genetic studies in several different species (Culotti and Merz, 1998; Hong et al., 1999). DCC receptors largely mediate attraction to netrins but can also participate in repulsion. UNC-5 receptors exclusively

function in repulsion which is mediated by UNC-5 alone or in combination with DCC receptors (Hedgecock et al., 1990; Hong et al., 1999).

1.3.1a2 Slits

Slits are large secreted glycoproteins first discovered in a genetic screen of embryonic patterning defects in *Drosophila* (Nusslein-Volhard et al., 1984). Their role in axon guidance was later observed in genetic screens for commissural axon guidance pathfinding defects in *Drosophila* (Hummel et al., 1999). Slits homologs have been characterized in *C. elegans* (Hao et al., 2001), *Xenopus* (Chen et al., 2000), zebrafish (Hutson and Chien, 2002), chick (Holmes and Niswander, 2001), as well as in mammals (Brose et al., 1999). Slits signal through Roundabout (Robo) family receptors. Gene encoding these receptors were first identified in *Drosophila* in a genetic screen for genes regulating midline guidance defects in the central nervous system (CNS). Genetic and biochemical studies showed that Slit can bind to Robo, which functions as midline repellent (Brose et al., 1999; Kidd et al., 1998). *Slit* mutants exhibit collapse of axon tracts onto the midline in Drosophila (Kidd et al., 1998). Similarly, in vertebrate *slit* mutant, commissural axons show defects in midline crossing (Long et al., 2004). Interestingly, *Robo* mutants also show defects in commissural axon pathfinding (Kidd et al., 1998).

1.3.1a3 Semaphorins

Semaphorins are a large family of cell surface and secreted guidance molecules. Semaphorins were first identified by searching for molecules expressed on specific axon fascicles. Molecules of this family share a conserved “sema” domain and are divided into eight classes based on their origin and structural elements (Raper, 2000). Semaphorins signal through multimeric receptor complexes consisting of a ligand binding component, neurophilin, and a signal transducing component, called plexin (Huber et al., 2003). Studies in flies and mice suggest that semaphorin primarily acts as short-range inhibitory cues that repel axons away from inappropriate regions. Interestingly there are studies suggesting that semaphorins may also act as attractive cues for certain axons. Class 3 semaphorins (Sema3s) are the most extensively studied vertebrate class. *In vitro* studies have revealed essential roles of class 3 semaphorins in eliciting growth cones responses as well as the understanding of signal transduction mechanisms that mediate these mechanisms. In addition, *in vivo* studies have implicated roles for Sema3 in the formation of several central and peripheral tracts as well as the axons of cranial, olfactory, motor, and hippocampal nerves (Cloutier et al., 2004; Falk et al., 2005; Huber et al., 2005; Kitsukawa et al., 1997; Liu and Halloran, 2005; Taniguchi et al., 1997; Wolman et al., 2004).

1.3.1a4 Ephrins

Ephs are a large group of receptor tyrosine kinases (RTKs) that bind to ephrins. Ephrin ‘ligands’ and Eph ‘receptors’ are membrane-bound resulting in signals that are localized to areas of cell contact (Lisabeth et al., 2013). After binding, both Eph- and

ephrin-expressing cells are capable of transducing signals that lead to changes in cellular behavior. Thus, Ephs and ephrins signal bidirectionally, with ephrin induction of Eph signaling termed ‘forward’ signaling and Eph induction of ephrin signaling called ‘reverse’ signaling. Bidirectional signaling allows regulation of axon and target cell responses after an interaction. Eph–ephrin proteins were first identified as contact repellents, however, Eph–ephrin proteins can promote adhesion or repulsion depending on the signaling context (Arvanitis and Davy, 2008). Phenotypic analyses of Eph and ephrin mutant mice have shown that Eph–ephrin signaling is used to regulate cell-cell interactions in a variety of developmental processes, including cell migration (Chin-Sang et al., 1999; George et al., 1998; Smith et al., 1997) and axon guidance (Williams et al., 2003; Yokoyama et al., 2001).

1.3.2 Ig superfamily (IgSF) CAMs in axon guidance and fasciculation

Navigation of axons depends on the interactions of growing axons with earlier grown axons of neighboring neurons which has already reached to its target. Axons adhere to either extracellular matrix or another cell surface by using specific cell surface receptors. Large number of IgSF-CAMs have been identified on growing axons, including NCAM1 (Cunningham et al., 1987), NCAM2 (Hamlin et al., 2004), L1CAM (Brittis et al., 1995), CHL1 (Schlatter et al., 2008), NRCAM (de la Rosa et al., 1990), CNTN1 (Falk et al., 2002), CNTN2 (Stoeckli and Landmesser, 1995; Suter et al., 1995),

and ALCAM (Avci et al., 2004). Ig superfamily CAMs mediate intracellular communication and adhesion by interacting homophilically (i.e. between IgSF-CAMs of the identical types) and heterophilically (i.e. between different types of IgSF-CAMs) in *cis* (i.e. located in the plane of the plasma membrane) and *trans* (i.e. located in two contacting cell surfaces) conformations on neuronal surfaces. IgSF CAMs have been shown to play an important role in correct navigation and axon fasciculation of axons using a diverse array of *in vitro* techniques. Animals deficient for certain IgSF-CAMs exhibit significant errors in pathfinding of corticospinal, callosal, retinal, and hippocampal axons, suggesting that these molecules are critical factors in mediating pathfinding *in vivo* (Maness and Schachner, 2007). However, it is unclear how Ig superfamily CAMs function *in vivo* and how these deficits influence the development and function of the neural circuits. *Therefore, in chapter 3, I investigate the roles of Cntn2, a member of Ig superfamily CAM, in the development and function of neural circuits in zebrafish.*

1.4 Cell types examined to analyze axon guidance and fasciculation

1.4.1 Interneurons of the nucleus of the medial longitudinal fascicle (nucMLF)

The axons of the nucleus of the medial longitudinal fascicle (nucMLF) are the first axons to extend in the zebrafish midbrain (Hjorth and Key, 2002). nucMLF are bilateral

clusters of neuronal cell bodies that lie in the ventral midbrain. nucMLF consists of a cluster of 6-8 neurons at the onset of MLF formation which occurs at 16 hpf. The cluster grows to approximately 30-35 neurons by 24 hpf (Chitnis and Kuwada, 1990; Ross et al., 1992). Each nucMLF cells extend an axon posteriorly along the ipsilateral ventral neural tube. The caudal-most nucMLF cell extends the leading MLF axon into the hindbrain, and then the more rostrally positioned cells extend axons that fasciculate with the leading axon (Wolman et al., 2007) (Fig. 1.3A).

Using *in vivo* time-lapse imaging of *Tg (pitx2c:gfp)* transgenic line which expresses a green fluorescent protein (GFP) in nucMLF neurons (Fig. 1.3B), Wolman and colleagues showed that nucMLF axon guidance is controlled by both positive axon-axon interactions and guidance by surrounding tissue (Wolman et al., 2008). Morpholino studies have shown that guidance molecule, Contactin-2 (Cntn2), a member of Ig superfamily CAMs, guides the direction of axon extension by interpreting environmental cues and mediating positive axon-axon contacts. However, knockdown of L1, another Ig superfamily CAM expressed by nucMLF (Tongiorgi et al., 1995) leads to MLF defasciculation in the hindbrain but does not cause any defects of the nucMLF (Wolman et al., 2007). These data suggest that not all CAMs expressed by these neurons are required for MLF axon guidance. The first axons to extend in the brain use the extracellular matrix (ECM) as growth substrate and guidance sources. Laminins, a component of the ECM, are heterotrimeric glycoproteins, consisting of α, β, and γ polypeptide chains which form a major component of the ECM in the central nervous system (Powell and Kleinman, 1997). A laminin-α1 mutant, *bashful (*Paulus *and*

Halloran, 2006) *also* exhibits nucMLF defects as seen in *cntn2* morphants. Loss of laminin-α1 causes nucMLF axons to extend into surrounding tissue in incorrect directions and reduces axonal growth rate. This has been shown to result in stunted nucMLF axons that fail to extend beyond the hindbrain (Wolman et al., 2008). However, unlike Cntn2, Laminin-α1 does not affect axon-axon interactions but does regulate neuronal polarity and influence growth cone responsiveness to surrounding cues (Wolman et al., 2008).

Optomotor response (OMR) is one of the innate sensory-driven locomotor behavior (Bilotta, 2000; Neuhauss et al., 1999). In this, larvae respond to the whole-field visual motion (Orger et al., 2000) by swimming and turning to maintain a stable position with respect to their visual environment (Portugues and Engert, 2009). nMLF is the most prominent group of neurons activated by visual stimulation that specifically elicits forward-directed locomotion (Orger et al., 2000). nucMLF is active in response to various stimuli including the spontaneous swimming and has been implicated in modulating locomotion in larval zebrafish (Sankrithi and O'Malley, 2010).

1.4.2 Rohon-Beard (RB) sensory neurons

Rohon-Beard (RB) neurons are multipolar primary sensory neurons present in the embryonic zebrafish spinal cord (Fig. 1.4A). They are located bilaterally in the dorsal spinal cord and have a cell body, two central axons, and a peripheral axon (Fig. 1.4B, C). RB neurons extend their central axons longitudinally within the dorsal spinal cord both rostrally and caudally and send their highly branched peripheral axons

dorsolaterally from the spinal cord. Peripheral axon runs through segmental myotomes and innervates skin that transmits sensory stimuli to the CNS (Bernhardt et al., 1990; Metcalfe et al., 1990; Ribera and Nusslein-Volhard, 1998). The RB neurons undergo programmed cell death resulting in complete elimination from the spinal cord by 5 days postfertilization (dpf), and their function is replaced by dorsal root ganglia neurons (Reyes et al., 2004; Williams et al., 2000).

Zebrafish embryos react to tactile stimuli from about 22 hpf. Tactile stimuli in the head region are mediated by a subset of trigeminal ganglion cells. However, tactile stimuli to the trunk are mediated by RB cells (Metcalfe et al., 1990). Tactile stimulation activates RBs, which synapse onto primary ascending commissural interneurons (CoPAs). CoPAs which contact contralateral descending interneurons then activates motor neurons located contralaterally to the site of tactile stimulation (Carmean and Ribera, 2010).

Previous studies have shown that guidance molecules Semaphorin 3d (Sema3d)/Plexin A4 (Plxna4), and Slit2/Robo affects the outgrowth of peripheral axons, but not the central axon. Similarly, Contactin-2 only affects the outgrowth of central axons of RB neurons (Liu and Halloran, 2005; Miyashita et al., 2004) but not the peripheral axons. These findings suggest that the outgrowth of peripheral and central axons is regulated by different molecular machinery.

1. 4.3 Retinal Ganglion Cell (RGC) neurons

Visual information is carried from the eye to the brain via the axons of retinal ganglion cell axons. RGC axons navigate through a series of intermediate targets on their route to their destination. Guidance molecules like netrins, slits, and ephrins play a key role in the guidance of RGC axon (Deiner et al., 1997; Thompson et al., 2009; Williams et al., 2003).

Due to optical transparency of embryos, zebrafish have proven to be an excellent model for studying axon guidance in an *in vivo* context. RGC axons must make several decisions along their pathway and respond to various attractive or repulsive cues to reach their appropriate target. In zebrafish, the first RGCs are born at 28 hpf, and all axons cross the midline. Retinal axons navigate dorsally through the optic tract and reach the tectum at 48 hpf. Sema3d, a secreted semaphorin, is expressed at the midline and guides the crossing of RGC axons (Sakai and Halloran, 2006). Laminins are important components of the basal lamina and are known to be highly permissive as well as an instructive cue. Laminin-1 has been shown to be a permissive substrate for neurite outgrowth for different neural cell types (Powell and Kleinman, 1997). In vivo, laminin-α1 has been shown to play an important role in guiding RGC axons (Paulus and Halloran, 2006). Cntn2, a cell adhesion molecule of Ig superfamily, has been shown to be required for the fasciculation of RGC axons in mouse (Chatzopoulou et al., 2008). In zebrafish, Cntn2 is expressed on RGC neurons and axons (see Fig. 3.11E-F). In

Chapter 3, we have examined the roles of Cntn2 in RGC axon guidance and fasciculation.

Since the roles mentioned above of Cntn2 in nucMLF and RB neuron development were implicated from morpholino studies, in ***Chapter 3****, I have examined the role of Cntn2 in development and function of nucMLF and Rohon-Beard neurons by using null mutants.*

1.5 ADDITIONAL PROJECTS CONDUCTED DURING PHD STUDIES

1.5.1: Novel Method for rapid cell ablation in zebrafish (in collaboration with Dr. Elizabeth Bryda)

Our cell ablation system utilized the human CD59 receptor (hCD59), and the bacterial toxin intermedilysin (ILY). Our data involving transient RNA injection and stable transgenic line suggest that hCD59/ILY method can ablate cells rapidly in zebrafish and can obviate limitations involving relatively slow onset of cell ablation seen with current methodologies. *I have described our findings in detail in* ***Chapter 6****.*

1.5.2: Establishment of a zebrafish model for Giant Axonal Neuropathy (GAN) (in collaboration with Dr. Mark Hannink)

Giant Axonal Neuropathy (GAN) is a rare neurodegenerative disorder affecting axons in the peripheral and central nervous system, accompanied by axonal swellings

and axon loss (Bruno et al., 2004; Sharma et al., 2012). While GAN is caused by presumptive loss-of-function mutations in the human *GAN* gene (Tazir et al., 2009), the etiology of the disease is poorly understood. We aimed to establish a zebrafish model of GAN to gain insight into the cellular and biochemical mechanisms underlying the disease phenotype. *GAN* encodes a 468 amino-acid protein, Gigaxonin, a member of the BTB-Kelch superfamily involved in the ubiquitin-proteasome pathway. In mice, *gan* is expressed extensively in multiple tissues, including the brain and spinal cord (Bomont et al., 2000). Similarly, we found that zebrafish *gan* is expressed from 18 hpf to 4 dpf, with high expression in the brain at 4 dpf.

To investigate roles of *gan* in disease, we generated loss-of-function mutations in *gan* using the CRISPR/Cas9 system. We have identified two alleles with frameshift mutations resulting in premature stop codons. Since sensory-motor functions are compromised in GAN patients, we examined two behaviors in zebrafish *gan* mutants involving sensorimotor circuits: touch-evoked escape response and food intake. Wild type and mutant larvae exhibited normal escape responses when touched in the trunk. In contrast, a significantly larger proportion of mutants responded when touched on the head, consistent with extensive *gan* expression in the hindbrain, where touch responses are processed. Feeding is a complex behavior requiring the coordination of sensory (vision, olfaction) and motor (jaw movement, locomotion) activities. At 7 dpf, mutant larvae exhibited a significant decrease in food intake compared to wild type siblings, consistent with *gan* expression in the hindbrain, where the motor neurons driving jaw movements are located. These data suggest that zebrafish *gan* mutants have defects in

sensorimotor functions consistent with the defects seen in the mouse GAN model and in human patients, and may represent a good model for GAN in a simple vertebrate.

1.6 FIGURES AND LEGENDS

Figure 1.1: Radially migrating neurons moving along radial glia processes in three repetitive steps

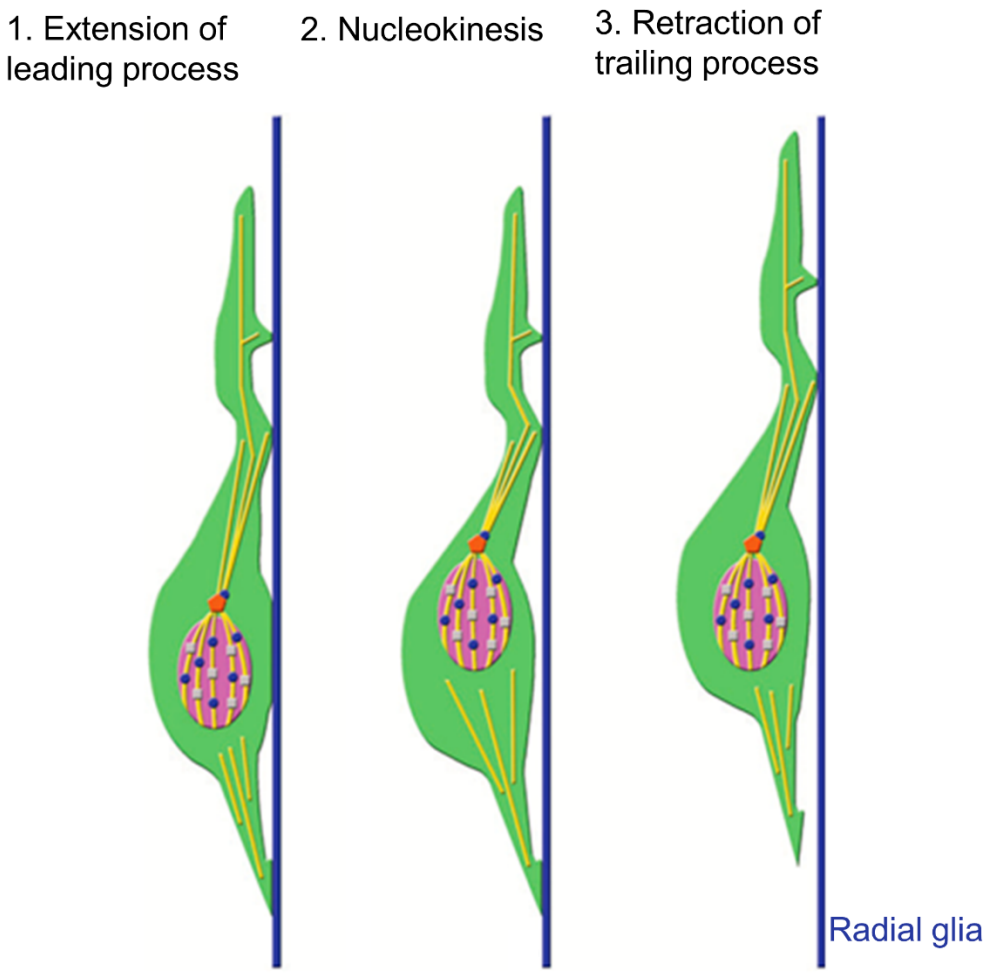

Figure 1.1: Radially migrating neurons moving along radial glia processes in three repetitive steps. (1) Migrating neurons first extend a leading process in the direction of migration. (2) This is followed nucleokinesis which causes forward movement. (3) In the final step, retraction of the trailing process takes place which enables the cell to move forward. *Adapted from (Solecki et al., 2006).*

Figure 1.2: Facial branchiomotor (FBM) neuron migration in zebrafish

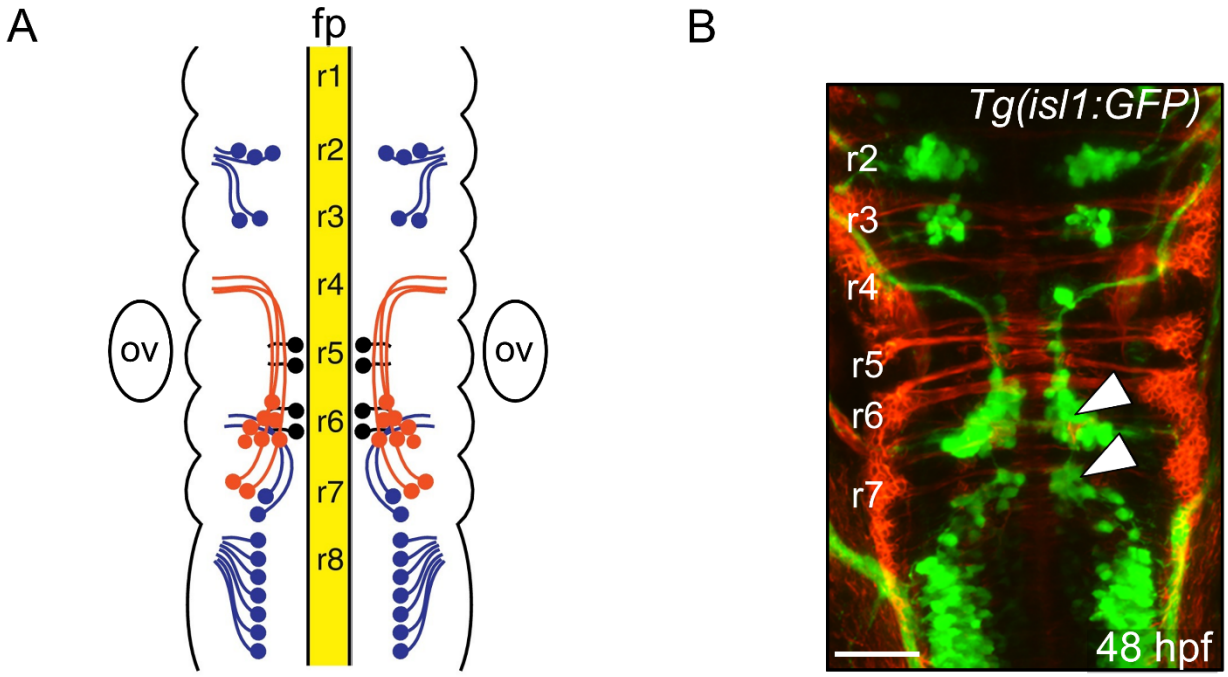

Figure 1.2: Facial branchiomotor (FBM) neuron migration in zebrafish. (A) Schematic rendering of 48 hpf zebrafish BMN organization. FBM neurons in red, other BM neurons in blue, abducens motor neurons in black; ov, otic vesicle; fp, floor plate (yellow). (B) *Tg(isl1:gfp)* embryos were fixed at 48 hpf, and processed for immunohistochemistry with zn5 antibody (red) to label hindbrain commissural neurons and axons at rhombomere boundaries, and anti-GFP antibody (green) to label FBM neurons (arrowheads). Dorsal views of the hindbrain with anterior to the top. Scale bar in B= 50 μm. *Panel A modified from (Wanner and Prince, 2013).*

Figure 1.3: MLF axons extension and convergence

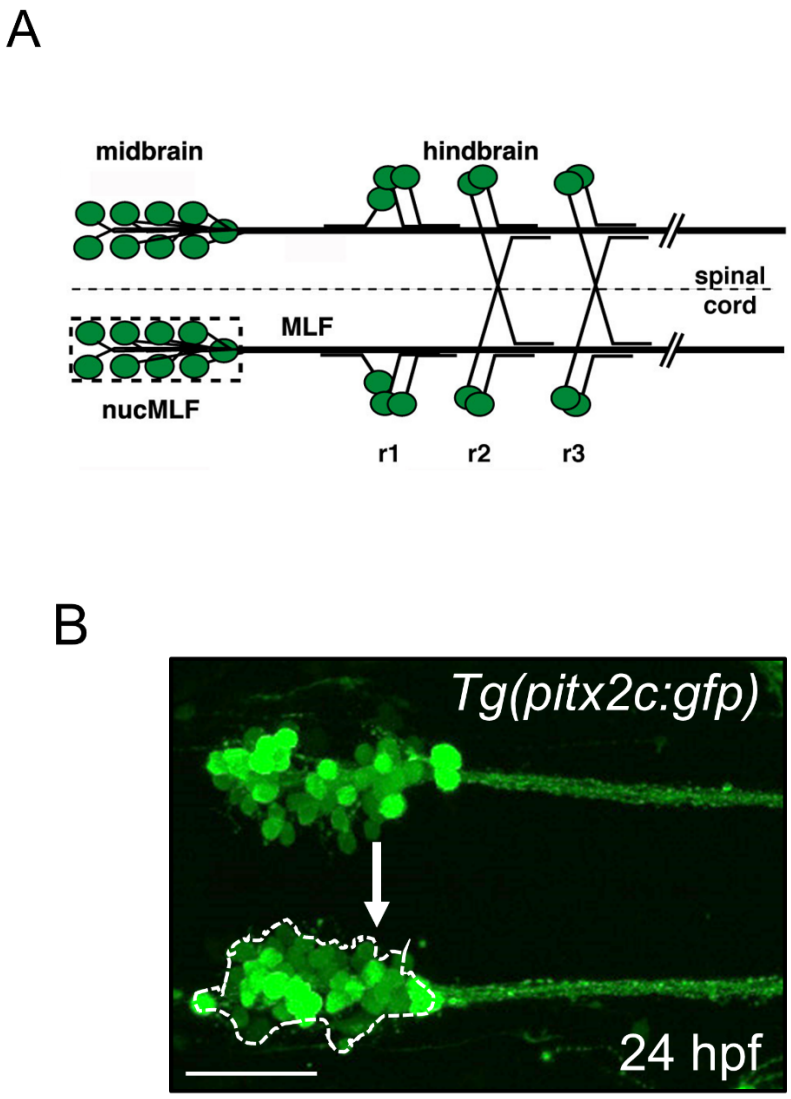

Figure 1.3: MLF axons extension and convergence. Ventral views with anterior to the left. (A) Schematic representation of MLF axons extending from midbrain to spinal cord. The dashed line denotes the ventral midline and dashed box surrounds the 'nucMLF zone'. r represents rhombomere. (B) Confocal projections of *Tg(pitx2c:gfp)* embryos labeled with anti-GFP antibody at 24 hpf. Ventral views of the midbrain with anterior to the left. Scale bar in B = 50 μm. *Panel A from (Wolman et al., 2008).*

Figure 1.4: Rohon-Beard neurons in zebrafish trunk

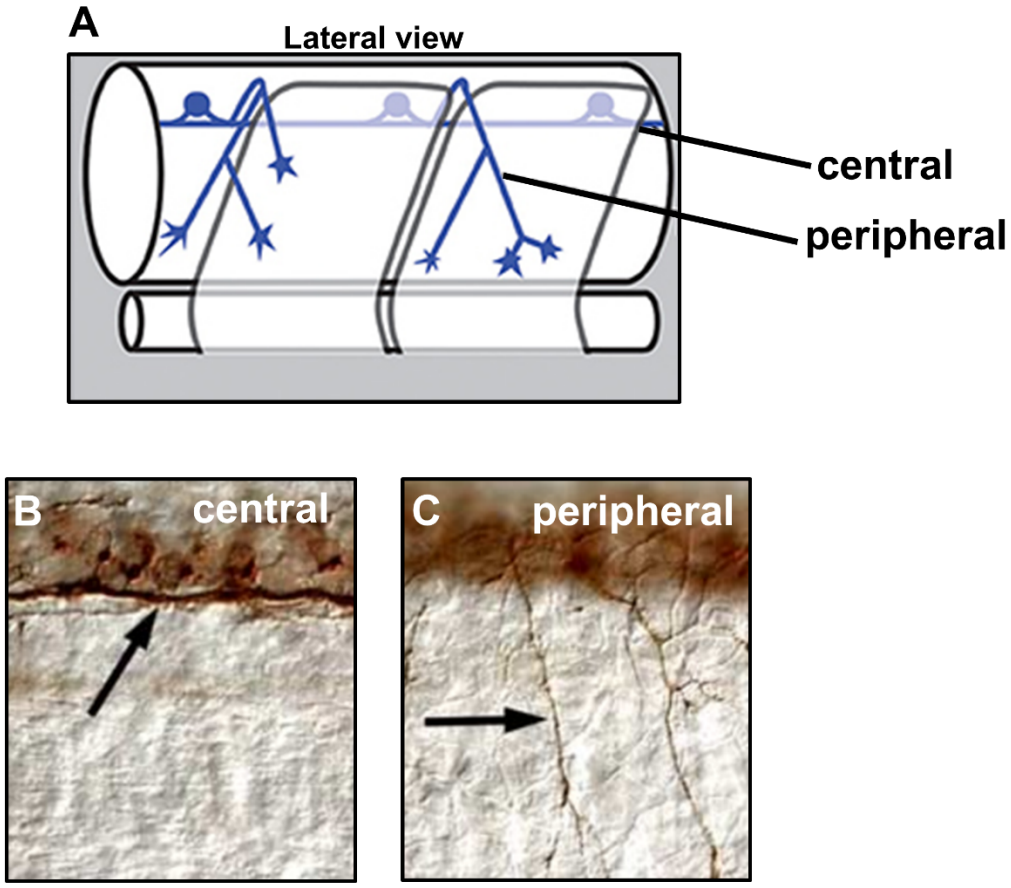

Figure 1.4: Rohon-Beard neurons in zebrafish trunk. Lateral views with anterior to the left. (A) Schematic of trunk showing Rohon-Beard axon pathways. (B, C) Zn-12 labeled 22 hpf embryo showing central axons in spinal cord focal plane (B, arrow) and peripheral axons in the epidermal focal plane (C, arrow). *Adapted from (Liu and Halloran, 2005).*

CHAPTER 2: MATERIAL AND METHODS

2.1 FISH MAINTENANCE

Zebrafish (*Danio rerio*) stock lines were maintained on a 14 hour light/ 10 hour dark cycle as described previously (Westerfield, 1995). Embryos were easily obtained by crossing adult fish. Depending on the nature of the experiment, embryos were obtained from pairwise crossing (1 pair) or population crossing (2-3 pairs). Embryos were grown at 28.5°C in embryo medium (E3) and staged by hours post fertilization (hpf) (Kimmel et al., 1995). The age of embryo was verified at somitogenesis stages. Embryos were treated with phenylthiourea (PTU, Sigma), a pharmacological pigmentation blocker, around 24 hpf if prevention of pigmentation was desired. Embryos were fixed overnight at 4°C at appropriate ages in 4% paraformaldehyde in phosphate-buffered saline (PBS). Embryos were fixed for 2 hours at room temperature if they required light fixing.

2.2 GENOTYPING EMBRYOS

To genotype embryos, genomic DNA from individual embryos was extracted using NaOH/Tris-HCl (Meeker et al., 2007). Single embryo was then incubated in 50 µl of 50 mM NaOH and boiled at 95°C for 10 minutes vortexting 2-3 times in between. Tubes containing genomic DNA were then cooled, and 5 µl of 1M Tris-HCl (pH 8) was added. Samples were then centrifuged at 13,000 RPM for 5 minutes at room temperature. 3 µl of supernatant containing genomic DNA was used in a standard 25 µl PCR reaction with appropriate primers.

2.3 GENOTYPING ADULTS

To genotype adult fish, fish were briefly anesthetized using tricaine. Using a pair of fine scissors, the caudal fin was clipped halfway between the tip of the fin to a point at which fish scales end. Fish were returned to holding cages and allowed to revive before putting them in a circulating system. Fin-clipped fish were maintained in isolation in the aquarium for 2-3 weeks until the clipped fin was fully regenerated. The fin clip tissue was immersed in 0.5 ml of lysis buffer and digested by rocking overnight at 55°C. The following day, tubes with fin clip tissue were centrifuged for 20 minutes at room temperature. Clear supernatant containing genomic DNA was transferred to new 1.5 ml centrifuge tubes containing 0.5 ml 100% ethanol. The samples were then rocked for 2-3 hours at room temperature until white/yellow strands were visible. Genomic DNA was then pelleted by centrifuging at 4°C for 20 minutes. The pellet was washed in cold 70% ethanol and the pellet was then resuspended in 20 µl ddH_2O. 2 µl of this resuspension was used in a standard 25 µl PCR reaction with appropriate primers.

2.4 MUTANT AND TRANSGENIC LINES

2.4.1 *trilobite*

Trilobite allele (*tri*^{tc240a}) was identified based on their morphology during somitogenesis (Hammerschmidt et al., 1996; Solnica-Krezel et al., 1996). Through positional cloning, the gene encoded by *trilobite* was identified as *vangl2* (Jessen et al., 2002). The *tri*^{tc240a} allele contains a 30 base pair insertion which results in the in-frame

addition of 13 amino acids at Arg 21 (Jessen et al., 2002). Homozygous mutant larvae usually die by 6-7 days of development, although about 10% of homozygotes escaped lethality and grow into fertile adults (Bingham et al., 2002). Homozygous mutants exhibit convergence extension defects as well as exhibit fully penetrant branchiomotor neuron defects.

2.4.2 *sleepy*

Sleepy allele *(sly^{ti263a})* was identified through large-scale zebrafish mutagenesis screens. This allele was identified based on defects in notochord differentiation resulting in shorter embryos with thin notochords (Odenthal et al., 1996). The *sleepy* locus maps to the *lamc1* gene, which encodes laminin γ1. In addition to undersized retinas and displacement of the lens (Parsons et al., 2002), homozygous mutants also show defects in FBM neuron migration (Chandrasekhar, 2004).

2.4.3 *off-limits*

Off-limits allele *(olt^{rw689})* was identified from mutagenesis using *N*-ethyl-*N*-nitrosourea (ENU). Both zygotic, as well as maternal-zygotic *olt* embryos, display FBM neuron migration defects (Wada et al., 2006). The *olt* locus maps *to* zebrafish Frizzled3a and the olt^{rw689} carries a missense mutation which disrupts proper folding and thereby their function.

2.4.4 *gpr125^{stl40}*

Gpr125 is an adhesion G protein-coupled receptor shown to act as a modulator of the Wnt/planar cell polarity (PCP) signaling system (Li et al., 2013). *gpr125^{stl40}* allele was generated by Dr. Lilianna Solnica-Krezel's lab at Washington University. The allele was generated using TALENs which targeted GPCR proteolytic site. The *gpr125^{stl40}* allele contains 19 base pair insertions resulting in early termination.

2.4.5 *cdh2^{hi3644}*

Cadherin 2 allele (*cdh2^{hi3644}*) came out the Hopkin's laboratory at MIT who generated and identified insertional mutations in 315 genes that resulted in visible morphological defects or lethality by 5 days post fertilization (Amsterdam et al., 2011; Golling et al., 2002). *Cdh2* mutants exhibit defasciculation of optic nerves. However, retinal ganglion cell axons appropriately cross the midline (Barresi et al., 2010).

2.4.6 *dtr^{te370a}*

Detour allele *(dtr^{te370a})* was ENU-generated and originally identified based on its midline and retinotectal phenotypes (Brand et al., 1996; Karlstrom et al., 1996). The *detour* (*dtr*) locus maps to the *gli1* gene. Cranial motor neurons are missing in *dtr^{te370a}* embryos (Chandrasekhar et al., 1999).

2.4.7 Islet1-GFP transgenic line *Tg(isl1:gfp)*

The islet1-GFP transgenic line was generated using the promoter/enhancer of the *islet (isl1)* gene to drive GFP expression in cranial motor neurons (Higashijima et al., 2000). *Isl1*, a member of the Lim/homeobox gene family, is expressed in all post mitotic motor neurons early during the development (Inoue et al., 1994). *Tg(isl1:gfp)* fish express GFP in all branchiomotor neurons (nV, nVII, nX), except the nIX motor neurons. Unless otherwise stated, data presented here on FBM neuron migration analysis were performed in this transgenic line.

2.4.8 Pitx2c-GFP transgenic line *Tg(pitx2c:gfp)*

The Pitx2c:GFP transgenic line was generated using an internal promoter of the Pitx2 gene to drive GFP expression in trigeminal ganglia and the nucMLF neurons (Wolman et al., 2008). Unless otherwise stated, data presented here on nucMLF axon convergence analysis were performed in this transgenic line.

2.5 GENOTYPING MUTANT LINES

2.5.1 *gpr125^{stl40}*

The following primers were used for genotyping:

Fwd: 5'-GATCTGCTGAGTCCGGTGAACGTGACGCTG- 3'

Rev: 5'-CACCATCAGCACGGCGTAGCTATTGAGTGA -3'

The PCR products were run on 2.5% MetaPhor agarose (Lonza, Catalog # 50181) gel for 2 hours at 35 volts to separate the bands. The *gpr125^{stl40}* allele contains 19 bp

insertion, so the predicted fragment sizes are 195 bp and 214 bp for wildtype and mutant samples respectively. Heterozygotes show several bands due to heteroduplex formation between 195 bp and 214 bp.

The PCR settings used were as follow:

95˚C: 2 min

94˚C: 40 sec

68˚C: 40 sec } X 40 cycles

72˚C: 40 sec

72˚C: 5 min

10˚C Hold

2.5.2 *cdh2*^{hi3644}

The following primers were used for genotyping by PCR.

A: 5'- AACACGTCCTCAGAGTGCCAC - 3'

B: 5'- GTACGGTTACCAAGTCAATGTG - 3'

D: 5'- CTGTTCCATCTGTTCCTGAC - 3'

E: 5'- GTTCCTTGGGAGGGTCTCCTC - 3'

The PCR products were run on 1% agarose gel for 1 hours at 118 volts to separate the bands. The allele contains ~ 3 kb insertion. Wildtype sample generates product at 603 bp with AB primer set only. Heterozygous sample generates products at 603 bp, 363 bp, and 428 bp with primer sets AB, AE, and BD respectively. Homozygous sample

generates products at 363 bp, and 428 bp with primer sets AE and BD respectively. Homozygous sample does not produce any product with AB primer set.

The PCR settings used were as follow:

94˚C: 2 min

94˚C: 40 sec

60˚C: 30 sec

73˚C: 60 sec

X 35 cycles

73˚C: 5 min

4˚C Hold

2.6 CRISPR/Cas9

2.6.1 Design and synthesis of guideRNA and Cas9 RNA

The sgRNA design tool at http://crispr.mit.edu was used to identify possible target sites. Two criteria were employed while choosing sgRNA. First, since we were using T7 RNA polymerase in our synthesis, we only selected sgRNAs that began with 5' G nucleotide. Second, we selected sgRNA target site with a restriction site for assaying the rate of mutagenesis in F_0-injected embryos as well as genotyping putative founders. Two complementary oligonucleotides corresponding to the sgRNA target site were ligated to pT7-gRNA (Addgene 46759, (Jao et al., 2013). sgRNA was transcribed from BamH1 (Promega) linearized pT7-gRNA using MEGAshortscript T7 kit (Ambion). Following *in vitro* transcription reaction, guide RNA was purified using Micro Bio-Spin P-

30 gel columns (Bio-Rad #732-6250). *Cas9* mRNA was synthesized using pT3TS-nls-zCas9-nls (Addgene 46757, (Jao et al., 2013) plasmid. The plasmid was linearized using Xba1 (New England BioLabs, R0145S) and DNA was purified using QIAquick PCR purification kit (Qiagen). 1 µg of linear DNA was used for *in vitro* transcription reaction (T3 mMESSAGE mMACHINE kit, Life Technologies, AM1338M). The mix of *Cas9*-encoding mRNA (150 pg/embryos) and sgRNA (50 pg/embryos) were injected into single cell *Tg(isl1:gfp)* embryos. Injected embryos were grown to adulthood to generate founder fish.

2.6.2 Test of sgRNA cleavage efficiency

To assay the rate of mutagenesis in F_0-injected embryos, genomic DNA from individual injected embryos were extracted using NaOH/Tris-HCl (Meeker et al., 2007). Single 24 hpf embryos were incubated in 50 µl of 50 mM NaOH and boiled at 95°C for 10 minutes vortexing 2-3 times in between. Tubes containing genomic DNA were then cooled, and 5 µl of 1M Tris-HCl (pH 8) was added. Samples were then centrifuged at 13,000 RPM for 5 minutes at room temperature. 3 µl of supernatant containing genomic DNA was used in a standard 25 µl PCR reaction with primers spanning sgRNA target site. 15 µl of PCR products were digested overnight at 37°C in a 30 µl reaction containing unique restriction enzyme to the target site. Samples were then run on a 2.5% agarose gel. Successful mutagenesis is indicated by the loss of restriction site.

2.6.3 Founder screening and F1 genotyping

To screen for germline transmission of CRISPR-induced mutations, each putative founder fish was crossed with wild-type fish. At 24 hpf, about 10 F1 embryos were randomly screened for germline transmission from each founder fish following the procedure described above. Remaining F1 embryos from founder fish successfully transmitting mutations into germline were grown to adulthood for individual screening. Genomic DNA from individual F1 adult heterozygotes was extracted from tail tissue and genotyped following the procedure described for the injected embryos. PCR products from individual F1 heterozygotes exhibiting restriction site polymorphism were cloned into TOPO pcr2.1 vector using the TOPO TA cloning kit (Invitrogen). Plasmid DNA was isolated from individual transformants and sequenced using a T7 primer to identify the type of CRISPR-induced mutations.

2.7 mRNA SYNTHESIS AND RNA GEL ELECTROPHORESIS

Sense mRNA was synthesized using Ambion Message Machine kit (T7 or Sp6) following manufacturer's recommendations. Linear template (1 µg) was incubated at 37°C with RNase-free water, 2X ribonucleotide mix, 10X transcription buffer and 10X RNA polymerase mix (T7 or SP6), generating a final reaction volume of 20 µl. The tube was then incubated for 2-4 hours at 37°C. 30 µl of nuclease-free ddH20 and 30 µl of Lithium Chloride was added, and mRNA was precipitated at -20°C overnight. The next day, samples were microcentrifuged for 20 minutes at 4°C. The pellet was washed with cold 70% ethanol and resuspended in 25 µl of nuclease-free ddH20. mRNA was stored at -20°C. Yields and quality were determined by nano spectrophotometer and RNA gel

electrophoresis. Formaldehyde agarose gels were used for visualizing the quality of synthesized RNA. 1 gram of agarose was melted in 84.8 ml of ddH20. Under the fume hood, 5.2 ml of room-temperature 37% formaldehyde was added and swirl gently. Next, 10 ml of 10X MOPS (0.2 M MOPS, 0.05 sodium acetate, 0.01 M EDTA, pH 7.0, stored at 4°C) was added and swirled gently before casting gel. 1X MOPS buffer was used as running buffer. RNA samples were prepared by mixing 2 µl of RNA, 1 µl of 1:10 diluted Ethidium bromide and 16 µl of 1.25x RNA loading buffer. RNA sample was then heated at 65°C for 10 minutes before loading in the gel. Smeared bands indicate a low-quality synthesis while single clean band typically indicate a successful transcription reaction.

2.8 MORPHOLINO/RNA INJECTION

Zebrafish embryos were injected at 1 to 2 cell stage. Embryos were lined up on glass slide glued to a Petri dish. Embryos were orientated with animal poles pointing towards the injection needle. Microcapillary needles (Stoelting Inc.) was pulled on a pipette puller, and the tip of the needle is broken using a micro-tweezer. Microcapillary needles were loaded with either mRNA or morpholino depending on the experiment and then installed into a micro-manipulator. The micro-manipulator was connected to a gas-pressure pulse regulator that permits controlled pressure injections (~3-4 nl per embryos). The injection volume was calibrated by measuring the diameter of droplets injected into mineral oil placed on a slide containing an etched micrometer scale. mRNA or morpholino either was injected into the blastomere or the boundary between blastomere and yolk. The needle was withdrawn slowly from the embryo and care was

taken to do as little damage to the embryo as possible. The injected embryos are then rinsed off the slide with egg water into a Petri dish. The injected embryos were examined under the light microscope for mortality that might have occurred during injection. Dead embryos were removed to prevent contamination of remaining living embryos.

2.9 IN SITU HYBRIDIZATION

Embryos fixed in 4% paraformaldehyde for at least 12 hours (typically overnight) at 4ºC were dehydrated in 100% methanol (Fisher) for at least 5 hours (typically overnight) at -20ºC. Embryos were rehydrated in a series of PBST/MeOH washes as follows: 1X5 minutes in 50% MeOH/50% PBST, 1X5 minutes in 30% MeOH/70% PBST, then 2X5 minutes in PBST. Following an hour room temperature fixation in 4% paraformaldehyde, embryos were washed 3X5 minutes in PBST and then treated with proteinase K (Sigma; 23 mg/ml diluted to 10 µg/µl) for 5 to 20 minutes depending on the age of the embryo. Embryos were washed fast 2X and washed 2X5 minutes in PBST. Embryos were then fixed for one hour at room temperature. After fixing, embryos were washed 3X5 minutes in PBST and 1X10 minute in 50%PBST/50% hybridization buffer and incubated in hybridization buffer for at least two hours at 70ºC. Embryos were incubated overnight in ~100 ng probe (1:100 dilution of the stock probe in hybridization buffer) at 65ºC. Following the overnight incubation, the probe was saved at -20°C (probes can be re-used 3-5 times without affecting the efficiency of the signal produced). Embryos were then washed at 65ºC for 1 hour in fresh hybridization buffer,

then washed 2X30 minutes in wash A, 1X30 minutes in wash B and 2X30 minutes in wash C, all at 65ºC. Embryos were then washed 1X10 minutes at room temperature in 50% wash C/50% Maleic Acid Buffer + 0.1% (v/v) Tween20, 2X10 minutes in Maleic Acid Buffer + 0.1% (v/v) Tween20, and 1X10 minutes in blocking solution. Embryos were then incubated overnight in anti-digoxygenin antibody (diluted 1:5000 in blocking solution) after blocking for 3 hours at room temperature. Next, embryos were washed 8X15 minutes in Maleic Acid Buffer + 0.1% (v/v) Tween20, then 3X10 minutes in TMNT. For color development, embryos were incubated in the dark in TMNT containing 0.45% (v/v) NBT and 0.35% (v/v) BCIP (Vector) for blue chromogenic reaction. The color reaction was stopped by washing embryos 3X5 minutes in 1X PBS. Embryos were fixed overnight in 4% paraformaldehyde at 4ºC, then were put through a glycerol series (25%, 50%, then 70% glycerol) and mounted on 70% glycerol. Embryos can be stored in glycerol for extended periods before mounting if necessary.

Solution recipes

Hybridization Buffer (30 ml)	Final Concentration
15 ml formamide (Fisher)	50%
7.5 ml 20X SSC	5X
30 µl 50 mg/ml heparin (Fisher)	50 µg/ml
1.5 ml 10 mg/ml yeast tRNA (Roche)	500 µg/ml
30 µl 100% Tween-20 (Sigma)	0.1%
276 µl 1M citric acid, pH 6.0 (LabChem, LC131180-1)	9.2 mM

5.664 ml DEPC-treated ddH20 -

Vortex at highest setting after adding each component.

Store at -20°C.

Wash A (10 ml)	Final Concentration
1 ml 20X SSC	2X
5 ml formamide	50%
10 µl 100% Tween-20	0.1%
4 ml ddH20 -	

Wash B (10 ml)	Final Concentration
1 ml 20X SSC	2X
10 µl 100% Tween-20	0.1%
9 ml ddH20 -	

Wash C (10 ml)	Final Concentration
1 ml 100% Wash B	10% (0.2X SSC)
9 µl 100% Tween-20	0.09%
9 ml ddH20 –	

Maleic Acid Buffer (1.6L)	Final Concentration
18.58 g Maleic Acid (Fisher)	100 mM

14.03 g NaCl	150 mM
9.6 g NaOH	150 mM

Adjust pH to 7.5 with 10N NaOH.

Bring to final volume with ddH20.

Sterilize by autoclaving for 20 minutes.

10% Stock Blocking Reagent (100 ml)	Final Concentration
10 g Blocking Reagent (Roche, 1096176)	10%
100 ml Maleic Acid Buffer	

Dissolve granular blocking reagent in a microwave.

Sterilize by autoclaving for 15 minutes.

2% Blocking Solution (10 ml)	Final Concentration
2 ml 10% Stock Blocking Reagent	2%
8 ml Maleic Acid Buffer	
10 µl 100% Tween-20	0.1%

TMNT Buffer (10 ml)	Final Concentration
8.23 ml ddH20-	
1 ml 1M Tris•HCl, pH 9.5	100 mM
500 µl 1M MgCl2	50 mM
250 µl 4M NaCl	100 mM

10 µl 100% Tween-20	0.1%
10 µl 1M Levamisole	1 mM

Do not autoclave. Use immediately.

2.10 DAB IMMUNOHISTOCHEMISTRY

Embryos were dechorionated and fixed in 4% paraformaldehyde in PBS at room temperature for 3-4 hours. Embryos were washed in PBS with 0.1% tween 20 (PBST) 3X10 minutes then blocked in incubation buffer (IB) (1% sheep serum, 2 mg/ml Bovine Serum Albumin (BSA), 1% DMSO, and 0.5% Triton-X100 in PBS) for at least 1 hour in room temperature on a rotator. Embryos were incubated in primary antibody (diluted in incubation buffer) overnight at 4ºC. Next day, embryos were washed 2Xfast, then 5X10 minutes with IB on a rotator. Embryos were incubated for 8 hours in secondary antibody (2 µl biotinylated universal antibody, 5 µl horse serum, and 493 µl IB) at room temperature. Embryos were then washed 2X fast, then 5X10 minutes with IB (no sheep serum or BSA) on a rotator. During the third wash, the tertiary solution was made. Avidin-biotin color development (A/B) solution was mixed as follows: 1% (v/v) reagent A, 1% (v/v) reagent B (Vectastain) in IB (no sheep serum or BSA) and allowed to sit for 30 minutes. Embryos were then incubated in the tertiary solution overnight at 4°C. The next day, embryos were washed 2X fast, then 5X10 minutes with PBST on a rotator. Embryos were then transferred to 24-well plate where they were rinsed 3X5 minutes with PBS. The next day, embryos were incubated in 750 µl diaminobenzidine (DAB) solution (0.5 mg/ml in PBS) for 20-30 minutes. While the embryos were incubating, start

solution was made by adding 5 µl 30% H_20_2 to 5 ml dH_20. HRP color reaction was started by adding 75 µl start solution to the embryos in the DAB solution. The color reaction was watched closely under dissecting scope. Once desired staining was achieved, the reaction was stopped replacing the DAB solution with stop solution (cold 0.2% azide in PBS). Embryos were washed 2X5 minutes in PBS and washed with 25%, 50%, and 70% glycerol in PBS. Finally, embryos were mounted in 70% glycerol. Embryos can be stored in glycerol for extended periods before mounting if necessary.

2.11 FLUORESCENT IMMUNOSTAINING

Embryos were fixed in 4% paraformaldehyde in PBS for at least 12 hours at 4ºC or 6-8 hours at room temperature. Embryos were washed with IB (1 % w/v BSA, 0.5% v/v Triton, and 1% v/v DMSO in PBS) 4X30 minutes then blocked once for 30 minutes in IB + 1% horse serum (Sigma). Embryos were then incubated in primary antibody diluted in IB + horse serum overnight at 4ºC. Next day, embryos were washed 2X30 minutes with IB and blocked once for 30 minutes in IB + 1% horse serum. Embryos were then incubated in the dark (covered with aluminum foil) for 8-12 h in fluorescent secondary antibody diluted in 1:500 in IB+HS. Next day embryos were rinsed 3X5 minutes in PBS and fixed overnight in 4% paraformaldehyde. After 4X5 minutes wash with PBS, embryos were put through a glycerol series (25%, 50%, then 70% glycerol) and mounted on 70% glycerol. It is important to store the embryos at 4ºC in the dark to avoid fading of the fluorescent signals. Fluorescent signals are stable up to a week after placing in 70% glycerol.

2.12 ANTIBODY AND PROBE CONCENTRATION

- Rabbit anti-GFP: 1:2000 (Invitrogen)
- Mouse anti-Zn8: 1:10 (Developmental Studies Hybridoma Bank)
- Mouse anti-Zn12: 1:250 (ZIRC)
- Rabbit anti-Cntn2: 1:500 (Kindly provided by Dr. Claudia Stuermer)
- Chicken anti-rabbit Alexa Flour 488: 1:500 (Invitrogen)
- Goat anti-mouse Alexa Flour 568: 1:500 (Life technologies)
- Donkey anti-rabbit Alexa Flour 568: 1:500 (Invitrogen)
- *cntn2* ISH probe: 1:100

2.13 QUANTIFICATION OF FBM NEURON

Z-stack images (0.5 µm thickness, 150-200 slices) were taken of dorsally-mounted stained embryos with Leica TCP SP8 MP confocal microscope at 40X magnification. Leica Application Suite X (LAS X) software was used to generate a 3D image of selected stacks of confocal images. FBM neurons at all dorsoventral levels were counted in the 3D image by examining each level.

2.14 DiI LABELING OF AXONS AND PHOTOCONVERSION

Embryos were fixed overnight at 4°C in 4% paraformaldehyde, washed in PBS, and embedded in 0.6% agarose (in Danieu buffer) on a glass slide. A 2 mg/ml solution of the lipophilic dye, *1,1'-Dioctadecyl-3,3,3',3'-Tetramethylindocarbocyanine Perchlorate* (DiI, ThermoFisher Scientific) in dimethylformamide, was pressure injected into the

structure of interest. Following overnight incubation at room temperature to allow for transport of DiI, the fluorescent signal was converted into a brown precipitate. Deyolked embryos were incubated in 3,3'-diaminobenzidine (DAB, Sigma; 0.5 mg/ml in PO_4 buffer) for 15 minutes, mounted in DAB on a slide, and the fluorescence was photoconverted by examining the structures of interest under epifluorescence for 20-30 minutes. Photoconverted embryos were post-fixed and mounted in 70% glycerol.

2.15 WESTERN BLOTTING

10 ml of lysis buffer was prepared fresh containing 1 ml of 10X Cell Lysis Buffer (#9803, Cell Signaling), 100 µl of 0.1 M PMSF, 1 complete protease inhibitor cocktail tablet (Roche), and 9 ml distilled water. Protein was isolated using 200 µl of lysis buffer per 100 decapitated 48 hpf heads. Samples were homogenized on ice by mechanical grinding, then rotated at 4°C for 20 minutes at 13,000 and immediately stored at -80°C at least overnight. Upon thawing, samples were centrifuged at 13,000 rpm for 5 minutes to pellet insoluble material. 30 µl of the supernatant from each sample was diluted 1:1 in 2X loading buffer (prepared from 4X NuPAGE LDS Sample Buffer, Invitrogen) with 20% β- mercaptoethanol, and boiled for 5 minutes at 95°C. Western blotting was performed using standard protocols (Pan et al., 2014).

2.16 TOUCH EVOKED ESCAPE RESPONSE ASSAY

Larvae at 2 dpf were placed in Petri dishes in E3 medium and aligned to the center of the field of view (20 mm in diameter). The tactile stimulus was a single touch to the head or trunk of the larva with a dissection needle. Each larva was tested only

once. The larval responses were binned into three categories: No response (no movement after touch), Weak Response (muted movement with larva remaining in the field of view), and Strong Response (rapid and vigorous movement with larva swimming out of the field of view).

2.17 SWIMMING ANALYSIS

For analysis of swimming behavior, 7 dpf larvae were placed singly in individual wells of a 24-well plate. Swimming activity was monitored at room temperature (21-22°C) using a DanioVision system and EthoVision XT 8.0 locomotion tracking software (Noldus). Larvae were allowed to acclimate in the DanioVision system for 30 minutes in the dark. Swimming activity was then monitored for an hour each in light and dark phases. Distance moved and moving duration parameters were analyzed using EthoVision. Larvae were processed for genotyping, and tracking data were pooled for analysis according to genotype. All of this analysis was performed at Georgia Southern University in Dr. Sittaramane's lab.

CHAPTER 3: DISTINCT ROLES FOR THE CELL ADHESION MOLECULE CONTACTIN2 IN THE DEVELOPMENT AND FUNCTION OF NEURAL CIRCUITS IN ZEBRAFISH

Suman Gurung[1], Emilia Asante[1], Devynn Hummel[1], Ashley Williams[2], Oren Feldman-Schultz[3], Mary C. Halloran[3], Vinoth Sittaramane[2], and Anand Chandrasekhar[1]

1, Division of Biological Sciences and Bond Life Sciences Center, University of Missouri, Columbia, MO 65211, USA.

2, Department of Biology, Georgia Southern University, Statesboro, GA 30458, USA.

3, Department of Integrative Biology, Department of Neuroscience, University of Wisconsin, Madison, WI 53706, USA.

Corresponding Author:

Dr. Anand Chandrasekhar

Division of Biological Sciences

Room 340D Bond Life Sciences Center

1201 Rollins St

University of Missouri, Columbia, MO 65211-7310

Running Title: Distinct roles for Cntn2 adhesion molecule in zebrafish

Keywords: zebrafish; Neuronal Migration; Axon guidance; Facial Branchiomotor Neuron; nucMLF; Cell adhesion molecule; Cntn2; Vangl2; Morpholino; CRISPR/Cas9

Submitted to Mechanisms of Development

3.1 ABSTRACT

Contactin2 (Cntn2)/Transient Axonal Glycoprotein 1 (Tag1), a neural cell adhesion molecule, has established roles in neuronal migration and axon fasciculation in chick and mouse. In zebrafish, antisense morpholino-based studies have indicated roles for *cntn2* in the migration of facial branchiomotor (FBM) neurons, the guidance of the axons of the nucleus of the medial longitudinal fascicle (nucMLF), and the outgrowth of Rohon-Beard (RB) central axons. To study functions of Cntn2 in later stages of neuronal development, we generated *cntn2* mutant zebrafish using CRISPR-Cas9. Using a null mutant allele, we detected genetic interactions between *cntn2* and the planar cell polarity gene *vangl2*, as shown previously with *cntn2* morphants, demonstrating a function for *cntn2* during FBM neuron migration in a sensitized background of reduced planar cell polarity signaling. In addition, maternal-zygotic (MZ) *cntn2* mutant larvae exhibited aberrant touch responses and swimming, suggestive of defects in sensorimotor circuits, consistent with studies in mice. However, the nucMLF axon convergence, FBM neuron migration, and RB outgrowth defects seen in morphants were not seen in the mutants, and we show here that they are likely off-target effects of morpholinos. However, MLF axons exhibited local defasciculation in MZ*cntn2* mutants, consistent with a role for Cntn2 in axon fasciculation. These data demonstrate distinct roles for zebrafish *cntn2* in neuronal migration and axon fasciculation, and in the function of sensorimotor circuits.

3.2 INTRODUCTION

Neuronal migration and axon guidance are critical developmental processes that are essential for establishing functional neural circuits underlying complex cognitive and motor functions. During development of the central nervous system, many newborn neurons travel long distances away from the germinal zone to their final locations, whereupon they extend axons and dendrites to assemble functional neural networks. Precise neuronal migration and axon guidance are dependent upon cell-cell and cell-substrate interactions (Chao et al., 2009; Marin et al., 2010), which are mediated by a number of membrane-associated molecules. Membrane proteins playing important roles in neurodevelopment include the cell adhesion molecules of the immunoglobulin superfamily (IgSF-CAMs), which are anchored to the membrane by a glycosylphosphatidyl inositol (GPI) linkage or a single transmembrane domain, have varying numbers of Ig-like extracellular domains, and are widely expressed during vertebrate neural development (Gennarini et al., 2016; Stoeckli, 2004; Stoeckli and Landmesser, 1995).

Contactin2 (Cntn2)/Transient Axonal Glycoprotein 1 (Tag1), a GPI-linked IgSF-CAM, has six Ig-like domains and four fibronectin domains (Furley et al., 1990), and can bind homophilically (Kunz et al., 1998) as well as heterophilically with other IgSF CAMs such as L1, NgCAM, and NrCAM (Buchstaller et al., 1996; Fitzli et al., 2000; Kuhn et al., 1991; Kunz et al., 1998; Pavlou et al., 2002; Suter et al., 1995). Cntn2 can also interact with contactin-associated protein-like 2 (Caspr2) at the juxtaparanode region in neurons (Tzimourakas et al., 2007). Cntn2 is broadly expressed by various cortical, cranial

nerve, and spinal neurons and axons (Dodd et al., 1988; Yamamoto et al., 1986). It has been demonstrated to play a role in the fasciculation and guidance of dorsal root ganglion axons in mice (Kunz et al., 1998; Law et al., 2008) and spinal commissural axons in chick (Stoeckli and Landmesser, 1995), in the migration of mitral cells in the mouse olfactory bulb (Bastakis et al., 2015), and in sensorimotor gating and coordination in mice (Savvaki et al., 2008).

In zebrafish, *cntn2* is expressed in specific neuronal types during development (Liu and Halloran, 2005; Sittaramane et al., 2009; Warren et al., 1999; Wolman et al., 2008) (Fig. 3.1). Morpholino (MO)-mediated knockdown studies indicated that *cntn2* is required for the organization of the midbrain nucleus of the medial longitudinal fascicle (nucMLF) and the convergence of nucMLF axons into the fascicle (Wolman et al., 2008), the growth and fasciculation of Rohon-Beard (RB) central axons in the spinal cord (Liu and Halloran, 2005), and the caudal migration of facial branchiomotor (FBM) neurons in the hindbrain (Sittaramane et al., 2009). Interestingly, *cntn2* genetically interacts with the planar cell polarity gene *vangl2*, which encodes a four-pass transmembrane protein (Jessen et al., 2002), during FBM neuron migration (Sittaramane et al., 2009), suggesting that Cntn2 and Vangl2 participate in a common mechanism to regulate this process. While these MO-based data are consistent with Cntn2-associated functions in mouse and chick, potential later functions for zebrafish *cntn2* in sensorimotor circuits and behavior could not be examined because of reduced efficacy of MO-mediated knockdown after 1-2 days of development (Bill et al., 2009).

Moreover, although appropriate controls (Eisen and Smith, 2008) were performed, a caveat of MO-mediated knockdown experiments is the possibility of off-target effects.

Therefore, to investigate roles for zebrafish *cntn2* at later developmental stages and to address potential concerns with the MO knockdown studies, we generated loss-of-function mutations in *cntn2* using CRISPR/Cas9. We generated two *cntn2* mutant lines (*cntn2*^{zou20} and *cntn2*^{zou22}) representing null alleles. Using the null mutants, we detected genetic interactions between *cntn2* and *vangl2*, as shown previously with morphants, definitively demonstrating a function for *cntn2* in FBM neuron migration. In addition, maternal-zygotic (MZ) *cntn2* mutant larvae exhibited aberrant touch responses and swimming, suggestive of defects in sensorimotor circuits, consistent with studies in mice. However, the nucMLF axon convergence, FBM neuron migration defects, and RB outgrowth defects seen in *cntn2* morphants were not seen in MZ*cntn2* mutants, and our data indicate that the morphant phenotypes are likely off-target effects of the morpholino. Interestingly, MLF axons exhibited local defasciculation in MZ*cntn2* mutants, consistent with a role for Cntn2 in axon fasciculation. These data demonstrate distinct developmental roles for zebrafish *cntn2* in neuronal migration and axon fasciculation, and in the function of sensorimotor circuits.

3.3 MATERIALS AND METHODS

3.3.1 Animals

Zebrafish (*Danio rerio*) were maintained following standard protocols and University of Missouri ACUC guidelines as described previously (Sittaramane et al., 2013; Westerfield, 1995). Embryos were grown in E3 medium at 28.5 °C, staged by hours post fertilization (hpf) (Kimmel et al., 1995), and embryo age was verified at somitogenesis stages. *Tg(isl1:gfp)* (Higashijima et al., 2000) and *Tg(pitx2c:gfp)* (Wolman et al., 2008) fish were used to analyze FBM neuron migration, and nucMLF neurons and axons, respectively. The following two mutant lines were used: *trilobite* (*tri*^{tc240a}, (Hammerschmidt et al., 1996)) and *sleepy* (*sly*^{ti263a}, (Odenthal et al., 1996); kindly provided by Dr. Clarissa Henry, University of Maine, Orono) fish carrying mutations in the *vangl2* and *lamc1* genes, respectively. CRISPR-Cas9 *cntn2* mutant lines were generated in the *Tg(isl1:gfp)* background.

3.3.2 Generation of *cntn2* null alleles using CRISPR-Cas9

The sgRNA design tool at http://crispr.mit.edu was used to identify possible target sites. Two complementary oligonucleotides (5' -TAGGCTAACAATGGTGCCGCAT-3'; 5'–AAACATGCGGCACCATTGTTAG-3') corresponding to the sgRNA target site in exon 4 (Fig. 3.2A) were used. sgRNA and Cas9 RNA were synthesized as described (Jao et al., 2013). The following primers were used for genotyping: Fwd: 5' -GACATATCATTTGCTGAAGAGTCG- 3'; Rev: 5' -CTCGCGTTAGCAAGATACAAGTTA -3'. PCR products spanning the target site were digested overnight with BanI (NEB), and successful mutagenesis was indicated by the loss of the BanI site and the presence of an undigested PCR product (Fig. 3.2C).

Injected embryos were grown to adulthood to generate founder fish, which were identified by outcrossing to wildtype fish and genotyping the F1 progeny for mutations in *cntn2*.

3.3.3 Morpholino injections

Antisense *cntn2* morpholino (5' -CCACACCCAGACCAGACACTTATTT- 3';(Liu and Halloran, 2005; Sittaramane et al., 2009) and standard control morpholino (5' -CCTCTTACCTCAGTTACAATTTATA- 3') were obtained from Gene Tools (Corvallis, OR). The *cntn2* MO used in this study was previously shown to knockdown Cntn2 protein levels (Liu and Halloran, 2005), which we validated (Fig. 3.3).

3.3.4 Immunohistochemistry and in situ hybridization

Immunohistochemistry and in situ hybridization were performed using standard protocols (Sittaramane et al., 2009; Vanderlaan et al., 2005). The following primary antibodies were used: rabbit anti-GFP (Invitrogen, 1:2000 dilution), zn5/8 (Developmental Studies Hybridoma Bank (DSHB), 1:10 dilution), rabbit anti-Cntn2 (kindly provided by Dr. Claudia Stuermer, University of Konstanz (Lang et al., 2001); 1:500 dilution), zn-12 (ZIRC, 1:250 dilution). The following secondary antibodies were used: chicken anti-rabbit Alexa Fluor 488 (Invitrogen; 1:500 dilution), goat anti-mouse Alexa Flour 568 (Life technologies, 1:500 dilution), donkey anti-rabbit Alexa Flour 568 (Invitrogen, 1:500 dilution). Images were taken with an Olympus BX60 or Leica TCP

SP8 MP confocal microscope, processed for brightness and contrast, and composed into Figures using Photoshop or Powerpoint software.

3.3.5 Western blot

Total protein was isolated from the heads of 2 dpf larvae as previously described (Hoffman et al., 2016). Western blotting was performed using standard protocols (Pan et al., 2014). The following primary antibodies were used: rabbit anti-Cntn2 ((Lang et al., 2001); 1:500 dilution), anti-acetylated α-tubulin (Sigma, 1:2000 dilution). The following secondary antibodies were used: goat anti-rabbit IgG, HRP conjugate (Santa Cruz Biotechnology, 1:5000 dilution) and HRP-goat anti-mouse IgG (H+L) (Invitrogen, 1:2500 dilution).

3.3.6 Quantification of FBM neurons in the hindbrain

Z-stack images (0.5 μm thickness, 150-200 slices) were taken of dorsally-mounted stained embryos with Leica TCP SP8 MP confocal microscope at 40X magnification. Leica Application Suite X (LAS X) software was used to generate a 3D image of selected stacks of confocal images. FBM neurons at all dorsoventral levels were counted in the 3D image by examining each level.

3.3.7 Genotyping immunostained embryos

The head fragments of antibody-stained embryos were mounted for quantification of FBM neuron migration, and the corresponding tail fragments were genotyped. Genomic region spanning the point mutation in the *trilobite* (*tri*^{tc240a}) allele (Jessen et al., 2002) was PCR amplified using following primers: Fwd: 5′-GCCTGGATGGTCACAGATTT-3′; Rev: 5′ CCGGAAGTTTATCAGTATGGGAAACAC-3′. PCR product was purified using a PCR purification kit (Qiagen) according to the manufacturer's instructions and sequenced to detect the point mutation in each sample.

3.3.8 DiI injections and photoconversion of DiI fluorescence

Embryos were fixed overnight at 4°C in 4% paraformaldehyde, washed in PBS, and embedded in 0.6% agarose (in Danieu buffer) on a glass slide. A 2 mg/ml solution of the lipophilic dye, *1,1'-Dioctadecyl-3,3,3',3'-Tetramethylindocarbocyanine Perchlorate* (DiI, ThermoFisher Scientific) in dimethylformamide, was pressure injected into the nasal retina, targeting the retinal ganglion cell layer. Following overnight incubation at *room temperature* to allow for transport of DiI, the fluorescent signal was converted into a brown precipitate as previously described (Chandrasekhar et al., 1997). Deyolked embryos were incubated in 3,3'-diaminobenzidine (DAB, Sigma; 0.5 mg/ml in PO_4 buffer) for 15 min, mounted in DAB on a slide, and the fluorescence was photoconverted by exposing the labeled axons to epifluorescence for 20-30 min. Photoconverted embryos were post-fixed, and mounted in 70% glycerol.

3.3.9 Quantification of outgrowth of central axons of Rohon-Beard (RB) neurons

Rohon-Beard neurons were sparsely labeled by injecting 12.5 pg of *ngn1:GFP-caax* DNA (Andersen et al., 2011) and 25 pg of Tol2 transposase RNA per embryo at the one-cell stage. Injected embryos were fixed at 18 hpf for 4 hours at room temperature, and immunostained for GFP. RB neurons were binned into three groups based on the position of the cell body along the anterior-posterior (A-P) axis (1-5 somites, 6-10 somites, 11-16 somites). As a proxy to measuring the lengths of the central axons, the somite numbers corresponding to the tips of the anteriorly- and posteriorly-extending axons (ascending and descending axons, respectively) were recorded.

3.3.10 Analysis of larval behaviors

Larvae at 2 dpf were placed in petri dishes in E3 medium, and aligned to the center of field of view (20 mm in diameter). The tactile stimulus was a single touch to the head or trunk of the larva with a dissection needle. Each larva was tested only once. The larval responses were binned into three categories (Fig. 3.9): No response (no movement after touch), Weak Response (muted movement with larva remaining in the field of view), and Strong Response (rapid and vigorous movement with larva swimming out of the field of view).

For analysis of swimming behavior, 7 dpf larvae were placed singly in individual wells of a 24-well plate. Swimming activity was monitored at room temperature (21-22°C) using a DanioVision system and EthoVision XT 8.0 locomotion tracking software (Noldus). Larvae were allowed to acclimate in the DanioVision system for 30 minutes in the dark. Swimming activity was then monitored for an hour each in light and dark phases. Distance moved and moving duration parameters were analyzed using EthoVision. Larvae were processed for genotyping the *cntn2* locus, and tracking data were pooled for analysis according to genotype.

3.3.11 Statistical analysis

We performed the chi-square tests using online software (www.quantpsy.org/calc.htm) to detect any significant differences in the distribution of: 1) FBM neuron migration phenotypes among groups used for genetic interaction studies, 2) touch-evoked escape responses for *cntn2*+/+ and MZ*cntn2* mutant embryos following a head touch or a trunk touch, and 3) MLF defasciculation phenotypes in *cntn2*+/+ and MZ*cntn2* mutants. We performed unpaired t-tests using GraphPad Prism 7 software to detect any significant differences in: 1) distance moved and moving duration between *cntn2*+/- and MZ*cntn2* mutant embryos, 2) RGC axon fascicle thickness in *cntn2*+/+, *cntn2*+/- and MZ*cntn2* mutant embryos, and 3) RB central axon length in *cntn2*+/+ and MZ*cntn2* mutant embryos.

3.4 RESULTS

3.4.1 CRISPR-generated *cntn2* alleles are null

To examine roles for *cntn2* in larval zebrafish, and to test the validity of the *cntn2* morphant phenotypes, we generated loss-of-function mutations in *cntn2* using CRISPR-Cas9 technology (Jao et al., 2013). We injected a single guide RNA (sgRNA) targeting exon 4, which encodes the second Ig domain of Cntn2 (Fig. 3.2A, B). We identified three independent alleles (*cntn2*^{zou20}, *cntn2*^{zou21}, and *cntn2*^{zou22}), and established lines for the *cntn2*^{zou20} and *cntn2*^{zou22} alleles. The *cntn2*^{zou20} allele has a 7 base pair (bp) insertion, and the *cntn2*^{zou22} allele has an 11 bp deletion (Fig. 3.2A, C), which generate frameshifts and premature stop codons (Fig. 3.2B). Whole-mount in situ hybridization revealed that *cntn2* expression is reduced in *cntn2*^{zou20} (Fig. 3.2D) and *cntn2*^{zou22} (data not shown) homozygous mutant embryos, consistent with nonsense-mediated decay (Chang et al., 2007). Importantly, a polyclonal antibody raised against the full-length Cntn2 protein (Lang et al., 2001) failed to detect any protein following immunohistochemistry (Fig. 3.2D) or western blotting (Fig. 3.2E) in both zygotic *cntn2*^{zou20} and *cntn2*^{zou22} homozygous mutants. These results strongly suggest that the CRISPR-generated *cntn2* alleles are null. Interestingly, zygotic as well as maternal-zygotic (MZ) *cntn2* homozygous mutants are viable and fertile, and appear morphologically normal.

3.4.2 FBM neurons migrate normally in *cntn2* mutants

In zebrafish, facial branchiomotor (FBM) neurons are born in rhombomere 4 (r4) and migrate posteriorly into r6 and r7 (Chandrasekhar et al., 1997; Higashijima et al., 2000) (Fig. 3.4A). *cntn2* is expressed in FBM neurons in zebrafish and mouse (Garel et al., 2000; Sittaramane et al., 2009; Warren et al., 1999) (Fig. 3.1B). In *cntn2* morpholino (MO)-injected embryos (morphants), FBM neurons exhibit migration defects, frequently failing to migrate out of r4 (Sittaramane et al., 2009). In *cntn2* morphants (4-6 ng MO dose/embryo), FBM neurons migrated normally in ~50% of the embryos, and either migrated poorly (Partial block) or largely failed to migrate (Severe block) in the remaining embryos (Fig. 3.4B, E). “Partial block” indicates reduced FBM neuron migration out of r4 on one or both sides, with FBM neurons found throughout the migratory pathway from r4 to r7, whereas “Severe block” indicates that a large majority of FBM neurons (estimated to be substantially greater than 50%) remained in r4 on both sides, in the characteristic pattern seen previously in genetic mutants like *trilobite* (Bingham et al., 2002). To our surprise, FBM neurons migrated normally into r6 and r7 in 100% of zygotic *cntn2* homozygotes (Fig. 3.4C, E) of both alleles. The discrepancy in FBM migration phenotypes between *cntn2* morphants and mutants may be explained by the presence of maternally contributed mRNA/protein in mutants but not in morphants. To test this possibility, we examined the migration of FBM neurons in maternal-zygotic (MZ) *cntn2* mutants. FBM neurons migrated normally in 95% of MZ*cntn2-/-* embryos (Fig. 3.4D, E), strongly suggesting that *cntn2* does not have an essential function during FBM neuron migration, and may play a subtle role at best.

3.4.3 Genetic interaction between *cntn2* and *vangl2* for FBM neuron migration is preserved in mutants

Vangl2, a four-pass transmembrane protein and a core component of Wnt/planar cell polarity pathway (Gray et al., 2011), is expressed ubiquitously in the hindbrain during the period of FBM neuron migration (Sittaramane et al., 2013; Sittaramane et al., 2009). We showed previously that *cntn2* and *vangl2* genetically interact during FBM neuron migration since injection of a suboptimal dose of *cntn2* MO enhances the weak FBM neuron migration phenotype of *vangl2* heterozygotes (Sittaramane et al., 2009). To test whether *cntn2* mutants support this conclusion, we examined the offspring of MZ*cntn2-/-* homozygous females and *vangl2-/-* homozygous mutant males, which are 100% double heterozygous embryos. FBM neuron migration defects were more severe and frequent in *cntn2+/-; vangl2+/-* double heterozygotes (Fig. 3.5D, E), compared to *cntn2+/-* or *vangl2*+/- embryos alone (Fig. 3.5B, C, E). FBM neurons migrated normally in 100% of *cntn2+/-* embryos (Fig. 3.5B, E), and failed to migrate out of r4 in only 5% of *vangl2+/-* embryos (Fig. 3.5C, E). By contrast, FBM neurons failed to migrate out of r4 in 17% of *cntn2+/-; vangl2+/-* embryos (Fig. 3.5D, E). To further strengthen this subtle genetic interaction phenotype, we quantified FBM neuron migration in embryos obtained from a cross between *vangl2+/-* heterozygotes and *cntn2-/-* homozygous mutants, generating 50% *cntn2+/-; vangl2*+/+ and 50% double heterozygous (*cntn2+/-; vangl2+/-*) embryos. Since the genotypes of the embryos was unknown at the time of neuronal quantification, we selected ten immunostained embryos from each of three phenotypic

groups corresponding to normal migration, partial and severe migration block (Fig. 3.5F-H), counted the number and examined the distribution of motor neurons in r4, r5, and (r6+r7) (Fig. 3.5I). Nearly 70% of FBM neurons failed to migrate out of r4 in “severe block” embryos, while 87% and 65% of neurons migrated out of r4 in “normal migration” and “partial block” embryos, respectively, providing high confidence in our phenotypic classes (Fig. 3.5E). Importantly, all embryos in the partial (n=10) and severe block (n=10) categories were subsequently genotyped as double heterozygotes, while most of the “normal migration” embryos (8/10) were genotyped as *cntn2+/-; vangl2*+/+. Taken together, the distribution of FBM migration phenotypes generated in two different genetic crosses supports the likelihood of genetic interactions between *cntn2* and *vangl2*. This genetic requirement for *cntn2*, defined using a null allele, is revealed only in a sensitized genetic background of reduced planar cell polarity signaling, suggesting that *cntn2* plays a definitive but minor role during FBM migration.

To further explore a role for *cntn2* in FBM neuron migration, we examined another sensitized genetic background known to affect FBM neuron migration. We showed previously using suboptimal *cntn2* MO doses and the *bashful* mutant that *cntn2* genetically interacts with *laminina1* (*lama1*), which encodes a broadly expressed Laminin subunit Laminina1 (Sittaramane et al., 2009). Since FBM neurons exhibit similar migration defects in *bashful* (*lama1-/-*) and *sleepy* (*lamc1-/-*) mutants (Chandrasekhar, 2004), which affect different Laminin subunits, we tested for genetic interactions between *cntn2* and *lamc1*. We examined the offspring of MZ*cntn2-/-* homozygous females and *lamc1*+/- heterozygous males, 50% of which are double

heterozygous embryos. We found no embryos with severe FBM neuron migration defects, and the fraction of embryos with partial defects was comparable to that seen in *cntn2+/-* and *lamc1+/-* populations (data not shown). These data indicate that *cntn2* and *lamc1* do not interact genetically for FBM neuron migration, and suggest that some morphant-associated phenotypes may not reflect true functions of *cntn2*.

3.4.4 *cntn2* mutants lack nucMLF axon convergence defects seen in morphants but exhibit MLF defasciculation

Given the discrepancy between *cntn2* morphant and mutant FBM neuron migration phenotypes, we examined other phenotypes previously seen in morphants, such as the nucMLF axon convergence defects (Wolman et al., 2008). First, we confirmed the morphant phenotype by injecting *cntn2* MO into *Tg(pitx2c:gfp)* embryos, which express GFP in nucMLF cell bodies and axons (Wolman et al., 2008). In control MO-injected embryos, the nucMLF was found as bilateral groups of tightly clustered cells, which extended tight axon fascicles posteriorly (Fig. 3.6A, E). However, in *cntn2* MO-injected embryos, the nucMLF cells were loosely packed, their axons were defasciculated and they failed to converge normally (Fig. 3.6B, E). In contrast to the morphants, we did not find any nucMLF axon convergence defects in either zygotic (Z*cntn2-/-*) or maternal-zygotic (MZ*cntn2-/-)* embryos (Fig. 3.6C-E), consistent with the difference between morphant- and mutant-associated FBM neuron phenotypes (Fig. 3.4).

We also examined the ability of MLF axons to maintain fasciculation in the absence of Cntn2. MLF axons remained tightly fasciculated as they extended through the midbrain and anterior hindbrain (Fig. 3.6F). Interestingly, MZ*cntn2-/-* embryos showed defasciculation of MLF axons in these regions (Fig. 3.6G-I). Because the MLF axons are often loosely fasciculated posterior to r2, we restricted our analysis to the area anterior to r2 (delineated by dotted line in Fig. 3.6F, corresponding to the hindbrain entry point for trigeminal sensory axons). We categorized embryos in blinded fashion into three groups based on the severity of the defasciculation phenotype: None (no defasciculation), Weak (small splits in the fascicle or very short stretches of defasciculated axons on one or both sides (Fig. 3.6G), and Strong (extensive stretches of split fascicles or axon defasciculation on one or both sides (Fig. 3.6H, I)). About ~85% of MZ*cntn2* mutant embryos (n=32) exhibited strong defasciculation, and <5% showed no defects (Fig. 3.6J). In marked contrast, only ~28% of *cntn2*+/+ embryos (n=32) exhibited strong defasciculation, and ~50% showed no defasciculation (Fig. 3.6J). These data suggest strongly that Cntn2 is involved in maintaining adhesions between MLF axons in the zebrafish midbrain and anterior hindbrain.

3.4.5 FBM neuron and nucMLF defects in *cntn2* morphants are likely off-target effects

The difference between *cntn2* morphant and mutant phenotypes can be explained either by off-target effects of the morpholino (MO) (Eisen and Smith, 2008;

Kok et al., 2015) or by genetic compensation from related genes in mutants but not in morphants (Rossi et al., 2015). To distinguish between these alternatives, we examined the effects of injecting *cntn2* MO into *cntn2*+/+ and MZ*cntn2*-/- embryos. If *cntn2* MO injection causes defects in *cntn2*+/+ embryos but not in MZ*cntn2*-/- embryos, then it would suggest genetic compensation (Fig. 3.7A). However, defects in both *cntn2*+/+ and MZ*cntn2*-/- embryos following *cntn2* MO injection would imply an off-target effect of the MO (Fig. 3.7A). As expected, FBM neuron migration and the development of nucMLF neurons and axons occurred normally in control MO-injected *cntn2*+/+ and MZ*cntn2*-/- embryos (Fig. 3.7B-E, J, K). Consistent with previous studies (Sittaramane et al., 2009), migration of FBM neurons was strongly affected in *cntn2*+/+ embryos injected with *cntn2* MO (Fig. 3.7F, J). Similarly, the organization and axonogenesis of nucMLF neurons was greatly perturbed in *cntn2*+/+ embryos injected with *cntn2* MO (Fig. 3.7G, K), as shown previously (Wolman et al., 2008). Surprisingly, MZ*cntn2*-/- embryos, which lack functional *cntn2* mRNA and contain no detectable Cntn2 protein, also exhibited FBM neuron migration and nucMLF convergence phenotypes following *cntn2* MO injection (Fig. 3.7H-K). These data demonstrate that the FBM and nucMLF neuronal defects seen in *cntn2* morphants are likely due to off-target effects of the MO.

3.4.6 *cntn2* mutants exhibit a defective escape response and have swimming deficits

While some of the *cntn2* morphant phenotypes appear to be off-target effects, the definitive phenotypes seen in MZ*cntn2* mutants (*cntn2-vangl2* genetic interaction for FBM neuron migration and MLF defasciculation) motivated us to look for phenotypes in other *cntn2*-expressing cell types. In *cntn2* morphant embryos, Rohon-Beard (RB) central axons grew more slowly and showed some defasciculation compared to control embryos (Liu and Halloran, 2005). To test whether the growth of RB central axons was affected in *cntn2* mutants, we compared the lengths of RB central axons in equivalent-stage *cntn2+/+* and MZ*cntn2-/-* embryos. RB neurons were sparsely labeled using a *ngn1:GFP-caax* Tol2 construct (Andersen et al., 2011). There was no reduction in RB central axon lengths in MZ*cntn2* mutants (Fig. 3.8), suggesting that the loss of Cntn2 does not affect RB central axon growth rates as seen in morphants. In addition, we did not observe obvious defasciculation of RB central axons in zn-12 antibody-stained MZ*cntn2-/-* embryos at 24 hpf (data not shown). However, because the RB central axon defasciculation effect was variable in the morphants (Liu and Halloran, 2005), we reasoned that a behavioral test such as the touch-evoked escape response (Granato et al., 1996) would be a more sensitive assay for putative functional defects associated with these neurons. The escape responses of 2 dpf larvae to head or trunk touch were binned (blinded to genotype) into three categories: No response, Weak response, and Strong response (see Materials and Methods). Larvae of both genotypes (*cntn2+/+* and MZ*cntn2-/-*) behaved similarly when touched on the head (Fig. 3.9A). However, larger numbers of MZ*cntn2-/-* mutant larvae than *cntn2+/+* larvae exhibited weak responses when touched in the trunk (Fig. 3.9B). Touch-evoked escape response defects in the

trunk but not in the head suggest that MZ*cntn2* mutants may have a defect associated specifically with the RB neuron-mediated spinal sensorimotor circuit. Importantly, outgrowth of spinal motor axons was not affected in mutants (Fig. 3.10) consistent with a role for *cntn2* in assembling the sensory component of the escape response circuit. While there was no clear defect in RB central axon outgrowth in mutants, we cannot rule out defects in other aspects of RB morphology or differentiation.

To further examine the effects of Cntn2 protein loss on the function of sensorimotor circuits, we analyzed swimming activity using the DanioVision system. Since Cntn2 is expressed in a subset of retinal ganglion cells (RGCs) and their axons (Fig. 3.1E-F), we examined light-evoked behaviors by measuring the swimming activity of 7 dpf *cntn2+/-* and MZ*cntn2-/-* larvae during “Lights off” and “Lights on” phases (60 minutes each) (Fig. 3.11A). Larval genotypes were determined after swimming activity measurements (See Materials and Methods). Total swimming distance and swimming duration were significantly lower in MZ*cntn2-/-* mutants compared to *cntn2+/-* siblings during both phases (Fig. 3.11B, C). Importantly, total distance moved and activity during the “Lights off” phase were significantly lower than during the “Lights on” phase in both *cntn2+/-* and MZ*cntn2-/-* larvae (Fig. 3.11B, C), indicating that light-dependent movement is conserved, and suggesting that the swimming deficits of MZ*cntn2* mutants result from circuit defects downstream of the visual pathway. We tested directly for visual pathway defects by examining the morphology of RGC axons following anterograde labeling with lipophilic dye DiI and photoconversion (see Materials and Methods). Since RGC axon fascicles were thinner in MZ*cntn2* mutants when compared

to *cntn2*+/+ cousins, but not when compared to *cntn2*+/- siblings (Fig. 3.12), potential defects in the visual system cannot be ruled out. Taken together, the escape response and swimming activity phenotypes suggest that MZ*cntn2* mutants have deficits in sensorimotor circuitry, consistent with *cntn2* expression in cell types (RB and RGC neurons) associated with these circuits.

3.5 DISCUSSION

A large number of membrane-associated molecules have been implicated in the guidance of migrating neurons and projecting axons during nervous system development (Maness and Schachner, 2007). With the advent and ease of application of CRISPR/Cas9 technology, it is now possible to readily test the biological role of any gene in zebrafish (Hwang et al., 2013). Here, we used CRISPR/Cas9 to generate a null mutant for a neural cell adhesion molecule Cntn2. Our data demonstrate that while some of the previously-described morphant phenotypes may result from off-target effects, *cntn2* also plays definitive roles in assembling neural circuits in zebrafish.

3.5.1 Comparison of *cntn2* morphant and mutant phenotypes

Morpholino-mediated knockdown experiments previously suggested roles for *cntn2* in the caudal migration of FBM neurons (Sittaramane et al., 2009), the guidance of axons from the nucMLF (Wolman et al., 2008), and the growth of RB central axons (Liu and Halloran, 2005). However, MZ*cntn2* mutants did not phenocopy most of these morphant phenotypes. There are several explanations for the differences between the

morphant and mutant phenotypes. First, the mutant might make partially functional Cntn2 protein due to translation in-frame from start codons downstream of the mutation in exon 4. Second, the use of alternative, cryptic splice sites may skip exon 4 and yet generate truncated but functional Cntn2 protein. However, these outcomes appear unlikely since no Cntn2 protein is detected in MZ mutants (both alleles) using a polyclonal antibody generated using full-length Cntn2 protein (Lang et al., 2001). Such an antibody would likely recognize epitopes distributed throughout the length of the protein, and therefore detect truncated protein generated by alternative splicing or translational start sites. Exhaustive analysis of the genome assembly (GRCz11, 2017) did not identify any closely related genes (>75% similarity in Immunoglobulin and Fibronectin domains), suggesting that the absence of a strong mutant phenotype is not due to genetic redundancy.

Although a few studies have shown that morphants and mutants for some genes have similar or overlapping phenotypes (Bill et al., 2009; Phillips et al., 2011), there are other cases where the two phenotypes do not match (Lebedeva et al., 2017; Moore et al., 2016). An analysis of several genes affecting development and organogenesis showed that 80% of the morphant phenotypes were not seen in mutants, and concluded that morpholinos produce a high false-positive rate (Kok et al., 2015). Two models can explain the discrepancy in phenotypes between morphants and mutants. In the first model, MOs can generate off-target effects by specifically knocking down the expression of another unidentified gene, but they can also be toxic and generate non-specific phenotypes. In the second model, genetic compensation from related genes

may occur in mutants, but not in morphants, resulting in the absence of a loss-of-function phenotype (Rossi et al., 2015). For instance, in *egfl7* mutants, vascular defects generated in *egfl7* morphants were not seen. However, several members of the *emilin* gene family were upregulated in mutants, potentially compensating for the loss of *egfl7* (Rossi et al., 2015). It is possible that genomic disturbances caused by deleterious mutations activate compensatory pathways in mutants, while MOs, which only block the translation of mRNA, fail to do so.

In light of these studies, one explanation for the difference between the *cntn2* morphant and mutant phenotypes is that other Cntn-like or other Ig superfamily CAM genes may be overexpressed and compensate for loss of *cntn2* function in mutants but not morphants. The genetic compensation and off-target effect models were distinguished by examining the effect of injecting MO into the mutants (Fig. 3.7A; (Stainier et al., 2017)). Since the *cntn2* morphant phenotypes for FBM and nucMLF neurons were readily seen in null mutants injected with *cntn2* MO, it is unlikely that these phenotypes are due to loss of Cntn2 function, but rather are due to off-target effects. Nevertheless, we have also documented *cntn2* mutant-specific phenotypes associated with the FBM and nucMLF neurons, indicating that *cntn2* plays definitive roles in the development of these neuronal populations.

3.5.2 Role for Cntn2 in FBM neuron migration

During nervous system development, migrating neurons respond to several cues in the environment, and interact with neighboring cells (Marin et al., 2010). Vangl2, a

core component of Wnt/Planar Cell Polarity (PCP) pathway (Gray et al., 2011), is expressed ubiquitously in the hindbrain, and functions both within the FBM neurons and in the surrounding neuroepithelial cells for FBM neuron migration (Davey et al., 2016; Jessen et al., 2002; Sittaramane et al., 2013; Sittaramane et al., 2009). *cntn2* is expressed in branchiomotor neurons, but not in the surrounding neuroepithelial cells, during FBM neuron migration (Sittaramane et al., 2009; Warren et al., 1999), which indicates that *cntn2* likely functions in a cell-autonomous fashion. *Laminina1* (*lama1*), which encodes a subunit of the extracellular matrix protein Laminin1, is expressed broadly (Sittaramane et al., 2009) and plays a role in FBM neuron migration (Paulus and Halloran, 2006). Using a combination of mutants and MOs, we previously showed genetic interactions between *cntn2* and *vangl2*, and between *cntn2* and *lama1* (Sittaramane et al., 2009). Here, using only mutants, we again observed genetic interactions between *cntn2* and *vangl2*, but not between *cntn2 and lamc1*, which encodes a different obligatory subunit of Laminin1. These data indicate that a role for *cntn2* in FBM neuron migration can be discerned in a sensitized *vangl2+/-* background but not in a sensitized *lamc1+/-* background. In addition to *vangl2* and *lamc1*, we tested for genetic interactions between *cntn2* and other PCP (*fzd3a*, *scrb1*) and non-PCP genes (*cdh2*, *gpr125*) that have been implicated in FBM neuron migration (Li et al., 2013; Rebman et al., 2016; Stockinger et al., 2011; Wada et al., 2005; Wada et al., 2006). We detected genetic interactions for *cntn2* only with *vangl2*, and not with any of the other genes tested (data not shown). Indeed, *vangl2* is rather unique in exhibiting genetic interactions with several PCP and non-PCP genes (*vangl2; fzd3a* and *vangl2;*

cdh2, for example), while many of the other combinations (*fzd3a; scrb1* or *fzd3a; cdh2*, for example) also do not exhibit genetic interactions (Gurung, S., Hummel, D., Chandrasekhar, A., in preparation). Given the central role of Vangl2 in Wnt/PCP signaling, only the *vangl2+/-* background may be sensitive enough to detect a subtle role for Cntn2 in FBM neuron migration.

3.5.3 Role for Cntn2 in nucMLF development

The nucMLF neurons extend dendrites toward retino-recipient areas and project axons to the spinal cord (Gahtan et al., 2005; Kimmel et al., 1982), and have been implicated in modulating locomotor speed, optomotor response, escape swimming and prey capture (Sankrithi and O'Malley, 2010; Severi et al., 2014). Morpholino-mediated knockdown experiments suggested roles for *cntn2* in the initial oriented growth of nucMLF axons, and their convergence into a tight fascicle (Wolman et al., 2008). We show here that MZ*cntn2* mutants do not recapitulate this nucMLF morphant phenotype. However, MLF axons in *cntn2* mutants do exhibit defasciculation in the midbrain and anterior hindbrain (rhombomeres 1-2). These data suggest that Cntn2 facilitates adhesions between MLF axons, which is consistent with its ability to interact homophilically, as well as heterophilically with other cell adhesion molecules (Brummendorf and Rathjen, 1996).

FBM neurons migrate in close proximity to MLF axons along the entire pathway from r4 to r7 (Bingham et al., 2005; Wada et al., 2006; Wanner and Prince, 2013). The migration of FBM neurons from r5 to r6 depends upon interactions between FBM

neurons and MLF axons mediated by the cell adhesion molecule Cadherin2 (Cdh2) (Wanner and Prince, 2013). Since MLF axons are frequently defasciculated in *cntn2* mutants, it is possible that the interactions between FBM neurons and MLF axons are also partially disrupted in *cntn2* mutants. It will be interesting to investigate potential roles for *cntn2* and *cdh2* in regulating FBM neuron migration indirectly through MLF axon-FBM neuron interactions.

3.5.4 Role for Cntn2 in sensorimotor circuits

In the mouse *Cntn2* mutant, retinal ganglion cell (RGC) sensory axons, which normally express Cntn2, lose their preference to extend on Cntn2-coated substrates, suggesting that RGC axon fasciculation requires homophilic Cntn2 interactions (Chatzopoulou et al., 2008). In zebrafish, Cntn2 is expressed on RGC neurons and axons (Fig. 3.11E-F). Although no obvious defects in RGC fasciculation or pathfinding were evident in MZ*cntn2* mutants (Fig. 3.12), the RGC axon fascicle was thinner in some cases, suggesting possible effects on outgrowth. We tested for a potential role in the visual system by measuring swimming activity in light and dark phases. While swimming duration and distance were significantly decreased in MZ mutants compared to controls in both light and dark conditions, both measures of swimming were similarly affected in control and MZ mutants when switching from light to dark phase, indicating that the regulation of motor activity by the visual system was not affected in mutants. It is more likely that the swimming deficits are generated by deficits in circuits downstream of the visual system for two reasons. First, given the nucMLF fasciculation defects in

MZ*cntn2* mutants, their swimming deficits are consistent with the role of the nucMLF in modulating locomotion in larval zebrafish (Severi et al., 2014). Second, some of the swimming deficits in MZ mutants may be attributed to a role for *cntn2* in the outgrowth or function of sensory neurons in the spinal motor circuits. While we did not find any growth defects in Rohon-Beard (RB) central axons in MZ*cntn2* mutants (Fig. 3.8), as seen previously in *cntn2* morphants (Liu and Halloran, 2005), other aspects of RB morphology or differentiation could potentially be affected. Therefore, our finding that *cntn2* mutants exhibit weaker escape responses to trunk touch compared to wildtype controls supports a role for *cntn2* in the function of the RB sensorimotor circuit. Since there are no defects in motor and RB axon outgrowth in *cntn2* mutants, defects in the connectivity and/or function of sensorimotor components seem more likely. Indeed, some of the motor deficits seen in the mouse *Cntn2* mutant (Savvaki et al., 2008) may result from improper development or function of dorsal root ganglion sensory axons (Kunz et al., 1998; Law et al., 2008).

In conclusion, our characterization of the *cntn2* CRISPR mutant has revealed definitive roles for the Cntn2 cell adhesion molecule in the zebrafish nervous system. It will be of interest to identify other membrane proteins that function in concert with Cntn2 to regulate FBM neuron migration and MLF axon fasciculation in zebrafish.

3.6 ACKNOWLEDGEMENTS

We thank members of the Chandrasekhar lab for discussion and fish care. We thank Dr. Clarissa Henry (University of Maine, Orono) for providing the *sleepy* (*lamc1*)

mutant fish, and Dr. Claudia Stuermer (University of Konstanz) for providing the Cntn2 antibody. We would also like to thank Dr. Jimann Shin (Lila Solnica-Krezel lab, Washington University) for reagents, help and advice on CRISPR protocols, and Dr. Martha Bagnall (Washington University) for help and advice on touch-evoked escape response experiments. This work was supported by NIH grants R01NS086934 (MH) and R01NS040449 (AC), and bridge funds from the University of Missouri Research Board and the Bond Life Sciences Center (AC).

3.7 FIGURES AND LEGENDS

Figure 3.1: Cntn2 protein expression during embryonic development

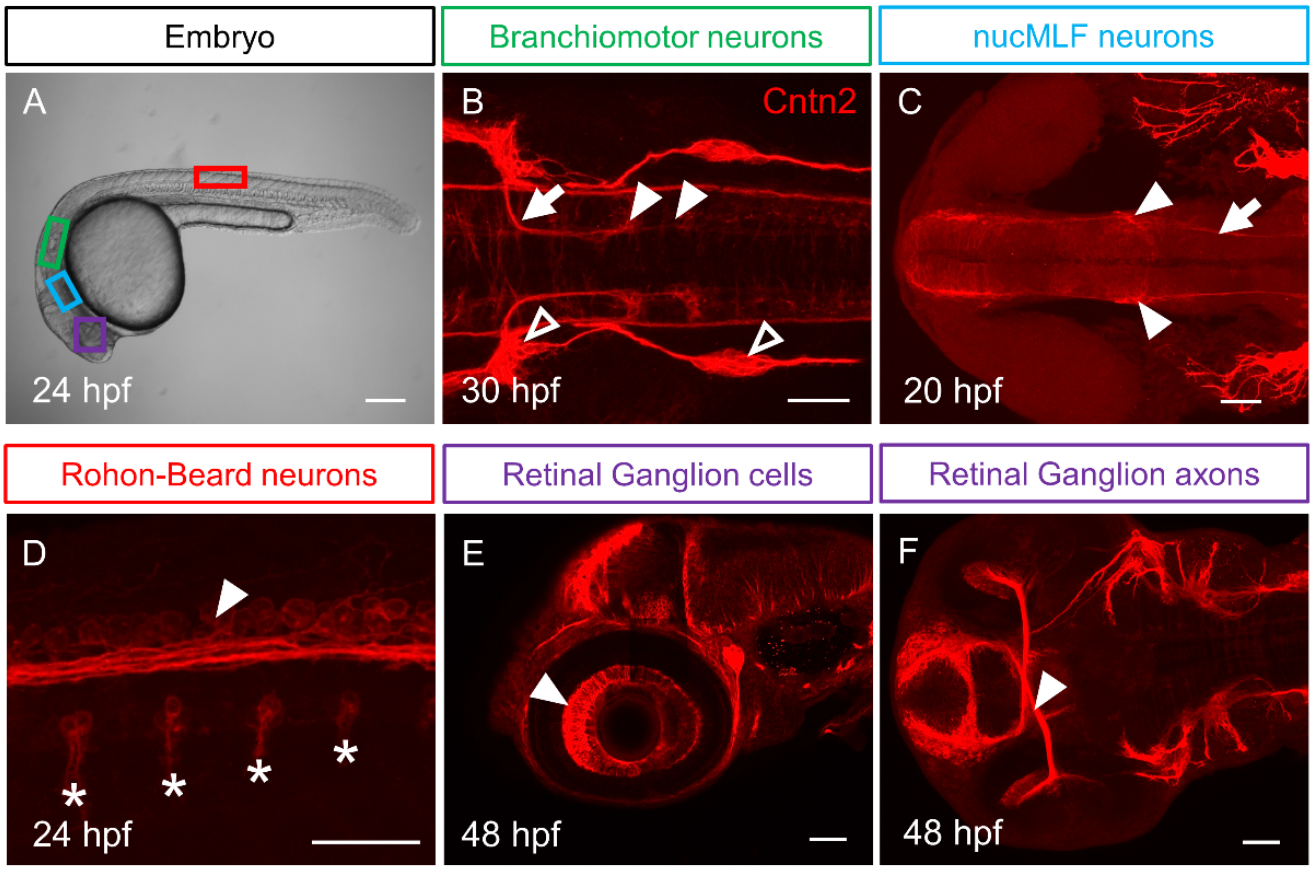

Figure 3.1: Cntn2 protein expression during embryonic development

(A) Lateral view of a 24 hpf embryo with boxes indicating the location of different neuronal cell types in B-F. Panels B-F show confocal projections of embryos labeled with anti-Cntn2 antibody (red). Panel B shows a dorsal view, and C and F show ventral views. Panels D and E show lateral views. All panels show anterior to the left. **(B)** A 30 hpf embryo showing Cntn2 expression in FBM neuron cell bodies in r6 and r7 (arrowheads), and their axons (arrow). Open arrowheads mark sensory ganglia. **(C)** A 20 hpf embryo showing Cntn2 expression in nucMLF cell bodies (arrowheads), and their axons (arrow). **(D)** A 24 hpf embryo showing Cntn2 expression in central axons (arrowhead) of Rohon-Beard (RB) neurons. Asterisks indicate axons of primary motor neurons exiting the spinal cord. **(E, F)** A 48 hpf embryo showing Cntn2 expression in nasal RGC (arrowhead, E) as well as RGC axons (arrowhead, F). Scale bars: A, 200 μm, and B-F, 50 μm.

Figure 3.2: Generation and validation of CRISPR-generated *cntn2* mutant

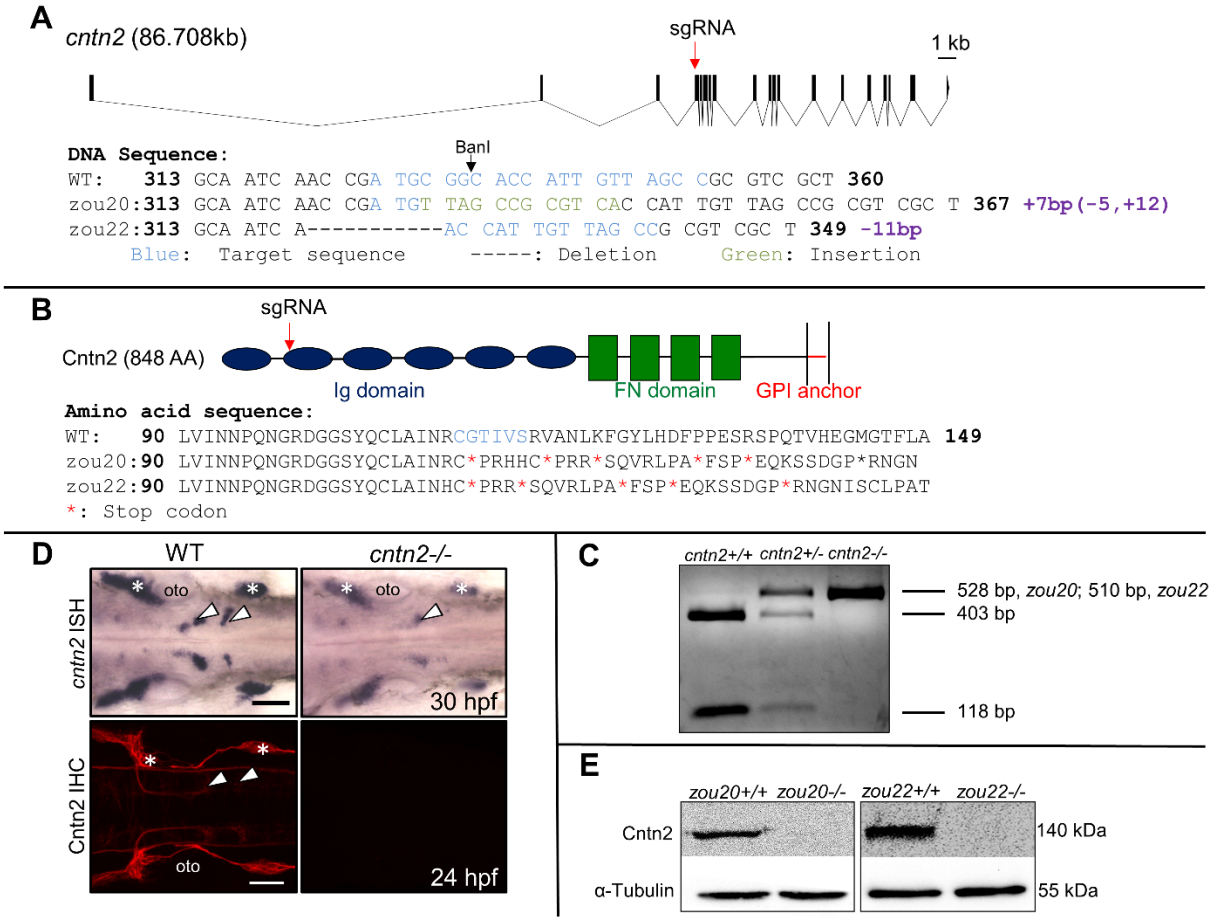

Figure 3.2: Generation and validation of CRISPR-generated *cntn2* mutant

(A) Genomic structure of *cntn2* containing 19 exons, with the CRISPR target site (sgRNA) in the 4th exon. The target site is highlighted in blue while the 7bp insertion and the 11bp deletion in *cntn2*^{zou20} and *cntn2*^{zou22} alleles are highlighted in green and indicated by dash marks, respectively. **(B)** Domain structure of Cntn2 containing six immunoglobulin (Ig) domains, four fibronectin (FN) domains, and a glycosylphosphatidylinositol (GPI)-anchor linked to the plasma membrane. Predicted amino acid sequences of wildtype (WT) *cntn2*, and *cntn2*^{zou20} and *cntn*^{zou22} alleles containing multiple stop codons (*). The highlighted AAs (blue) correspond to the CRISPR target site in the gene. **(C)** A PCR product (528bp, *zou20*; 510bp, *zou22*) spanning the target site digested with BanI differentiate between three genotypes: Wildtype (2 cut bands), heterozygote (1 uncut and 2 cut bands) and homozygote (1 uncut band). **(D)** Dorsal views of wildtype (WT) and mutant (*zou20*) hindbrains processed for *cntn2* in situ hybridization (ISH) (upper panels) and anti-Cntn2 immunohistochemistry (IHC) (lower panels). Arrowheads indicate migrated FBM neurons and asterisks mark sensory ganglia. In *cntn2* (*zou20*) mutants, *cntn2* expression is greatly reduced, and Cntn2 protein is not detectable. Scale bar = 50 μm. **(E)** Western blot analysis of Cntn2 in *cntn2*^{zou20} and *cntn*^{zou22} embryos at 48 hpf. Cntn2 protein is not detectable in *cntn2* mutants. Loading control is α-tubulin.

Figure 3.3: Knock down of Cntn2 expression with antisense MO

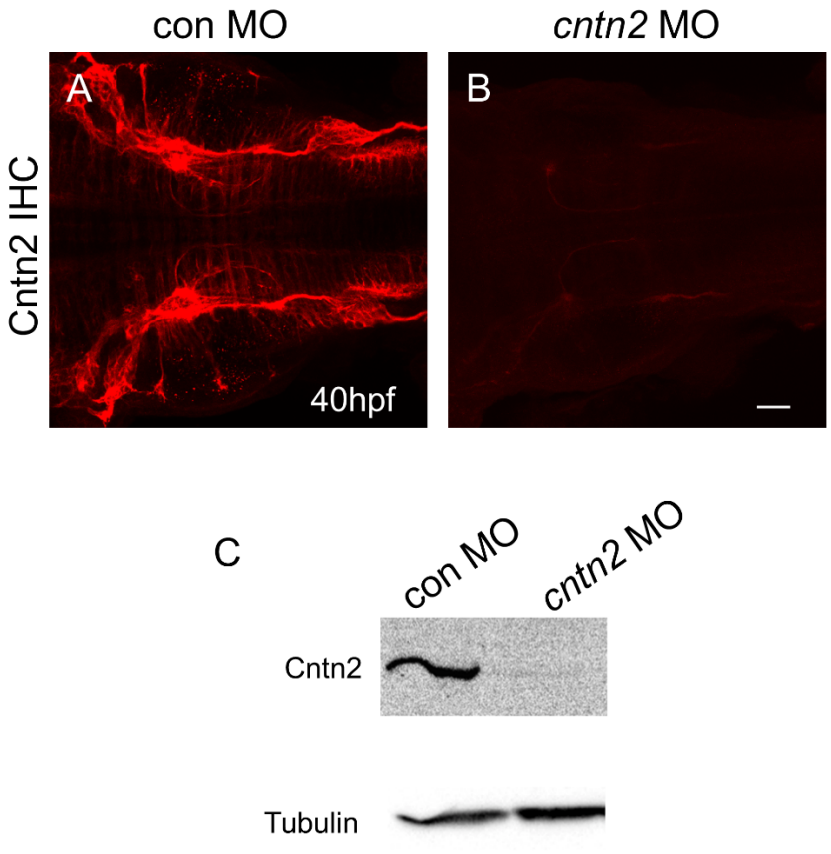

Figure 3.3: Knock down of Cntn2 expression with antisense MO

Top panels show dorsal view of hindbrain, with anterior to the left, in embryos labeled with the anti-Cntn2 antibody. **(A, B)** Cntn2 is highly expressed in a control MO-injected embryo (A). Cntn2 expression is almost completely eliminated in a *cntn2* MO-injected embryo (B). **(C)** Western blot analysis shows severe reduction of Cntn2 protein in *cntn2* MO-injected embryos at 48 hpf. Scale bar in B, 50 μm for A and B.

Figure 3.4: FBM neuron migration is affected in *cntn2* morphants but not in *cntn2* mutants

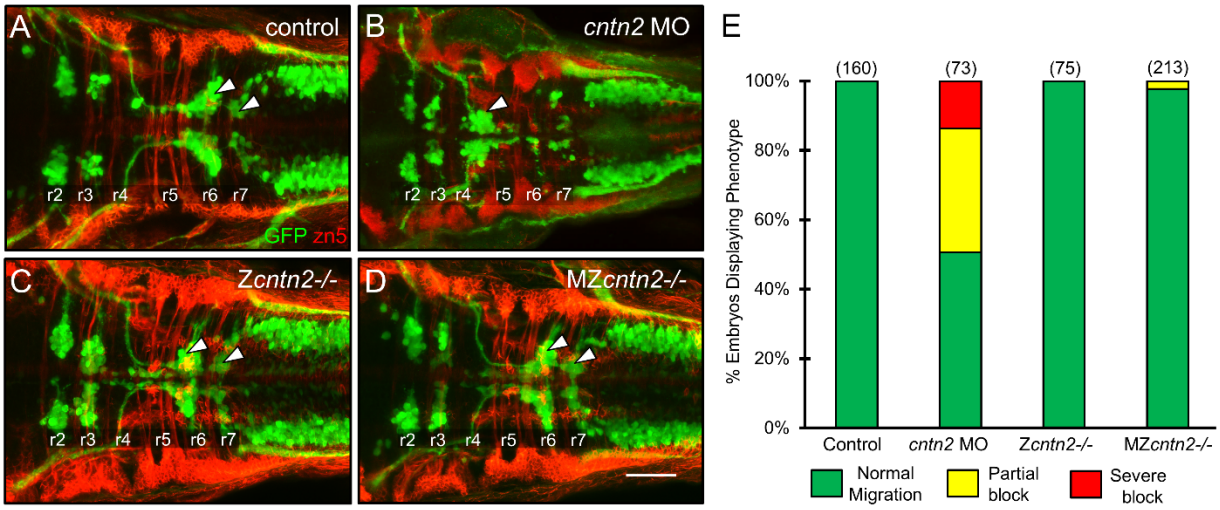

Figure 3.4: FBM neuron migration is affected in *cntn2* morphants but not in *cntn2* mutants

Panels A-D show dorsal views of the hindbrain with anterior to the left. *Tg(isl1:gfp)* embryos were fixed at 48 hpf, and processed for immunohistochemistry with zn5 antibody (red) to label hindbrain commissural neurons and axons at rhombomere boundaries, and anti-GFP antibody (green) to label FBM neurons (arrowheads). **(A)** FBM neurons (arrowheads) migrate normally into r6 and r7 in an uninjected embryo. **(B)** FBM neurons largely fail to migrate out of r4 in a *cntn2* MO-injected embryo. **(C, D)** FBM neurons migrate normally in zygotic mutant (Z*cntn2-/-*) (C), and maternal-zygotic mutant (MZ*cntn2-/-*) (D) embryos. Scale bar in D, 50 μm for A-D. **(E)** Quantification of FBM neuron migration defects. Number in parenthesis denotes number of embryos. Data are from 3 to 4 experiments.

Figure 3.5: *cntn2* interacts genetically with *vangl2* but not with *lamc1*

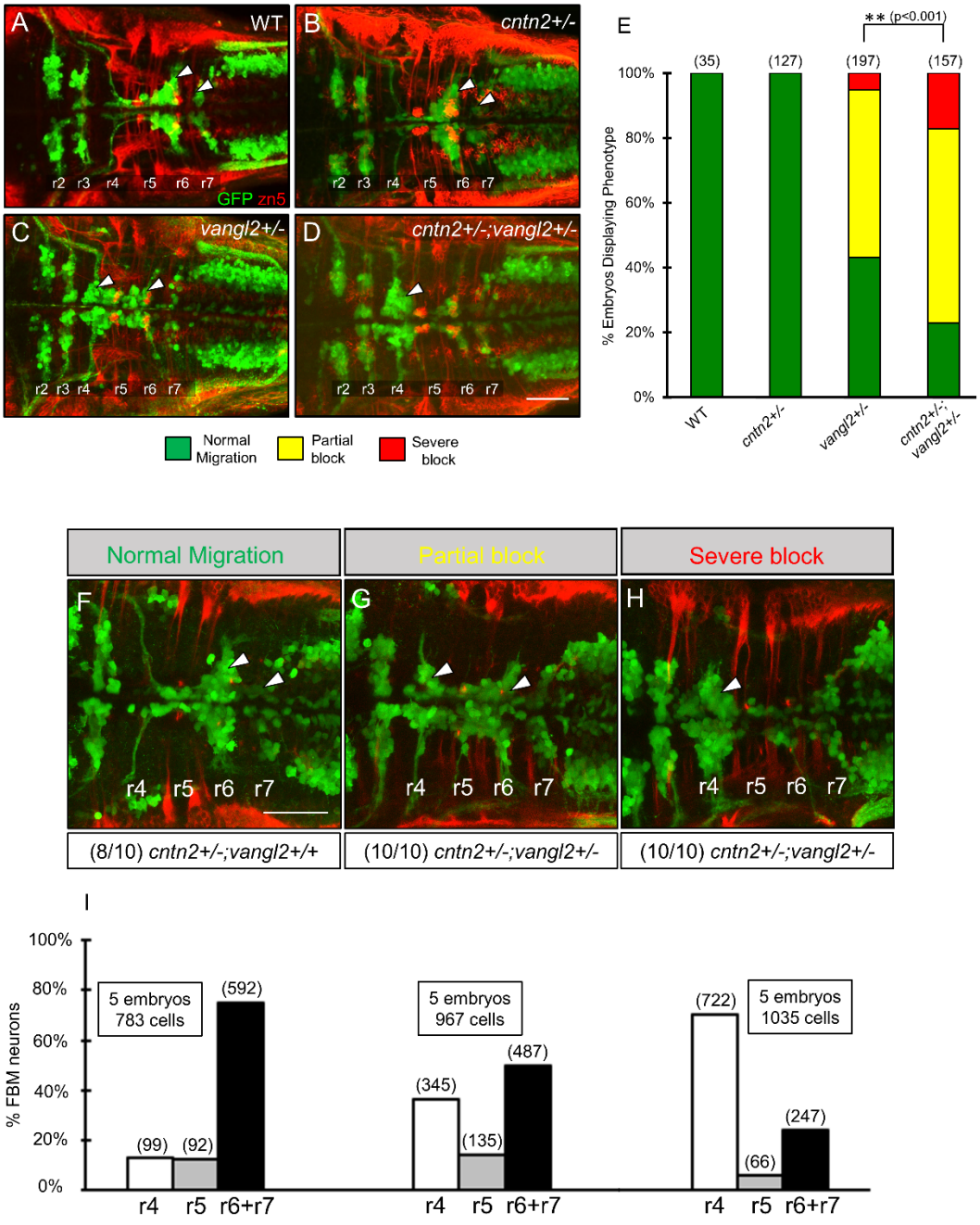

Figure 3.5: *cntn2* interacts genetically with *vangl2* but not with *lamc1*

Panels A-D and F-H show dorsal views of the hindbrain with anterior to the left. *Tg(isl1:gfp)* embryos were fixed at 48 hpf, and processed for immunohistochemistry with zn5 antibody (red) to label hindbrain commissural neurons and axons at rhombomere boundaries, and anti-GFP antibody (green) to label FBM neurons (arrowheads). **(A)** FBM neurons migrate normally in a control embryo. **(B)** FBM neurons migrate normally in a *cntn2* heterozygous (*cntn2+/-)* embryo. **(C)** FBM neurons migrate poorly in a *vangl2* heterozygous (*vangl2+/-)* embryo, with neurons located along the entire migratory pathway from r4 to r6. **(D)** FBM neurons fail to migrate out of r4 in a *cntn2; vangl2* double heterozygote (*cntn2+/-; vangl2+/-*). Scale bar in D, 50 μm for A-D. **(E)** Quantification of genetic interaction data. Number in parenthesis denotes number of embryos. **Chi-square test at $p<0.001$; NS: not significant. Data are from 2 to 4 experiments. **(F-H)** Offsprings of *vangl2+/-* heterozygous and *cntn2-/-* homozygous mutants exhibit normal, partial block, and severe block phenotypes for FBM neuron migration. Embryos exhibiting partial block (10/10) and severe block (10/10) were all identified as *cntn2; vangl2* double heterozygote (*cntn2+/-; vangl2+/-*) and a majority of embryos (8/10) exhibiting normal migration were identified as *cntn2+/-*; *vangl2+/+* by genotyping. **(I)** Quantification of non-migrated FBM neurons in r4, partially migrated FBM neurons in r5 and fully migrated FBM neurons in r6, and r7. Number in parenthesis denotes number of cells. Scale bar in F, 50 μm for F-H.

Figure 3.6: *cntn2* mutants show MLF defasciculation but lacks nucMLF defects seen in morphants

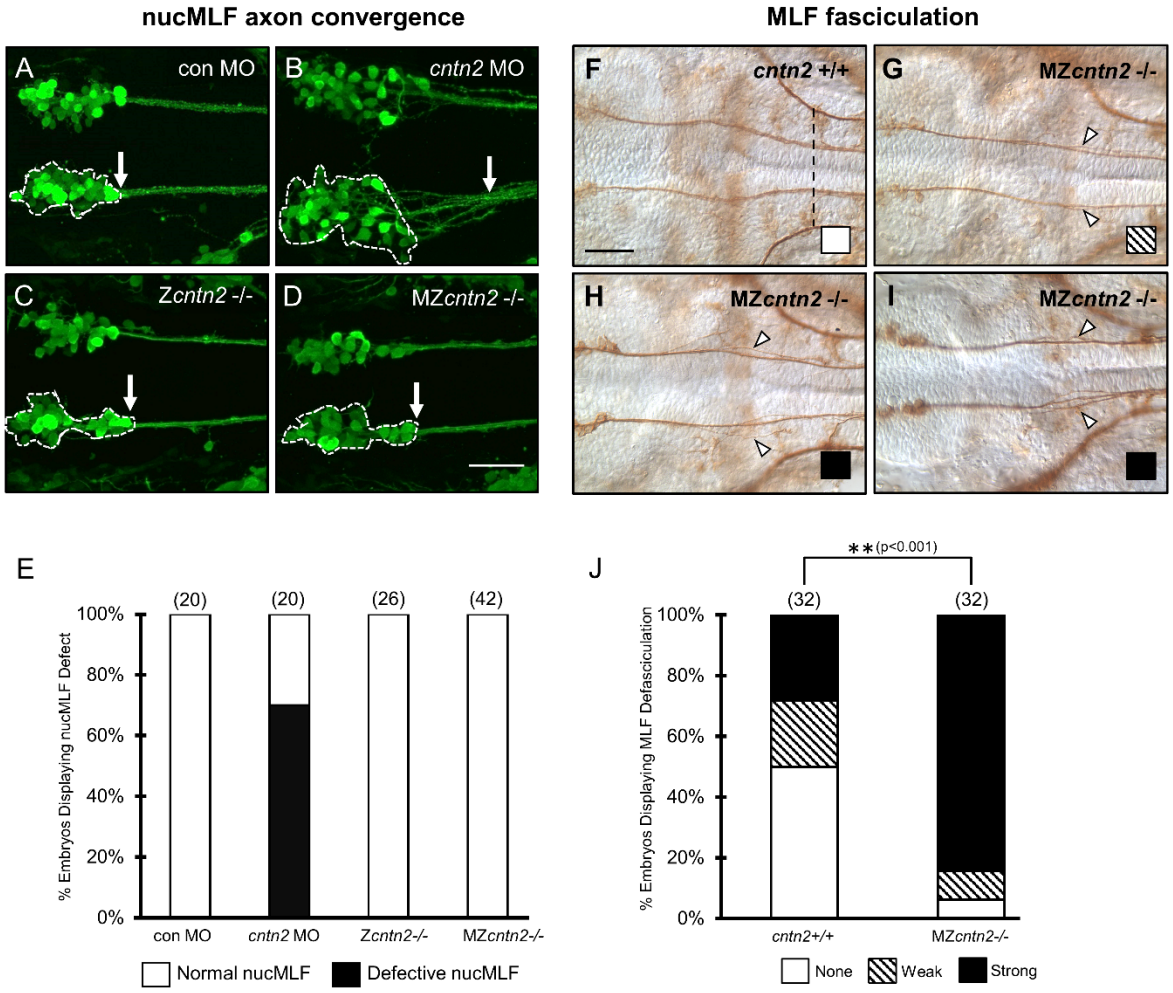

Figure 3.6: *cntn2* mutants show MLF defasciculation but lacks nucMLF defects seen in morphants

Panels A-D show ventral views of the midbrain with anterior to the left. (A-D) Confocal projections of *Tg(pitx2c:gfp)* embryos labeled with anti-GFP antibody at 24 hpf. Panels F-I show ventral views of the midbrain and anterior hindbrain region with anterior to the left. **(A)** In a control MO-injected embryo, the nucMLF is found as bilateral groups of tightly clustered cells (delineated by dashed outline). Their axons form tight fascicles (arrow) immediately posterior to the neuron clusters. **(B)** In a *cntn2* MO-injected embryo, the nucMLF neurons are loosely packed, and their axons are defasciculated. **(C, D)** The nucMLF neurons and axons converge normally in zygotic (Z*cntn2-/-*) and maternal-zygotic (MZ*cntn2-/-*) mutants. **(E)** Quantification of nucMLF defects. Number in parenthesis denotes number of embryos. Data are from 2 to 4 experiments. **(F-I)** Zn-12 antibody labeling of the MLF axons in 24 hpf embryos. MLF axons in a *cntn2*+/+ form a tight fascicle (F); however, MLF axons are defasciculated (arrowheads) in MZ*cntn2-/-* embryos (G-I). Black dotted line in F shows the cut-off point (for scoring) where the trigeminal sensory axons enter the hindbrain in r2. **(J)** Quantification of MLF defasciculation defects. Number in parenthesis denotes number of embryos. Data are from 2 experiments. Scale bar in D, 50 μm for A-D; Scale bar in F, 50 μm for F-I.

Figure 3.7: Some neuronal defects in *cntn2* morphants are likely to be off-target effects

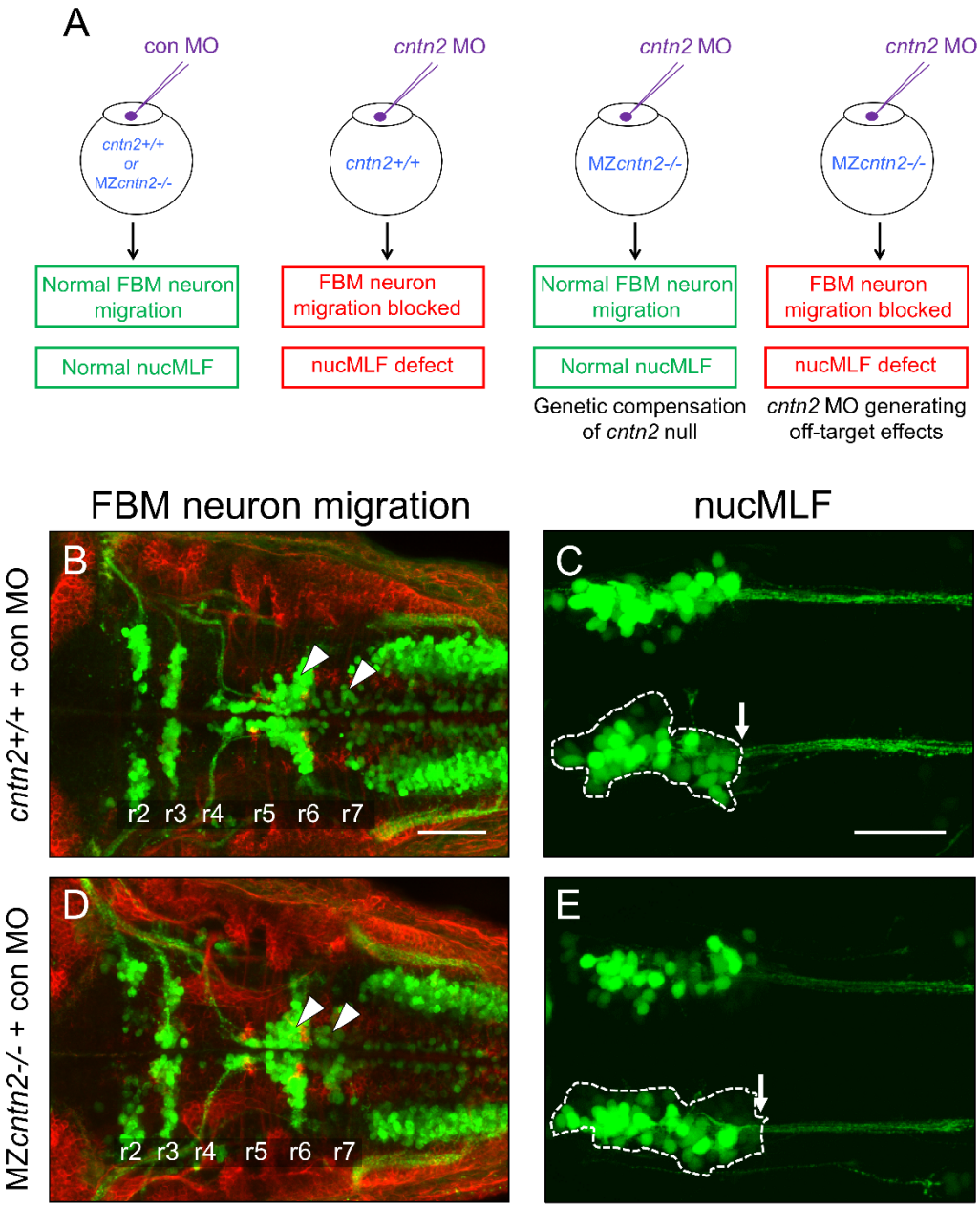

Figure 3.7: Some neuronal defects in *cntn2* morphants are likely to be off-target effects (continued)

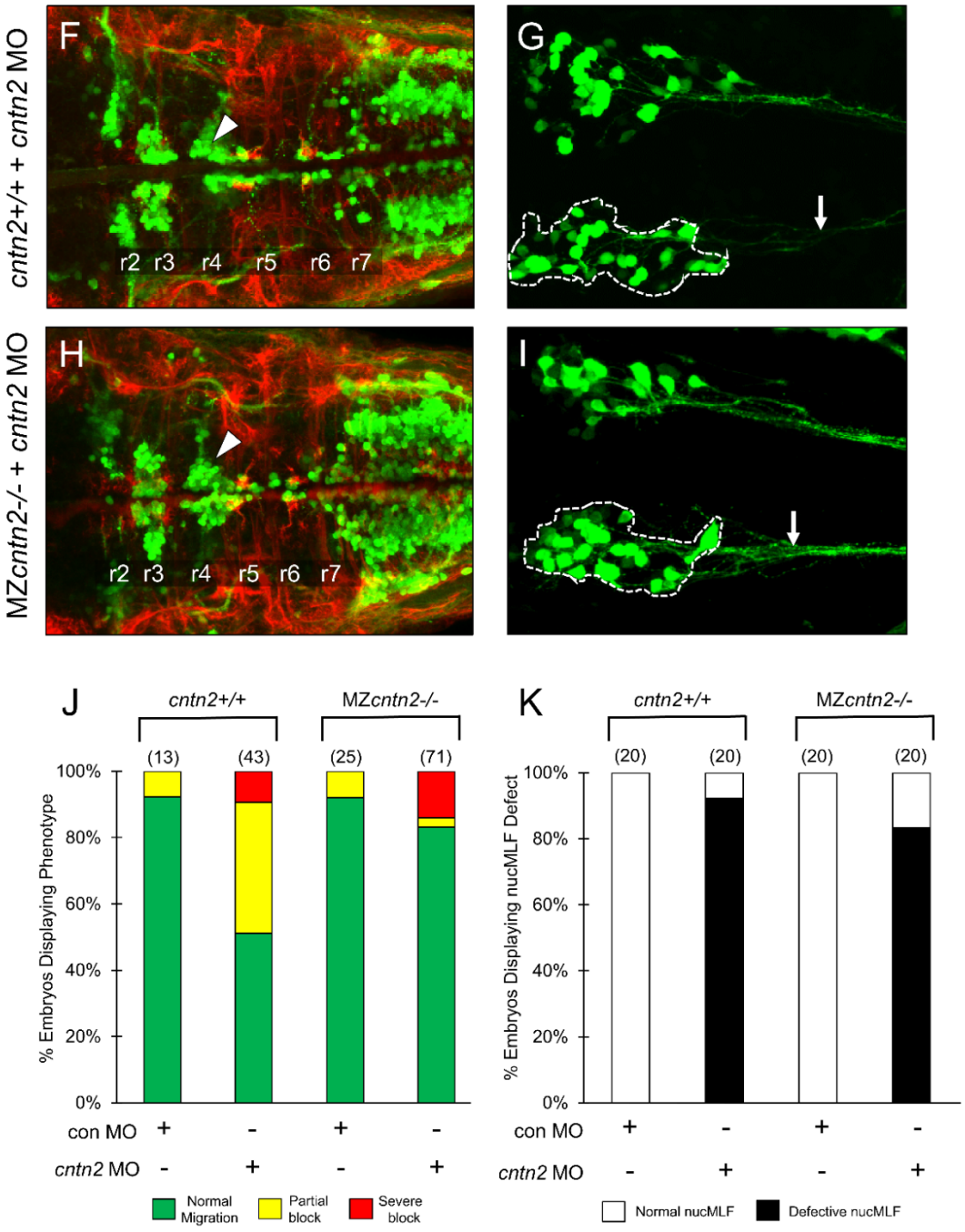

Figure 3.7: Some neuronal defects in *cntn2* morphants are likely to be off-target effects

(A) Experiments to distinguish between genetic compensation in MZ*cntn2-/-* mutants, and off-target effects of the *cntn2* MO. Normal development of FBM and nucMLF neuron in MZ*cntn2-/-* mutants injected with *cntn2* MO would suggest compensation. However, defective development of both cell types in these embryos would suggest off-target effects. (B, D, F, H) Dorsal views of the hindbrain with anterior to the left. *Tg(isl1:gfp)* embryos were fixed at 48 hpf, and processed for immunohistochemistry with zn5 antibody (red) to label hindbrain commissural neurons and axons at rhombomere boundaries, and anti-GFP antibody (green) to label FBM neurons (arrowheads). **(B, D)** FBM neurons migrate normally in control MO-injected *cntn2+/+* (B) and in MZ*cntn2-/-* (D) embryos. **(F, H)** Migration of FBM neurons is greatly reduced in *cntn2* MO-injected *cntn2+/+* (F) and MZ*cntn2-/-* (H) embryos. (C, E, G, I) Ventral views of the midbrain, with anterior to the left, of *Tg(pitx2c:gfp)* embryos labeled with anti-GFP antibody. **(C, E)** Normal nucMLF development in control MO-injected *cntn2+/+* (C) and MZ*cntn2-/-* (E) embryos. **(G, I)** Defective nucMLF development in *cntn2* MO-injected *cntn2+/+* (G) and MZ*cntn2-/-* (I) embryos. **(J)** Quantification of data presented in B, D, F and H. Number in parenthesis denotes number of embryos. **(K)** Quantification of data presented in C, E, G and I. Number in parenthesis denotes number of embryos. Scale bar in B, 50 μm for B, D, F, and H; Scale bar in F, 50 μm for C, E, G, and I.

Figure 3.8: Outgrowth of Rohon-Beard central axons is not affected in MZ*cntn2* mutants

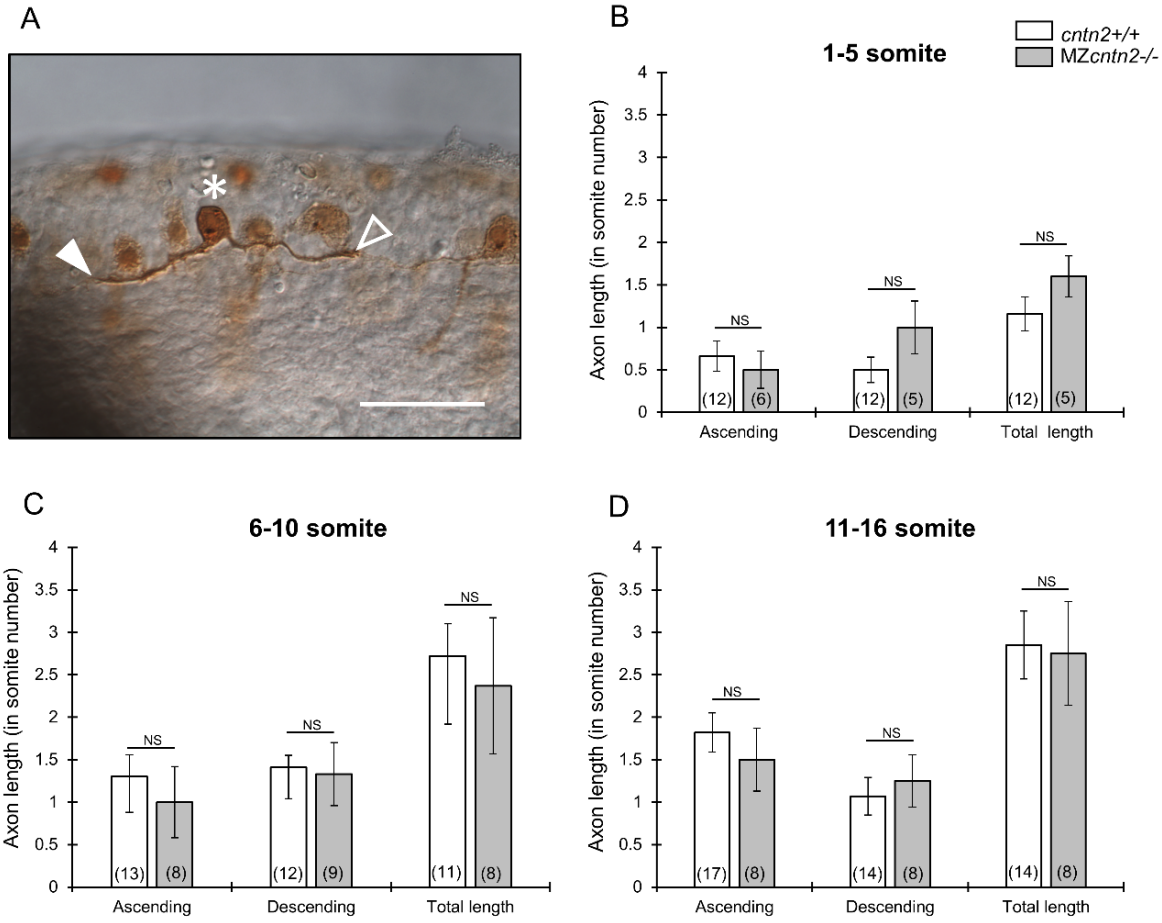

Figure 3.8: Outgrowth of Rohon-Beard central axons is not affected in MZ*cntn2* mutants

(A) Embryos injected with *ngn1:GFP-caax* DNA and Tol2 transposase RNA were fixed at 18 hpf, and processed for immunohistochemistry with anti-GFP antibody to label Rohon-Beard (RB) neurons . Asterisk indicates cell body, and the filled and open arrowheads indicate ascending and descending central axons, respectively, of a labeled RB neuron. Scale bar, 50 μm. **(B-D)** Quantification of the lengths of ascending and descending central axons, and total length (sum of ascending and descending lengths) of central axons of RB neurons located in the anterior (somites 1-5), intermediate (somite 6-10) and posterior (somites 11-16) regions of the spinal cord. There were no significant differences in the length of RB central axons between wildtype and MZ*cntn2* mutant embryos. Number of RB neurons scored is shown in parenthesis. Unpaired t-test; NS: not significant. Error bars show Mean ± SEM.

Figure 3.9: ***cntn2*** **mutants exhibit defective touch responses**

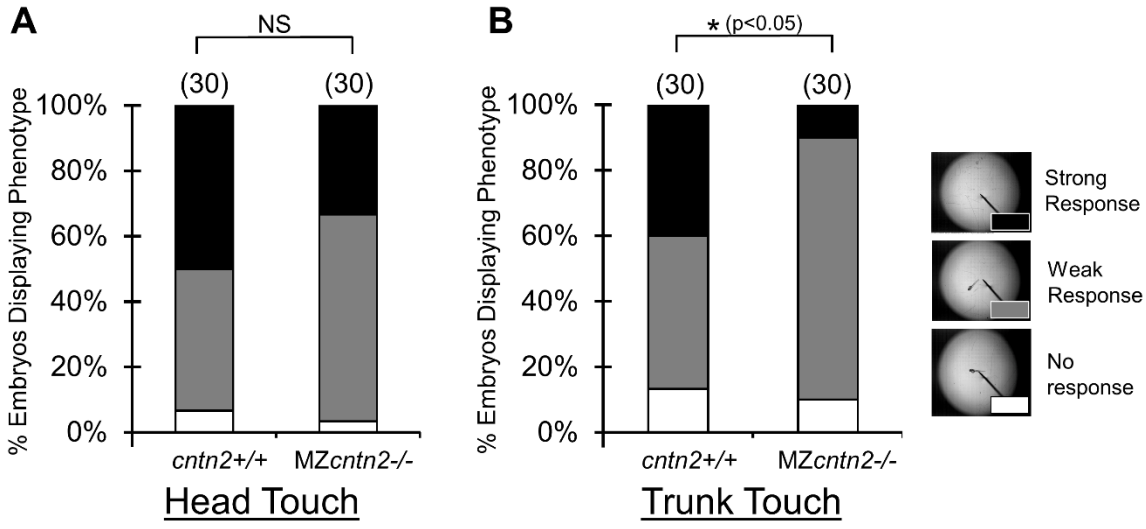

Figure 3.9: ***cntn2*** **mutants exhibit defective touch responses**

(A, B) Distribution of touch-evoked escape responses of 2 dpf *cntn2*+/+ and MZ*cntn2*-/- embryos following a head touch (A) or a trunk touch (B). The larval responses were binned into three categories: No response (no movement after touch), Weak Response (muted movement with larva remaining in the field of view), and Strong Response (rapid and vigorous movement with larva swimming out of the field of view). MZ*cntn2*-/- mutants responded similarly to control *cntn2*+/+ larvae when touched on the head. However, they exhibited much weaker escape responses compared to *cntn2*+/+ larvae when touched in the trunk. Data pooled from 2 experiments (number of embryos in parenthesis). *Chi-square test at $p<0.05$; NS: not significant.

Figure 3.10: Spinal motor axons develop normally in *cntn2* mutants

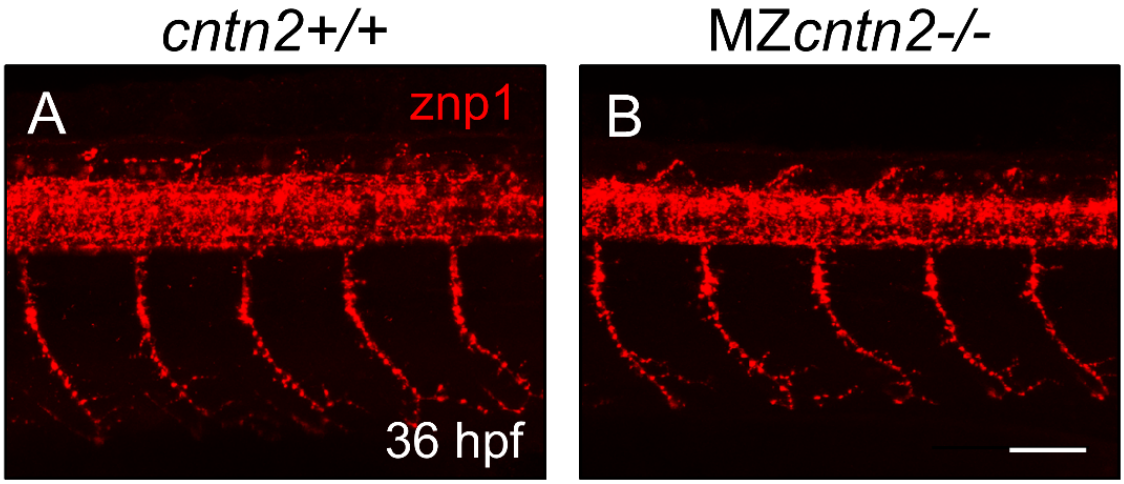

Figure 3.10: Spinal motor axons develop normally in *cntn2* mutants

Lateral views of the trunk with anterior to the left, in 36 hpf embryos stained with znp1 antibody. (A) In a wildtype embryo, the motor axon fascicles have extended into the ventral trunk musculature. (B) In a MZ*cntn2* mutant, the pattern of motor axon outgrowth is not affected. Scale bar in B, 50 μm for A and B.

Figure 3.11: *cntn2* mutants exhibit swimming deficits

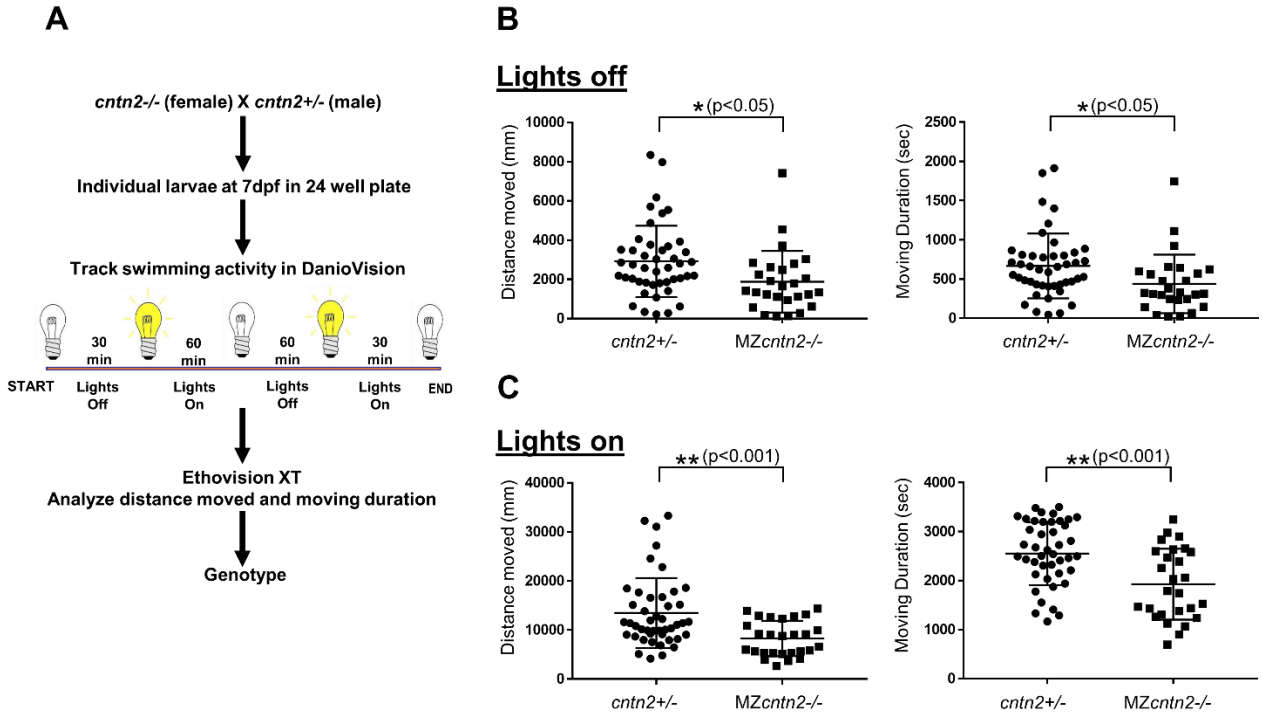

Figure 3.11: *cntn2* mutants exhibit swimming deficits

(A) Swimming assay and analysis. **(B, C)** Distance moved and moving duration are compared between *cntn2*+/- heterozygote and MZ*cntn2*-/- mutant larvae during Lights off (B) and Lights on (C) phases. There were significant differences between *cntn2*+/- (n=43) and MZ*cntn2*-/- (n=27). MZ*cntn2*-/- larvae moved less than *cntn2*+/- siblings during both lights off (unpaired t-test, *p<0.05) and lights on (unpaired t-test with Welch's correction, **p<0.001) phases (B, C). MZ*cntn2*-/- larvae also moved for shorter duration compared to *cntn2*+/- siblings during both lights off (unpaired t-test, *p<0.05) and lights on (unpaired t-test, **p<0.001) phases (B, C). Error bars show Mean ± SD.

Figure 3.12: Retinal ganglion cell axon fascicles are variably affected in *cntn2* mutants

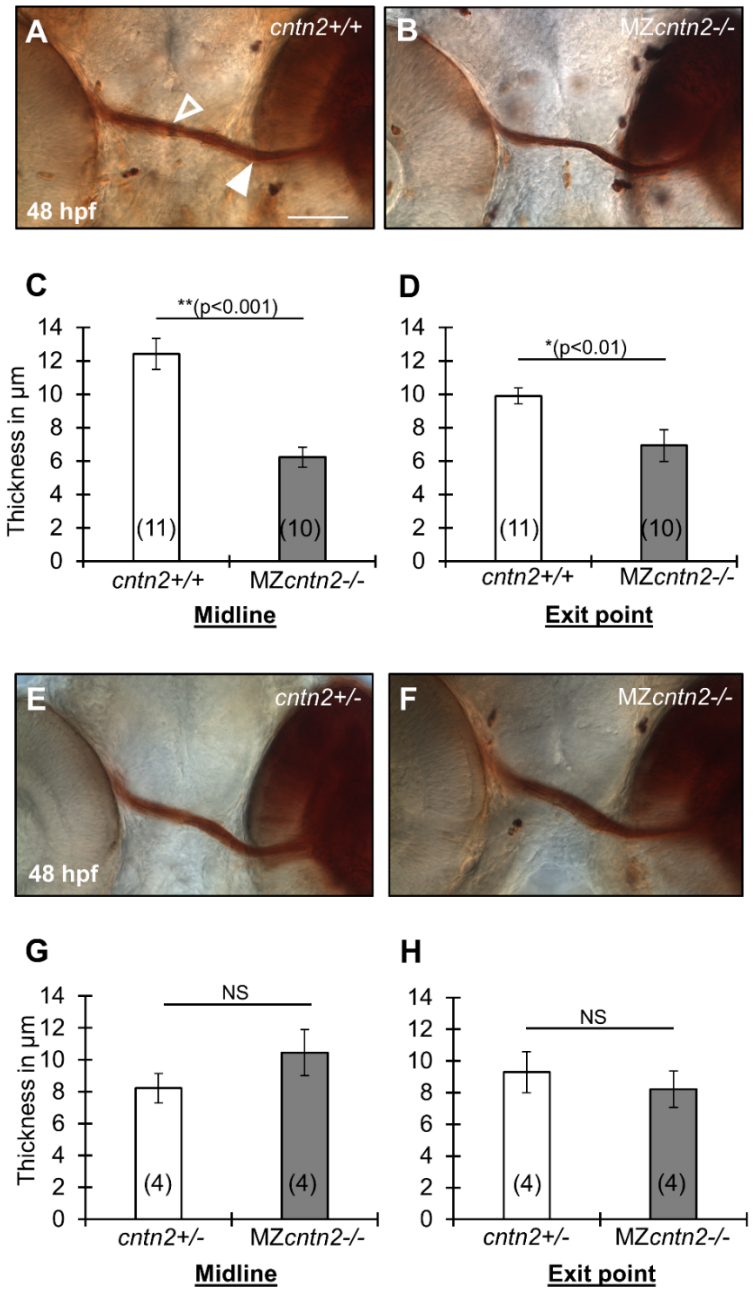

Figure 3.12: Retinal ganglion cell axon fascicles are variably affected in *cntn2* mutants

(A, B, E, F) Ventral view of DiI-labeled retinal ganglion cell (RGC) axon fascicles after photoconversion in *cntn2*+/+ (A), *cntn2*+/- (E) and MZ*cntn2*-/- (B, F) embryos at 48 hpf. The DiI-injected region targeting the nasal RGCs appears as a dark brown area on the right side in each panel. The filled arrowhead marks an RGC axon fascicle at the exit point from the eye, and the open arrowhead marks an RGC axon fascicle at the midline. **(C, D, G, H)** Summary of RGC axon fascicles thickness in wild-type and MZ*cntn2*-/- embryos. The RGC axon fascicles are significantly thinner at the midline (C) and at the exit point from the eye (D) in MZ*cntn2*-/- mutants (B) compared to *cntn2*+/+ cousins (A). However, these differences were not seen (G, H) when MZ*cntn2*-/- mutants (F) were compared to *cntn2*+/- siblings (E). Scale bar in A, 50 μm for A, B, E, and F. Unpaired t-test; NS: not significant. Error bars show Mean ± SEM.

CHAPTER 4: DIFFERENTIAL ROLES FOR SPECIFIC PLANAR CELL POLARITY (PCP) AND NON-PCP GENES DURING FACIAL BRANCHIOMOTOR NEURON MIGRATION IN ZEBRAFISH

Suman Gurung[1], Devynn Hummel[1], Isabelle Roszko[2], Diane S. Sepich[2], Lilianna Solnica-Krezel[2], and Anand Chandrasekhar[1].

1, Division of Biological Sciences and Bond Life Sciences Center, University of Missouri, Columbia, MO 65211, USA.

2, Department of Developmental Biology, Washington University School of Medicine, St Louis, MO 63110, USA.

Corresponding Author:

Dr. Anand Chandrasekhar

Division of Biological Sciences

Room 340D Bond Life Sciences Center

1201 Rollins St

University of Missouri, Columbia, MO 65211-7310

Running Title: Role of PCP and non-PCP genes in facial branchiomotor neuron migration

Keywords: Zebrafish; Neuronal Migration; Facial Branchiomotor Neuron; Wnt/PCP; Vangl2; Gpr125; Cdh2; Fzd3a; Scrb1; Cntn2; Genetic interaction

Manuscript in preparation

4.1 ABSTRACT

The caudal migration of facial branchiomotor (FBM) neurons in the vertebrate hindbrains are controlled by many genes. Many Wnt/Planar Cell Polarity (PCP) proteins are demonstrated or postulated to act at the cell surface, however, the contributions for the various proteins to neuron migration are unclear. Several but not all genes encoding components of the PCP pathway have been shown to play essential roles in FBM neuron migration in zebrafish. PCP proteins Vangl2, Pk1a, Scrb1, and Fzd3a are necessary while non-PCP proteins Cntn2, Gpr125, and Cdh2 have relatively minor roles for FBM neuron migration. In this study, we have evaluated the relative contributions of the PCP and non-PCP genes by performing several pairwise genetic interaction analyses. Several genetic combinations involving *vangl2* with PCP and non-PCP genes generate strong effects on FBM neuron migration. However, most combinations not involving *vangl2* generate weak or no effects. Together, Vangl2 appears to play a unique role in FBM neuron migration and suggest that it may play a key role in regulating the function of several PCP and non-PCP genes during FBM neuron migration.

4.2 INTRODUCTION

Neuronal migration is essential for the assembly of neural circuits that control complex behaviors. Many human brain disorders result from incorrect neuronal migration (McManus and Golden, 2005; Vajsar and Schachter, 2006). Therefore, an understanding of the molecular mechanisms regulating neuronal migration can provide insight into the pathological processes of these disorders. Migrating neurons respond to chemotactic cues in the environment and modulate cell-cell interactions with neighboring cells as they navigate from where they are born to where they end up forming functional neural circuits (Marin et al., 2010). During early development of the nervous system, migrating neurons employ two modes of migration: radial (parallel to radial glia) or tangential (orthogonal to radial glia, either occurring along the medial-lateral or anterior-posterior axes) (Pearlman et al., 1998; Rakic, 1974). Radially migrating neurons use radial glial fibers as a substrate (Campbell and Gotz, 2002), however, tangentially migrating neurons use interactions with neighboring cells and environmental cues to navigate to their final position. Cell-cell interactions, which are critical for precise neuronal migration, are mediated by a number of membrane-associated molecules (Marin et al., 2010).

Due to their conserved organization as well as the stereotypic migration, the facial branchiomotor (FBM) neurons have become an excellent model to study neuronal migration in the vertebrate embryo (Chandrasekhar, 2004; Song, 2007). Branchiomotor neurons are generated in specific rhombomeres in the hindbrain and innervate muscles

that arise in the pharyngeal arches (Chandrasekhar et al., 1997; Lumsden and Keynes, 1989; Noden, 1983). In zebrafish, the facial branchiomotor (FBM) neurons undergo a characteristic tangential migration along the rostral-caudal axis from rhombomere 4 (r4) to r6 and r7 where they form the facial motor nucleus (Chandrasekhar et al., 1997; Higashijima et al., 2000). Through forward genetic screens, several genes encoding components of the Wnt/Planar Cell Polarity (PCP) pathway have been shown to play essential roles in FBM neuron migration in zebrafish. The presumptive Wnt receptor Frizzled3a (Wada et al., 2006), the transmembrane protein Vangl2 (Bingham et al., 2002; Jessen et al., 2002), atypical cadherins Celsr 1a, 1b, and 2 (Wada et al., 2006), cytoplasmic adaptors Prickle1a (Carreira-Barbosa et al., 2003), Prickle1b (Mapp et al., 2011), and Scribble1 (Wada et al., 2005) are required for caudal migration of FBM neurons. However, in addition to these PCP genes, several non-PCP genes encoding Laminina1 (Grant and Moens, 2010; Sittaramane et al., 2009), Cadherin2 (Rebman et al., 2016; Stockinger et al., 2011), MAM domain containing glycosylphosphatidylinositol anchor 2A (Mdga2a) (Ingold et al., 2015) , chemokine receptor Cxcr4 (Cubedo et al., 2009), WAVE homology domain protein Nhsl1b (Walsh et al., 2011), RE1-silencing transcription factor (Rest) (Love and Prince, 2015), and elongation factor Spt5 (Cooper et al., 2005) have also been shown to be involved in FBM neuron migration. Interestingly, *vangl2* interacts genetically with non-PCP genes like *hdac1*, which encodes a histone deacetylase (Nambiar et al., 2007), *cntn2*, which encodes Ig superfamily cell adhesion molecule (Sittaramane et al., 2009) (Gurung et al., submitted to Mechanisms of Development), and *gpr125*, which encodes an adhesion GPCR (Li et

al., 2013), for FBM neuron migration. Moreover, mosaic analyses in zebrafish suggest that *vangl2, fzd3a, celsr2,* and *scrib* largely function non-cell autonomously during FBM neuron migration (Jessen et al., 2002; Wada et al., 2005; Wada et al., 2006)**,** and potential roles for non-neuronal cell types in regulating FBM neuron migration cannot be ruled out (Sittaramane et al., 2013). Furthermore, a ‘‘collective mode’’ of migration which depends on interactions between FBM neurons may work in a PCP-independent manner to regulate migration (Davey et al., 2016; Walsh et al., 2011). Thus far, the roles of most genes in FBM neuron migration have been examined in isolation. A notable exception is Vangl2, which plays a central role in Wnt/PCP signaling. It has been demonstrated to exhibit genetic interactions with several non-PCP (Li et al., 2013; Sittaramane et al., 2009) and PCP genes (Carreira-Barbosa et al., 2003; Montcouquiol et al., 2003; Murdoch et al., 2014). However, some of these data were generated using morpholinos. Therefore, to address the concerns with morpholino-based studies, and to obtain a more comprehensive picture of the genetic interaction landscape, we performed an extensive pairwise analysis of several PCP and non-PCP genes. We compared the FBM neuron migration phenotypes of several combinations of double heterozygotes to those of their single heterozygote siblings. We found that *vangl2* is rather unique in exhibiting genetic interactions with several PCP and non-PCP genes (*vangl2; fzd3a* and *vangl2; cdh2*, for example), while many of the other combinations (*fzd3a; scrb1* or *fzd3a; cdh2*, for example) did not exhibit genetic interactions. These data highlight the central role of Vangl2 in Wnt/PCP signaling and suggest that it may

play a key role in regulating the function of other PCP and non-PCP genes during FBM neuron migration.

4.3 RESULTS

4.3.1 *vangl2* genetically interacts with *gpr125* for FBM neuron migration

Migrating neurons likely regulate their behavior by interacting with neighboring cells. *vangl2* is expressed ubiquitously during the period of FBM neuron migration and is required for and functions non-cell autonomously during FBM neuron migration (Bingham et al., 2002; Jessen et al., 2002; Sittaramane et al., 2013). Gpr125, an adhesion G protein-coupled receptor, is maternally provided and broadly expressed (Li et al., 2013) in the zebrafish. However, morpholino-mediated knockdown of *gpr125* rarely causes FBM neuron migration defects (Li et al., 2013). Consistent with this, we did not observe FBM neuron migration defects in MZ*gpr125* mutants (data not shown) suggesting that *gpr125* does not have an essential function during FBM neuron migration. However, *gpr125* has been shown to genetically interact with *vangl2* during FBM neuron migration since injection of *gpr125* MO enhances the weak FBM neuron migration phenotype of *vangl2* heterozygotes (Li et al., 2013). Since these data were obtained from MO studies, we asked if the genetic interaction between *vangl2* and *gpr125* seen previously is preserved in mutants. To test this, we examined the offspring of MZ*gpr125-/-* homozygous females and *vangl2-/-* homozygous mutant males, which

are 100% double heterozygous embryos. The FBM neuron migration in double heterozygous embryos was binned into three categories based on the positioning of FBM neurons in different rhombomeres. 1) Normal migration indicates complete migration with more than 90% (estimated) of FBM neurons ending up in r6 and r7. 2) Partial block indicates reduced FBM neuron migration out of r4 on one or both sides, with FBM neurons found throughout the migratory pathway from r4 to r7, whereas 3) severe block indicates that a large majority of FBM neurons (estimated to be substantially greater than 50%) remained in r4 on both sides. FBM neuron migration defects were more severe and frequent in *gpr125+/-; vangl2+/-* double heterozygotes (Fig. 1D), compared to *gpr125+/-* or *vangl2*+/- embryos alone (Fig. 4.1B, C). FBM neurons migrated normally in 100% of *gpr125+/-* embryos (Fig. 4.1B, E), and failed to migrate out of r4 in only 5% of *vangl2+/-* embryos (Fig. 4.1E). By contrast, FBM neurons failed to migrate out of r4 in 45% of *gpr125+/-; vangl2+/-* embryos (Fig. 4.1D, E). This genetic interaction between *gpr125* and *vangl2* using null mutant alleles is revealed only in sensitized genetic background, suggesting that *gpr125* plays a definitive but minor role during FBM migration.

To further explore a role for *gpr125* in FBM neuron migration, we examined another sensitized genetic background known to affect FBM neuron migration. Li et al., 2013 showed previously using *gpr125* MO into the *scribble1 (scrb1)* mutant that *gpr125* genetically interacts with *scrb1*, a PCP gene shown previously to regulate tangential migration of FBM neuron (Wada et al., 2005). We examined the offspring of MZ*gpr125-/-* homozygous females and *scrb1+/-* heterozygous males, 50% of which are

double heterozygous embryos. We found no embryos with severe FBM neuron migration defects, and the fraction of embryos with partial defects was comparable to that seen in *gpr125+/-* and *scrb1+/-* populations (data not shown). These data indicate that *gpr125* and *scrb1* do not interact genetically for FBM neuron migration and suggest that some morphant-associated phenotypes may not reflect true functions of *gpr125* as seen previously between *cntn2* and *lamc1* (Gurung et al., submitted to Mechanisms of Development).

4.3.2 *vangl2* genetically interacts with cell adhesion gene *cdh2* and PCP gene *fzd3a* for FBM neuron migration

Cadherin-2 (N-cadherin; Cdh2), a family of calcium-dependent cell adhesion molecules, has been implicated to play a role in various processes during neural development including neuron migration, axon elongation, pathfinding and fasciculation, target recognition and synaptogenesis (Suzuki and Takeichi, 2008). Cadherin-2 is expressed in both migrating FBMNs and the surrounding neuroepithelial cells (Hong and Brewster, 2006; Lele et al., 2002; Stockinger et al., 2011), and is required for FBM neuron migration (Rebman et al., 2016; Stockinger et al., 2011; Wanner and Prince, 2013). *fzd3a*, a PCP gene, is expressed throughout the hindbrain during the migration of FBM neurons and is required for and functions non-cell autonomously during FBM neuron migration (Wada et al., 2006). Given the unique nature of *vangl2* in exhibiting genetic interactions with several non-PCP (Li et al., 2013; Sittaramane et al., 2009) and

PCP genes (Carreira-Barbosa et al., 2003; Montcouquiol et al., 2003; Murdoch et al., 2014), we tested for genetic interaction between *vangl2-cdh2* and *vangl2-fzd3a*. To test this, we examined the offspring of *vangl2+/-* heterozygous and *cdh2+/-* heterozygous fish, which are 50% *vangl2+/-* heterozygous embryos, out of which 50% are *vangl2+/-; cdh2+/-* double heterozygous embryos. FBM neuron migration defects were more severe and frequent in embryos obtained from crossing *vangl2+/-* heterozygous and *cdh2+/-* heterozygous fish, compared to embryos obtained from crossing *vangl2+/-* heterozygous fish to wildtype fish which also generates 50% *vangl2+/-* heterozygous embryos. FBM neurons failed to migrate out of r4 in only 10% of embryos obtained from crossing *vangl2+/-* heterozygous fish to wildtype fish (Fig. 4.2). By contrast, FBM neurons failed to migrate out of r4 in around 50% of embryos obtained from crossing *vangl2+/-* heterozygous and *cdh2+/-* heterozygous fish (Fig. 4.2).

To test for possible genetic interactions between *vangl2* and *fzd3a*, we examined the offspring of *vangl2+/-* heterozygous and *fzd3a+/-* heterozygous fish, which are 50% *vangl2+/-* heterozygous embryos, out of which 50% are *vangl2+/-; fzd3a+/-* double heterozygous. FBM neuron migration defects were more severe and frequent in embryos obtained from crossing *vangl2+/-* heterozygous and *fzd3a+/-* heterozygous fish, compared to embryos obtained from crossing *vangl2+/-* heterozygous fish to wildtype fish generating 50% *vangl2+/-* heterozygous embryos. FBM neurons failed to migrate out of r4 in only 10% of embryos obtained from crossing *vangl2+/-* heterozygous fish to wildtype fish (Fig. 4.2). By contrast, FBM neurons failed to migrate out of r4 in around 25% of embryos obtained from crossing *vangl2+/-* heterozygous and

cdh2+/- heterozygous fish (Fig. 4.2). Together these data suggest that *vangl2* genetically interacts with *cdh2* and *fzd3a* for FBM neuron migration.

4.3.3 Other PCP and non-PCP genes do not exhibit genetic interactions for FBM neuron migration

Since *vangl2* genetically interact with *cdh2* and *fzd3a* for FBM neuron migration. We tested for genetic interaction between *cdh2* and *fzd3a*. To do this, we crossed *cdh2+/-* heterozygous and *fzd3a+/-* heterozygous fish and examined the offspring which are 50% *cdh2+/-* heterozygous embryos, out of which 50% are *cdh2+/-; fzd3a+/-* double heterozygous. FBM neuron defects seen in embryos obtained from crossing *cdh2+/-* heterozygous and *fzd3a+/-* heterozygous fish was comparable to defects seen in *cdh2+/-* heterozygotes suggesting that *cdh2* and *fzd3a* do not interact with each other for FBM neuron migration. We also tested for genetic interaction between *fzda3a* and PCP gene (*scrb1)* and non-PCP genes *(lamc1 and gpr125).* However, we did not observe any pairwise genetic interaction for FBM neuron migration involving *fzd3a, scrb1, lamc1* and *gpr125*. (Fig. 4.3A).

Contactin2 (Cntn2)/Transient Axonal Glycoprotein 1 (Tag1), a GPI-linked IgSF-CAM, is implicated in the caudal migration of facial branchiomotor neuron (Sittaramane et al., 2009). Interestingly, *cntn2* and *vangl2* genetically interact during FBM neuron migration since injection of a suboptimal dose of *cntn2* MO enhances the weak FBM neuron migration phenotype of *vangl2* heterozygotes (Sittaramane et al., 2009). We

tested for genetic interaction between *cntn2* and several other PCP (*vangl2, fzd3a* and *scrb1*) and non-PCP genes (*gpr125*, *cdh2 and lamc1*) using genetic mutants. We detected interaction between *cntn2* and *vangl2* (see Chapter 3, figure 3.5) for FBM neuron migration. However, we did not observe any pairwise genetic interaction for FBM neuron migration involving *cntn2, cdh2, fzd3a, lamc1, gpr125* and *scrb1* (Fig. 4.3 and 4.4).

4.4 DISCUSSION

During the development of the nervous system, migrating neurons respond to several cues in the environment as well as the neighboring cells (Marin and Rubenstein, 2003). A large number of membrane associated molecules have been shown to play an important roles in guiding migrating neurons (Maness and Schachner, 2007). We performed an extensive pairwise analysis of several PCP (*vangl2, fzd3a, scrb1*) and non-PCP genes (*cntn2, gpr125, cdh2, lamc1*) that have been implicated in FBM neuron migration (Li et al., 2013; Rebman et al., 2016; Stockinger et al., 2011; Wada et al., 2005; Wada et al., 2006).

Vangl2, a core PCP molecule, has been shown to interact genetically with several PCP genes (Carreira-Barbosa et al., 2003; Montcouquiol et al., 2003; Murdoch et al., 2014) as well as non PCP (Li et al., 2013; Sittaramane et al., 2009) molecules. Using a combination of mutants and MOs, *vangl2* has been previously shown to genetically interact with *gpr125* for FBM neuron migration (Li et al., 2013). Interestingly, *gpr125* has also been shown to genetically with *scrb1*, a PCP gene, for FBM neuron

migration (Li et al., 2013). However, these data were generated using morpholinos. Therefore, to address the concerns with morpholino we only used genetic mutants to examine the genetic interaction. Here, using only mutants, we again observed genetic interaction between *vangl2* and *gpr125*, but not between *gpr125* and *scrb1*. These data indicate that a role for *gpr125* in FBM neuron migration can be discerned in a sensitized *vangl2+/-* background but not in a sensitized *scrb1+/-* background. These data also suggest that some morphant-associated phenotypes may not reflect true functions of *gpr125*.

Given the unique nature of *vangl2* in exhibiting genetic interactions we tested for genetic interaction between *vangl2* and a cell adhesion gene *cdh2* and PCP gene *fzd3a* for FBM neuron migration. We observed strong pairwise genetic interaction between *vangl2; cdh2* as well as *vangl2; fzd3a*. However, we did not observe any interaction between *cdh2* and *fzd3a* further suggesting the unique nature of *vangl2* for FBM neuron migration.

Together, after careful analysis of pairwise genetic interaction between several PCP and non- PCP genes, we observed strong pairwise genetic interaction involving *vangl2* with *gpr125, cdh2, cntn2* (Chapter 3) and *fzd3a* but failed to see any pairwise genetic interactions not involving *vangl2*. Vangl2 appears to play a unique role in FBM neuron migration, distinct from the roles of other PCP and non-PCP genes. The connection between identified genetic interactions and the underlying molecular mechanisms is unclear. However, these genetic interactions suggest that these proteins may participate in a multi-component signaling complex at the FBM neuron cell

membrane with membrane proteins on adjacent FBM neurons or non-neuronal cells (floor plate, neuroepithelial) to regulate neuronal migration. These data highlight the central role of Vangl2 in Wnt/PCP signaling and suggest that it may play a key role in regulating the function of other PCP and non-PCP genes during FBM neuron migration. On-going biochemical studies will determine if these proteins indeed are in a multi-protein complex.

4.4 FIGURES AND LEGENDS

Figure 4.1: *vangl2* genetically interacts with *gpr125* for FBM neuron migration

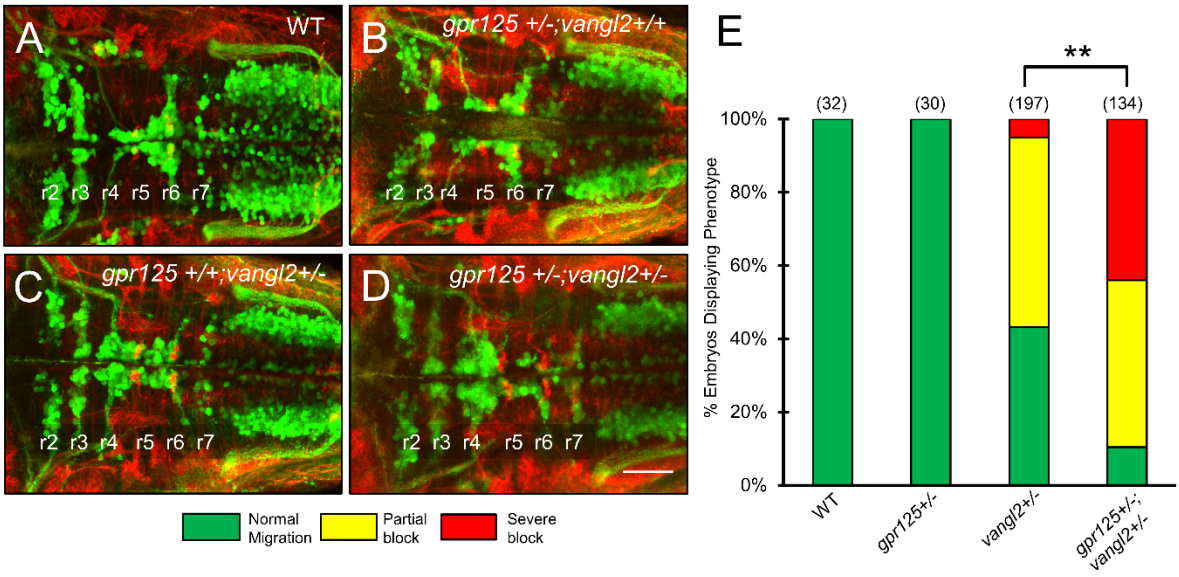

Figure 4.1: *vangl2* genetically interacts with *gpr125* for FBM neuron migration

All panels show dorsal views of the hindbrain with anterior to the left. *Tg(isl1:gfp)* embryos were fixed at 48 hpf, and processed for immunohistochemistry with zn8 antibody (red) t0 label commissural neurons and axons at rhombomere boundaries (A-D), and anti-GFP antibody (green) to label FBM neurons (A-D; arrowheads). (A) FBM neurons migrate normally in a control embryo. (B) FBM neurons migrate normally in a *gpr125* heterozygous (*gpr125+/-)* embryo. (C) FBM neurons migrate poorly in a *vangl2* heterozygous (*vangl2+/-)* embryo, with neurons located along the entire migratory pathway from r4 to r6. (D) FBM neurons fail to migrate out of r4 in a *gpr125; vangl2* double heterozygote (*gpr125+/-; vangl2+/-*). Scale bar in D, 50 μm for A-D. (E) Quantification of genetic interaction data. Number in parenthesis denotes number of embryos. **Chi-square test at $p<0.001$; NS: not significant. Data are from 2 to 4 experiments.

Figure 4.2: *vangl2* genetically interacts with cell adhesion genes *cdh2* and PCP gene *fzd3a* for FBM neuron migration

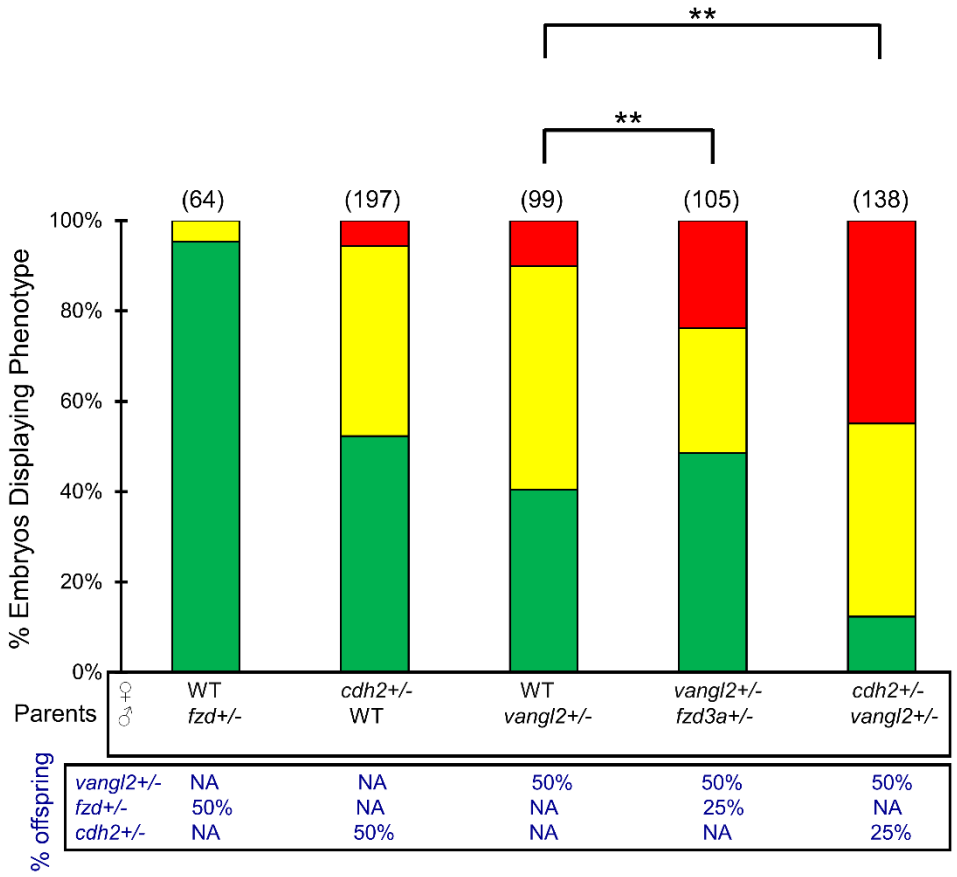

Figure 4.2: *vangl2* genetically interacts with cell adhesion genes *cdh2* and PCP gene *fzd3a* for FBM neuron migration

Quantification of genetic interaction data. Number in parenthesis denotes number of embryos. **Chi-square test at $p<0.01$; NS: not significant. Data are from 2 to 4 experiments.

Figure 4.3: Other PCP and non-PCP genes do not exhibit genetic interactions for FBM neuron migration

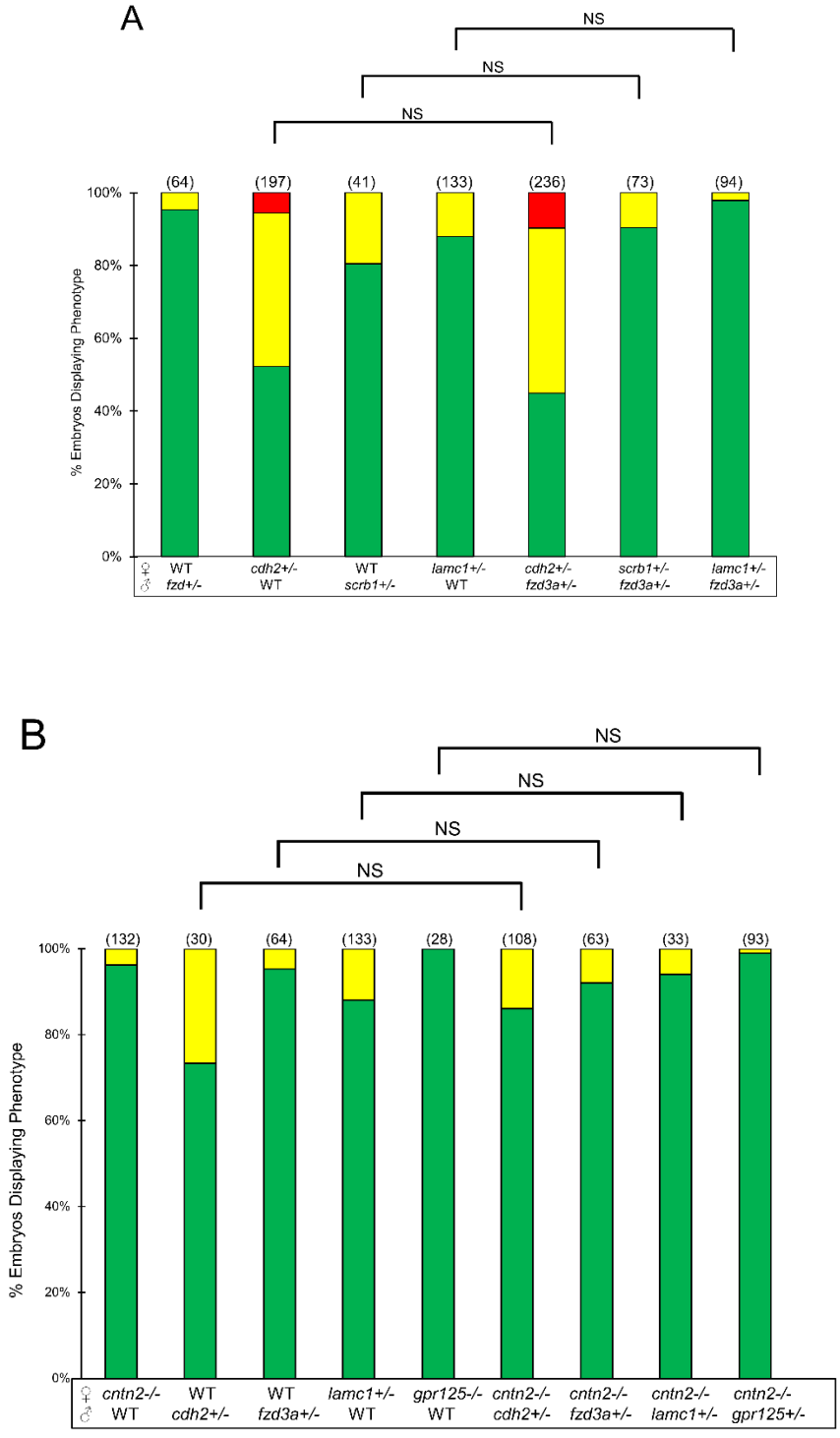

Figure 4.3: Other PCP and non-PCP genes do not exhibit genetic interactions for FBM neuron migration

Quantification of genetic interaction data. Number in parenthesis denotes number of embryos. Chi-square test. NS: not significant. Data are from 2 to 4 experiments.

Figure 4.4: Summary of pairwise genetic interaction analyses

	Vangl2	Fzd3a	Scribble 1	Gpr125	Lamc1	Cdh2	Cntn2
Vangl2	Yes						
Fzd3a	Yes	Yes					
Scribble 1	In progress	No	Yes				
Gpr125	Yes	No	No	No			
Lamc1	No	No	In progress	In progress	Yes		
Cdh2	Yes	No	In progress	In progress	In progress	Yes	
Cntn2	Yes	No	No	No	No	No	No

Figure 4.4: Summary of pairwise genetic interaction analyses

Pairwise genetic interaction tested for FBM neuron migration in this study. “Yes” indicates that the genes interact genetically for FBM neuron migration whereas “No” indicates no such genetic interaction was observed.

CHAPTER 5: CONCLUSIONS AND FUTURE DIRECTIONS

In the preceding chapters, I investigated the roles of the Ig superfamily cell adhesion molecule Cntn2 in development and function of neural circuits in zebrafish. First, I used CRISPR/Cas9 to generate *cntn2* null mutants and demonstrated that *cntn2* has a definitive but subtle role during FBM neuron migration (Chapter 3). Surprisingly, other phenotypes documented previously using morpholino-mediated *cntn2* knockdown were not seen in *cntn2* null mutants. My data showed that the dramatic morphant phenotypes were likely due to off-target effects of the *cntn2* morpholino. Importantly, however, specific neuronal and behavioral defects were seen in cntn2 null mutants. Maternal-zygotic (MZ) *cntn2* mutants exhibited axon fasciculation defects consistent with a role of Cntn2 in axon fasciculation. In addition, MZ*cntn2* mutant larvae exhibited aberrant touch responses and swimming, suggestive of defects in sensorimotor circuits, consistent with studies in mice. These data demonstrate distinct roles for zebrafish *cntn2* in neuronal migration and axon fasciculation, and in the function of sensorimotor circuits. An exhaustive genetic interaction analysis of several planar cell polarity (PCP) and non-PCP genes (Chapter 4) demonstrated that *vangl2* is rather unique in exhibiting genetic interactions with several PCP and non-PCP genes for FBM neuron migration. By contrast, all *(fzd3a, scrb1, gpr125, lamc1, cdh2)* other genes, PCP and non-PCP, involved in neuronal migration did not exhibit significant genetic interactions. These data suggest that *vangl2* might be playing a central role in regulating function of many PCP and non-PCP genes for FBM neuron migration. I discuss below some questions and ideas for future experimentation.

5.1 Do genetic interactions reflect physical interactions between membrane proteins during FBM neuron migration?

We observed genetic interactions between *vangl2* and three non-PCP genes *cntn2, gpr125*, and *cdh2*, and between *vangl2* and *fzd3a*, a PCP gene, for FBM neuron migration. These data suggest that Vangl2 might play a central role in regulating the function of many PCP and non-PCP proteins. These genetic interactions suggest that these proteins may participate in a multi-component signaling complex at the FBM neuron cell membrane with membrane proteins on adjacent FBM neurons or non-neuronal cells (floor plate, neuroepithelial) to regulate neuronal migration. We can perform biochemical studies to determine if these proteins can indeed interact within a multi-protein complex. To do this, these proteins can be tagged with distinct epitopes (GFP, V5, Myc), and the proteins can be transiently expressed in zebrafish embryos by RNA injection. Co-immunoprecipitation analysis would reveal whether any specific protein pairs are present within a membrane complex, potentially interacting physically. We have previously expressed tagged full-length Vangl2, Cntn2, and Itgα6 constructs separately in zebrafish embryos (Fig. 5.1). These analyses will be challenging because 1) all proteins being considered are membrane-associated, and coimmunoprecipitation analysis of membrane proteins is technically difficult, and 2) the proposed complexes are postulated to exist on a small group of migrating neurons and their neighboring cells in the zebrafish hindbrain, whereas these studies will employ protein-overexpressing cells isolated from the zebrafish at an earlier developmental stage.

5.2 What structural motif in Cntn2 is important for MLF axon fasciculation?

Cntn2 can act homophilically, as well as heterophilically, in cell adhesion and neurite outgrowth, and the immunoglobulin (Ig) and fibronectin (FN) domains have been implicated in both functions (Kunz et al., 2002; Pavlou et al., 2002). The FN domains and the two N-terminal Ig domains have been implicated in cell adhesion while neurite outgrowth functions may be uniformly distributed amongst the Ig and FN domains. We could test whether the Ig and FN domains have separable roles in MLF axon fasciculation by evaluating the abilities of various deletion constructs to rescue MLF defasciculation in MZ*cntn2* mutants. Variant proteins can be expressed specifically but transiently in MLF neurons by injecting Tol2-based plasmids containing *cntn2* cDNAs under the control of the *pitx2c* element (Essner et al., 2000; Kikuta and Kawakami, 2009) (see Chapter 3, Fig. 3.4). If transgene expression is variable or rescue is inconsistent in these transient-expression studies, we can perform the rescue experiments by generating stable transgenic lines for the various Cntn2 deletion variants.

5.3 Examine the function of genes misregulated in *vangl2*-deficient embryos

The membrane protein Vangl2, a core component of Wnt/Planar Cell Polarity (PCP) pathway, functions independently of PCP signaling to regulate the caudal migration of facial branchiomotor (FBM) neurons in the vertebrate hindbrain (Glasco et al., 2012; Sittaramane et al., 2013). To gain insight into the underlying mechanisms, we used transcriptomic and proteomic analyses to identify genes or proteins whose expression levels are altered in hindbrains isolated from 18 hpf Vangl2-deficient zebrafish embryos. Following bioinformatic analysis and manual curation of the top 300 misregulated genes, we generated a short list of roughly 50 candidate genes, and *itga6a, lrrtm1, and sema6dl* were among our top candidates for further analyses. These candidate genes are expressed in or around FBM neurons during the period of neuron migration (Fig. 5.2). Integrins are heterodimeric transmembrane receptors that mediate cell-adhesion (Hynes, 2002). Integrins interact with several extracellular and intracellular proteins to mediate their effects (Arnaout et al., 2007). Itga6 is a laminin binding integrin (Niculescu et al., 2011) . In zebrafish, *itga6a* is expressed broadly in the hindbrain. Interestingly, our preliminary data from morpholino studies that *itga6a* plays a role in FBM neuron migration (V. Sittaramane, S. Gurung, and A. Chandrasekhar, unpublished data). Leucine-rich repeats (LRR) are protein modules that are commonly involved in ligand receptor interactions or in cell adhesion (Kobe and Kajava, 2001).

Lrrtm1 is thought to be involved in brain development, neuronal connectivity, and synaptogenesis (Francks et al., 2007; Linhoff et al., 2009). Interestingly, *lrrtm1* is expressed in FBM neurons. The *semaphorin* gene family contains a large number of transmembrane and secreted proteins and function as repulsive and attractive cues of

axon guidance during development (Nakamura et al., 2000; Raper, 2000). *Sema6dl* is expressed in specific rhombomeres during the period of FBM neuron migration.

To directly examine the roles of these candidate genes in FBM neuron migration, I generated loss of function mutations in these genes using CRISPR-Cas9. I designed gRNAs (one target per gene) to generate frameshift mutations in several genes (*itga6a, lrrtm1, sema6dl*) at specific locations where small indels would likely cause loss of protein function. We have identified alleles for *itga6a, lrrtm1, and sema6dl* causing frameshifts that introduce early stop codons. Despite extensive analysis, I have not detected any defects in FBM neuron migration in zygotic or maternal zygotic mutants for any of these genes. However, other neuronal and behavioral phenotypes have not yet been characterized. Therefore, subtle phenotypes, as seen in MZ*cntn2* mutants, may be discovered in these mutants also.

5.4 FIGURES AND LEGENDS

Figure 5.1: Tagged constructs and their detection by western blotting.

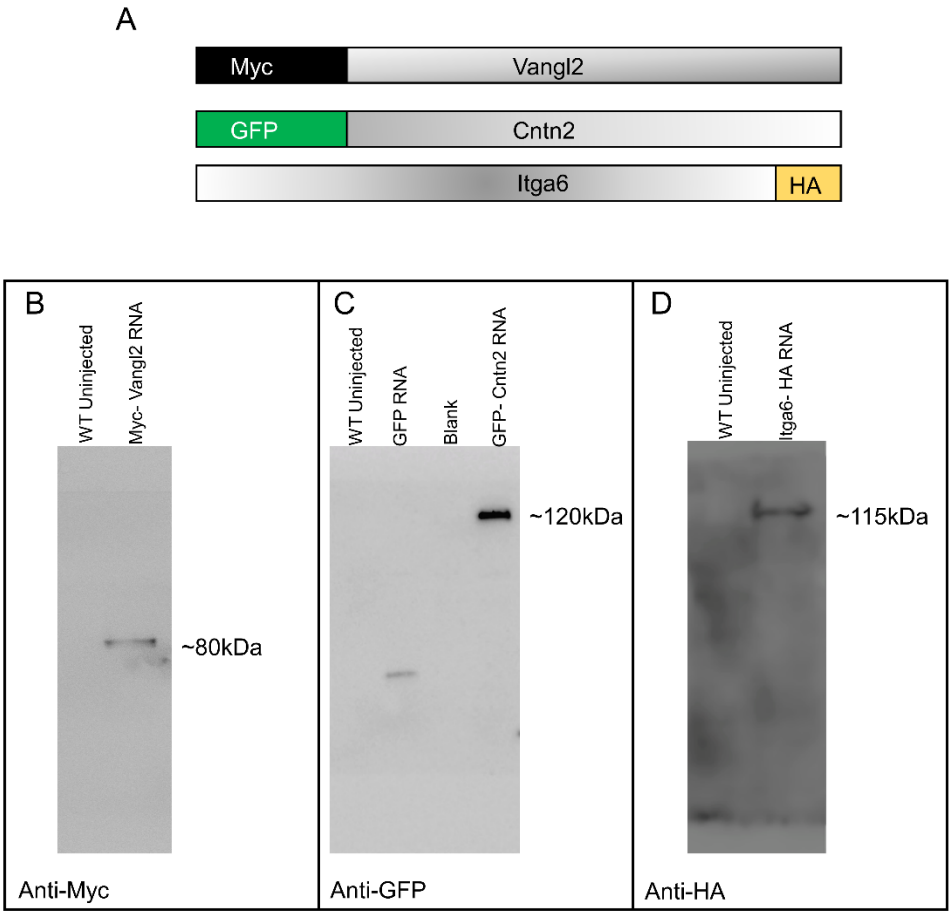

Figure 5.1: Tagged constructs and their detection by western blotting. Tagged constructs (A) Map of the tagged Vangl2, Cntn2, and Itgα6 constructs. (B, C, D) Western blots to detect tagged Vangl2, Cntn2, and Itgα6 proteins in lysates of 10 hpf zebrafish embryos injected with the synthetic capped mRNAs.

Figure 5.2: Expression pattern of candidate genes identified from transcriptomic analysis.

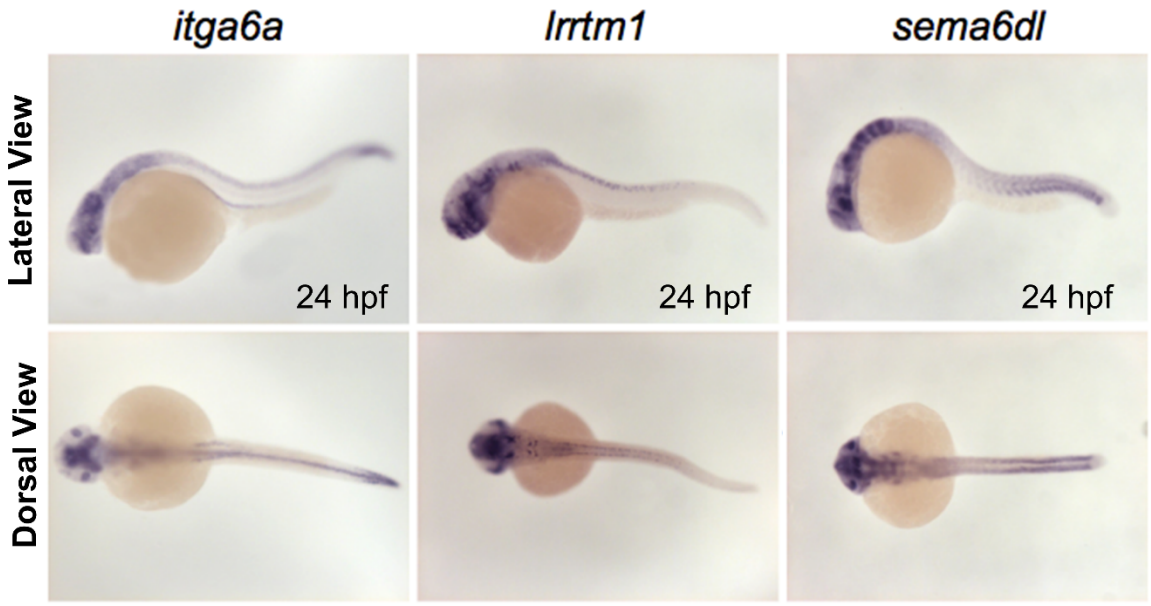

Figure 5.2: Expression pattern of candidate genes identified from transcriptomic analysis. In-situ hybridization performed at 24 hpf embryos reveal that candidate genes are expressed in or around FBM neurons during the period of neuronal migration. *Itga6a* is expressed in the lens, pronephric ducts, caudal somites and broadly in the hindbrain. *Lrrtm1* is expressed in the spinal cord, retina proliferative zone, telencephalon and diencephalon. In the hindbrain, *lrrtm1* is specifically expressed in the facial branchiomotor neuron. *Sema6dl* is expressed at the rhombomeres boundaries, somites, and the lens. In-situ images from *zfin.org*

5.5 TABLES

Table 5.1 CRISPR/Cas9 target site and oligonucleotides used to make gRNA for *itga6a*, *lrrtm1*, and *sema6dl*

Target gene	Target gene region	Target site	Oligonucleotides for annealing	
itga6a	exon 5	**GGTCGGGGATGAAAACCGTC**TGG	TA**GGTCGGGGATGAAAACCGTC**	AAAC**GACGGTTTTCATCCCCGA**
lrrtm1	exon 1	**GGGCTGATACTGTGCTCCCT**GGG	TA**GGGCTGATACTGTGCTCCCT**	AAAC**AGGGAGCACAGTATCAGC**
sema6dl	exon 3	**GGTATATTTGGTGAGTCTGA**GGG	TA**GGTATATTTGGTGAGTCTGA**	AAAC**TCAGACTCACCAAATATA**

Sequences of the genomic target sites and oligonucleotides for making the gRNA are shown. Sequence present in the gRNAs are in bold. PAM is underlined.

Table 5.2 Summary of CRISPR/Cas9 generated alleles of *itga6a*, *lrrtm1*, and *sema6dl*

Gene	Allele 1	Allele 2	Allele 3
itga6a	-11 bp (premature stop)	-4 bp (premature stop)	+7 (premature stop)
lrrtm1	-4 bp (premature stop)	+4 bp (premature stop)	-20 bp (premature stop)
sema6dl	-9 bp (in-frame deletion)	-6 bp (in-frame deletion)	-11 bp (premature stop)

CHAPTER 6: A NOVEL GENETIC CELL ABLATION TECHNOLOGY IN ZEBRAFISH

Suman Gurung[1], Marina M. Hanson[2], Devynn Hummel[1], Miriam Hankins[2], Xuebin Qin[3], Elizabeth C. Bryda[2], and Anand Chandrasekhar[1]

1, Division of Biological Sciences and Bond Life Sciences Center, University of Missouri, Columbia, MO 65211, USA

2, Department of Veterinary Pathobiology, College of Veterinary Medicine, University of Missouri, Columbia, MO 65211, USA

3, Department of Neuroscience, Temple University School of Medicine, Philadelphia, PA 19140, USA

Corresponding Author:

Dr. Anand Chandrasekhar

Division of Biological Sciences

Room 340D Bond Life Sciences Center

1201 Rollins St

University of Missouri, Columbia, MO 65211-7310

Tel: (573) 882-5166; Fax: (573) 884-9676

Email: AnandC@missouri.edu

Running Title: Genetic cell ablation technology in zebrafish

Keywords: zebrafish; cell ablation; hCD59; intermedilysin; zCREST, genetic; inducible

To be submitted to Zebrafish

6.1 ABSTRACT

Targeted cell ablation is a powerful approach to for investigating cellular functions, tissue regeneration, developmental processes and pathogenesis of human disease. Several methods have been developed to accomplish cell ablation, however, current methodologies have limitations including relatively slow onset of cell ablation. Intermedilysin (ILY) is a cytolytic pore-forming toxin secreted by *Streptococcus intermedius* that exclusively lyse human cells by specifically binding to human CD59 receptor. In this study, we have optimized physiological parameters for the application of the hCD59-ILY system in zebrafish. Embryos injected with RNA encoding wildtype hCD59 exhibited rapid tissue lysis upon ILY treatment. However, embryos injected with RNA encoding mutant hCD59 RNA, which lacks the ILY binding site, did not exhibit any cell lysis, demonstrating the specificity of the hCD59-ILY system. In addition, to validate the hCD59-ILY system in an intact embryo expressing hCD59 in specific neural cell types, we generated transgenic fish expressing hCD59 in branchiomotor neurons using zCREST promoter. ILY treatment of hCD59-expressing neurons plated in culture from this transgenic line resulted in rapid lysis, definitively demonstrating that zebrafish cells are susceptible to ablation using this system. We are currently testing the efficacy of the hCD59-ILY system to mediate rapid ablation of hCD59-expressing cells in intact embryos.

6.2 INTRODUCTION

Cell-specific ablation is a powerful tool for understanding cell lineage, cell function, developmental processes and disease mechanisms (Buch et al., 2005; Lahl et al., 2007; Luquet et al., 2005; Saito et al., 2001). Physical, chemical, and genetic methods have been developed to ablate cells ablation in various model organisms (Curado et al., 2007; Lewandoski, 2001; McGuire et al., 2004). However, current methodologies have limitations including lack of cell-type specificity, off-target effects, narrow pharmacological windows, and relatively slow onset of cell death.

Zebrafish is an excellent model system for studying development and disease. Due to their optical transparency, zebrafish embryos have proven to be an excellent experimental system for analyzing dynamic cellular processes including cell migration, axon guidance, and myelination (Bingham et al., 2002; Pogoda et al., 2006; Wolman et al., 2008), which involve intercellular interactions and signaling. Due to its regenerative abilities, zebrafish are also an excellent model system for understanding the mechanisms underlying tissue regeneration. To study the roles of specific cell types and interactions during development and regeneration, various cell ablation methods employing physical, chemical and genetic approaches have been developed. Physical ablation which includes laser ablation or tissue removal by surgery allows both temporal and spatial control (Gahtan and Baier, 2004; Yang et al., 2004). However, these methods are crude and often lack specificity, hence difficult to replicate. Furthermore, these methods are labor-intensive, requiring manual manipulation of individual samples during laser ablation or surgery. While chemical ablation such as 2-butoxyethanol (BE)

for erythrocyte ablation (Koshkaryev et al., 2003) can be less labor-intensive and time-consuming than physical ablation, it is difficult to induce ablation efficiently without toxic off-target effects (Dornfest et al., 1990; Klinken et al., 1987).

Genetically-mediated ablation involves the expression of toxin-producing enzymes or toxin-specific receptors in the cells being targeted for ablation. For example, the expression of diphtheria toxin A (DTA) using cell type-specific promoters can induce tissue-specific ablation (Kurita et al., 2003; Lee et al., 2015). However, off-target effects, as well as toxicity, have been observed. In addition, due to the high potency of DTA, leakiness of the minimal promoter can prevent the generation of transgenic zebrafish lines (Wan et al., 2006). Another genetic cell ablation system using bacterial Nitroreductase (NTR) and a nontoxic prodrug Metronidazole (Mtz), has been widely used in zebrafish to ablate cells with spatial and temporal control (Ariga et al., 2010; Chen et al., 2011; Zhao et al., 2009). Within cells expressing Nitroreductase, the enzyme converts the prodrug Mtz into a cytotoxic DNA cross-linking agent that induces cell death by apoptosis (Knox et al., 1988) (Curado et al., 2008). While the NTR/Mtz method offers clear advantages over physical and chemical ablation approaches, it can have bystander effects on neighboring cells when dying cells release the toxic drug (Grohmann et al., 2009). Another caveat of this method is the relatively slow onset of cell death. Therefore, it would be highly desirable to develop a genetic approach for targeted, rapid cell ablation.

We describe a novel cell ablation system for zebrafish that utilizes the human CD59 receptor (hCD59), and the bacterial toxin intermedilysin (ILY) (Hu et al., 2008).

hCD59 is a widely expressed cell surface 128 amino acid glycoprotein linked to the membrane through a glycosylphosphatidylinositol (GPI) anchor (Wickham et al., 2011). ILY is approximately 50 kDa toxin secreted by a Gram-positive pathogenic bacterium, *Streptococcus intermedius*, and is a member of cholesterol-dependent cytolysins (CDCs). ILY selectively binds to hCD59, but not to cognate receptors from other vertebrates (Nagamune et al., 1996), and induces pore formation and cell lysis. In mice, hCD59 has been specifically expressed particular cell types, which were lysed (ablated) rapidly following ILY treatment (Feng et al., 2016; Hu et al., 2008). We have tested the effectiveness of the hCD59-ILY cell ablation system in zebrafish.

6.3 MATERIALS AND METHODS:

6.3.1 Zebrafish husbandry and maintenance

Zebrafish (*Danio rerio*) were maintained following standard protocols and University of Missouri ACUC guidelines as described previously (Sittaramane et al., 2013; Westerfield, 1995). Embryos were grown in E3 medium at 28.5°C, staged by hours post fertilization (hpf) (Kimmel et al., 1995), and embryo age was verified at somitogenesis stages.

6.3.2 Testing for salt tolerance

For salt tolerance testing, embryos were dechorinated at 10 hpf, and exposed to a range of NaCl concentrations in E3 medium. Different NaCl concentrations were

generated by dilution using a 5 Molar NaCl stock solution. Mortality was assessed after overnight (~14 hours) incubation.

6.3.3 Assessing the effects of ILY treatment

Wildtype embryos were dechorinated at 23 hpf and incubated in E3 medium for one hour at 28.5°C. At 24 hpf, embryos were placed in the wells of a 12-well plate (20 embryos per well) containing E3 medium with 90 mM NaCl. Embryos were incubated at 37°C for 20 minutes to acclimate. Next, ILY was added to each well to a final concentration of 3-6 ng/μL, followed by incubation at 37°C. Embryo mortality (and tissue integrity) was assessed after 1 hour of incubation.

6.3.4 Intermedilysin (ILY)

ILY is a member of cholesterol-dependent cytolysins (CDCs) is composed of four structural domains (D1-D4) and is approximately 50 kDa (Nagamune et al., 1996; Ohkura et al., 2012; Tabata et al., 2014). ILY is secreted by the Gram-positive pathogenic bacterium, *Streptococcus intermedius*. Domain 1 is at the top of the molecule which acts as a foundation for other domains. Domain 2 connects domain 1 and 4. Domain 3 packs against domain 2 and forms the transmembrane β-barrel pore. Domain 4, which contains three membrane binding loops, contribute to the human specificity of ILY (Giddings et al., 2003; Giddings et al., 2004). ILY binding to CD59 triggers a series of conformational changes in ILY leading to its membrane

oligomerization which causes pore formation (Soltani et al., 2007). ILY is relatively stable between 0°C and 30°C but starts to lose its activity above 40°C with a complete loss at temperatures above 50°C (Nagamune et al., 1996).

6.3.5 hCD59 constructs and RNA synthesis

CD59, a small protein of approximately 77 amino acids and weighing 20 kDa, is ubiquitously expressed in all human tissues (Davies et al., 1989). The pCS2P+ plasmid was obtained from Addgene (#17095). In-fusion HD Cloning system (Clontech) was used to insert the ZsGreen-P2A-hCD59 fragment into the pCS2 backbone. The resulting construct is referred as wildtype (WT) *hCD59* from hereon. Mutant (Mut) *hCD59* was generated by modifying the pCS2- WT *hCD59* plasmid to delete the implicated ILY-binding domain of hCD59 (Hughes et al., 2009). The plasmids were linearized with enzyme PvuII (NEB), and capped WT *hCD59* and mut *hCD59* mRNA was synthesized using the mMessage mMachine SP6 Kit (Ambion) following manufacturer's protocol. The mRNA was checked for purity and size by gel electrophoresis, and concentration was determined using a Nanodrop spectrophotometer (Thermo Scientific).

6.3.6 Validation of *hCD59*-mediated cell ablation in transient expression assay

Wildtype nontransgenic embryos at the 1-2 cell stage were microinjected with wildtype *hCD59*, mutant *hCD59*, or *GFP* mRNA. The injection volume (and mRNA dose) was calibrated by measuring the diameter of droplets injected into mineral oil placed on a slide containing an etched micrometer scale. Approximately 600-1200 pg mRNA was injected into each embryo with an MPPI-2 pressure injector (Applied Scientific Inc.). Uninjected embryos and GFP mRNA-injected embryos from the same clutch served as controls. Injected embryos were examined for strong ZsGreen expression. Embryos with ubiquitous and high level of ZsGreen expression were dechorinated at 23 hpf and incubated in E3 medium for one hour at 28.5°C. At 24 hpf, embryos were placed in wells of 12 well plate (10 embryos per well) containing E3 medium with 90 mM NaCl, treated with ILY (4 ng/μl) or saline (control), and incubated at 37°C. Embryo health and mortality were assessed at 1 h and 24 h after ILY addition.

6.3.7 Generation of *zCREST:hCD59* transgenic zebrafish

We generated a transgenic line *Tg(zCREST:ZsGreen-hCD59),* expressing ZsGreen and hCD59 in branchiomotor neurons using Tol2 transposon-based transgenesis. The *ZsGreen-P2A-hCD59* fragment was released from the pCS2-WT *hCD59* vector and inserted into pME-MCS to generate pME-ZsGreen-P2A-hCD59 vector. The Tol2 kit was kindly provided by Kristen Kwan and Chi-Bin Chien, University of Utah (Kwan et al., 2007). We used p5E-zCREST, pME-ZsGreen-P2A-hCD59 vector, p3E-poly(A) and pDestTol2CG2 in a multiple cloning LR reaction (Kwan et al., 2007) to establish the final Tol2 vector for injecting into fertilized eggs (Fig. 6.4). 50 pg of the

Tol2-hCD59 vector was injected with 25 pg of Tol2 transposase mRNA into each fertilized egg obtained from crosses of wildtype nontransgenic fish. Injected embryos were screened at 24-36 hpf for GFP expression in the heart (Tol2 marker) and for ZsGreen expression in branchiomotor neurons and raised to adulthood. F1 progeny were screened for germline transmission of the *zCREST:ZsGreen-hCD59* transgene, and ZsGreen-expressing F2 embryos were raised to adulthood to establish the transgenic line.

6.3.8 Primary culture of zebrafish embryonic neurons

We employed a recently established protocol (Sassen et al., 2017) with minor modifications. Embryos (~200) were anesthetized with tricaine at 2-3 dpf, transferred to a 50 ml Falcon tube, and washed twice with 30% Danieau buffer. Embryos were resuspended in deyolking buffer 50% Ginzburg Fish Ringer (Whitlock and Westerfield, 2000) without calcium: 55 mM NaCl, 1.8 mM KCl, 1.25 mMNaHCO3), and deyolked by repeated trituration with 1 ml-pipette tip and brief vortexing. Deyolked embryos were pelleted at 300xg for 1 min, resuspended in 1 ml of deyolking buffer, and transferred to a sterile cell strainer (40 µm, Cat # 22-363-547, ThermoFisher) fitted for 50 ml Falcon tubes. The strainer containing deyolked embryos was dipped in 70% ethanol for 5 seconds to sterilize the tissue and submerged into culture medium (Leibovitz's L-15 medium supplemented with 10% (v/v) filtered bovine serum and 10,000 units/ml PenStrep). Embryos were transferred to a sterile 1.5 ml tube in culture medium (1 ml), and collagenase (Cat # 234155, MilliporeSigma) prepared in culture medium was added

to a final concentration of 4 mg/ml to obtain dissociated cells. The embryos were incubated on a rotator for 3 hours at room temperature with a brief vortex every 30 minutes. The dissociated embryo mixture was filtered through a sterile cell strainer into a 50 ml Falcon tube to remove debris, and washed with 1 ml of culture medium, and cells were pelleted by centrifugation (250xg, 5 min). The cell pellet was gently resuspended in 1 ml of culture medium, plated on poly-L-lysine coated plates (Cat # 08-774-124, ThermoFisher) and incubated at 28°C in a cell culture incubator without CO_2. The culture medium was replaced every 6 hours for first 12 hours, and every 12 hours thereafter. Cell density and viability were monitored using a Nikon TMS inverted scope.

6.3.9 Ablation in primary cell culture

Embryos from *Tg(zCREST:ZsGreen-hCD59)* crosses were screened for ZsGreen expression in branchiomotor neurons *Tg(isl1:gfp)* embryos (Higashijima et al., 2000), which express GFP in branchiomotor neurons, were used as controls. Primary cell cultures were established from ZsGreen- and GFP- expressing embryos, and ablation experiments were performed after 24 hours of plating. For imaging cells during the ablation process, a Zeiss Axiovert 200M inverted microscope with an environmental temperature control chamber was used with the chamber temperature set to 37°C. The cell culture dish was incubated in the chamber for 30 min to gradually bring the cultured cells up to 37°C. After locating small clusters or isolated ZsGreen- or GFP-expressing neurons, ILY was added to the culture medium, and the fluorescent cells were monitored for 30 min.

6.4 RESULTS

6.4.1 Establishing optimal conditions for testing the efficacy of ILY treatment in zebrafish embryos

Previous studies have shown that concentrations of NaCl below 50 mM completely abolish the cytolytic activity of ILY at 37°C (Nagamune et al., 1996). To evaluate the feasibility of ILY-mediated ablation in zebrafish, we first tested the tolerance of zebrafish embryos to elevated NaCl and temperature levels. Dechorionated embryos were incubated in E3 medium from 10 hpf at 28.5°C in NaCl concentrations ranging from 20 mM to 140 mM. Untreated (E3 only) embryos and embryos treated with up to 90 mM NaCl did not display any gross morphological defects or mortality (Fig. 6. 1A). However, embryos treated with NaCl concentrations greater than 90 mM exhibited significant mortality with only 20% survival at 140 mM NaCl concentration (Fig. 6.1A). This result suggests that the ILY treatments can be performed in 90 mM NaCl, which although not optimal, still supports ILY activity (Nagamune et al., 1996).

Next, to determine their tolerance to 37°C, the optimal temperature for ILY activity, zebrafish embryos at 24 hpf were incubated for 1 hour at 28°C and 37°C. No gross morphological differences or mortality were observed between the two groups and all embryos survived (data not shown), indicating that brief incubations at 37°C to induce cell death are not detrimental.

Finally, to test whether ILY itself has any detrimental effect, nontransgenic embryos were immersed in varying concentrations of ILY at elevated NaCl

concentration (90 mM) and temperature (37°C). In mammalian cells expressing hCD59, ILY induces rapid cell lysis (Hu et al., 2008). PBS-treated (control) embryos and embryos treated for 1 hour with up to 4 ng/μl of ILY did not exhibit any adverse effects or mortality (Fig. 6.1B). However, embryos treated with 5-6 ng/μl of ILY became morbid, with extensive embryo death (Fig. 6.1B), suggesting that ILY (or a breakdown product or other contaminant in the preparation) can have non-specific detrimental effects on zebrafish embryos at concentrations above 4 ng/μl. Together, these data establish that the hCD59-ILY system can be tested for feasibility in zebrafish within a defined range of NaCl and ILY concentrations.

6.4.2 ILY induces mortality in hCD59-expressing embryos, and requires the ILY-binding site

To rapidly assess the efficacy of ILY-mediated cell ablation in zebrafish, we tested the ability of ILY to kill cells in embryos expressing hCD59 transiently but ubiquitously following injection of synthetic mRNA. Uninjected or *GFP* mRNA-injected embryos were used as controls. Embryos injected with either *hCD59* or *GFP* mRNAs were positive for ZsGreen and GFP, respectively (Fig. 6.2B; data not shown). Following ILY addition, control embryos remained healthy for several hours (Fig. 6.2C, F, G), with no visible effect on any tissues. In sharp contrast, about 25% of WT hCD59-expressing embryos had dark, condensed yolk sacs within 1 hour of ILY exposure (Fig. 6.2D, F). At higher magnification, WT hCD59 expressing embryos showed vacuolation in the trunk

(Fig. 6.3). Moreover, all (100%) of the WT hCD59-expressing embryos were dead after 24 hours of ILY treatment, whereas uninjected embryos remained completely healthy (Fig. 6.2G). To determine whether ILY was inducing specific effects, we tested the effects of ILY treatment on embryos expressing a mutant hCD59 lacking the ILY-binding domain (hCD59ΔIBD; Fig. 6.2A). Embryos expressing hCD59ΔIBD remained completely healthy for 24 hours following ILY addition (Fig. 6.2E-G), suggesting strongly that ILY is specifically binding to hCD59 to induce tissue breakdown, leading to embryo mortality.

6.4.3 ILY-induced ablation of a specific cell type in transgenic embryos

To test the efficacy of the hCD59/ILY system for spatiotemporally-controlled cell ablation in zebrafish, we used the Tol2 system to generate a stable transgenic line in which ZsGreen and hCD59 are specifically expressed in branchiomotor neurons using the zCREST enhancer ((Uemura et al., 2005); Fig. 6.4A)). The generated transgenic line stably expresses ZsGreen-hCD59 in branchiomotor neurons (Fig. 6.4B). Initially we attempted to ablate ZsGreen-hCD59 expressing branchiomotor neurons by ILY treatment in transgenic embryos. However, we did not see any ablation of branchiomotor neurons after ILY treatment in intact embryos (Fig. 6.5).

Since it was unclear whether hCD59 cells within the intact embryo were being ablated following ILY treatment, we tested whether ILY could ablate hCD59-expressing cultured neurons. We cultured cells isolated from *Tg(zCREST:ZsGreen-hCD59)* embryos, which express ZsGreen and hCD59 specifically in branchiomotor neurons

(See Materials and Methods). Cells from *Tg(isl1:gfp)* embryos, which express GFP in branchiomotor neurons, were used as controls. Cultured fluorescent cells expressing GFP or ZsGreen could frequently be identified as neurons due to the presence of neurites or axonal processes. To detect dying cells unambiguously, only isolated fluorescent cells and small cell clusters (<5 cells) were analyzed. Within 5 min of ILY addition, there was a reduction of ZsGreen fluorescence intensity in these hCD59-expressing cells (Fig. 6.6B'). By 30 min, ZsGreen fluorescence intensity was greatly reduced or completely lost in the majority of cells analyzed (Fig. 6.6B'', C). In contrast, GFP fluorescence intensity in control neurons cultured from *Tg(islet1:gfp)* embryos remained unchanged up to 30 min after ILY addition (Fig. 6.6A' and 6.6A''). These data demonstrate that the ILY effectively ablated cultured zebrafish neurons expressing hCD59, while having no effect on cells not expressing hCD59. The data also suggest that the ILY-hCD59 system is working as expected in tissues within live embryos.

6.5 DISCUSSION

A large number of cell ablation techniques have been developed which have been instrumental in understanding the role of a specific cell lineage or tissue in developmental or physiological processes (Buch et al., 2005; Lahl et al., 2007; Luquet et al., 2005; Saito et al., 2001). Genetic cell ablation methods have proven to be superior over physical and chemical ablation methods which are labor intensive, time-consuming, and lack specificity. Current genetic cell ablation methods include expression of herpes simplex virus 1 thymidine kinase (HSVtk), bacterial nitroreductase,

and the diphtheria toxin (DT) receptor coupled with transgenic or viral delivery strategies. However, current genetic methodologies have limitations including lack of cell-type specificity, off-target effects, narrow pharmacological windows, and relatively slow onset of cell death.

To obviate these limitations, in this study, we aimed to provide proof of concept that ILY administration to ablate cells expressing hCD59 provides a sensitive and specific tool for cell ablation in zebrafish. The potent cytotoxin ILY, secreted by Streptococcus intermedius (SI), binds exclusively to the human cell membrane protein CD59 (hCD59) but not to CD59 of any other species tested to date (Nagamune et al., 1996). Once bound, ILY rapidly (within seconds) lyses the cells likely without creating an inflammatory reaction and without significant off-target effects. hCD59/ILY system has been recently proven successful at lysing a variety of cell types (e.g., erythrocytes and endothelia cells) in mouse transgenic models (Hu et al., 2008).

Zebrafish have become a favorite organism for studying vertebrate development. Zebrafish have large progeny clutch, breed all year, and are easily maintained. They also have transparent embryos that develop outside the mother allowing exquisite visual inspection of cell types for analysis of dynamic cellular processes. In addition, zebrafish embryo develops rapidly forming most of its tissues and organ primordia by 24 hours after fertilization. Therefore, in zebrafish, there is a great need for a rapid cell ablation system. In zebrafish, targeted conditional cell ablation system by combining the expression of bacterial Nitroreductase (NTR) enzyme in a tissue-specific manner, with treatment with the prodrug Metronidazole (Mtz), which is converted to a cytotoxic DNA

crosslinking agent by the enzymatic activity of NTR have been developed (Curado et al., 2008). The NTR/Mtz system is spatially controllable and strictly confined to the target cell population, temporally inducible, germline transmissible, and reversible (Curado et al., 2007). However, to achieve ablation using this system, fish must be treated with Mtz at near-toxic concentrations for 24 hours. In addition, a delayed continuous cell loss have been observed after Mtz removal (Mathias et al., 2014). Therefore, given this limitation of NTR/Mtz ablation system involving slow onset of cell death, we aimed to develop a rapid ablation technique and demonstrate the wide application and utility of the hCD59-ILY cell ablation system in zebrafish. In this study, using transient RNA injection and development of stable zebrafish transgenic line, we have shown that the hCD59/ILY system can be used to effectively ablate cells in zebrafish.

Since the system was optimized for mammals with different physiology than fish, our initial work involved finding optimal physiological parameters, optimal route of administration, and optimal dose. Since zebrafish embryos can easily uptake drugs in water, we employed immersion which is a non-invasive commonly used route of administering drugs in fish (Pisharath and Parsons, 2009). Moreover, this method also offers temporal control because the drugs can be added to and removed from the fish water at will (Curado et al., 2007).

Previous study has shown that the activity of ILY begins to decrease at temperatures below 20°C and is completely lost at salt concentrations less than 50 mM NaCl (Nagamune et al., 1996). Since zebrafish embryos are kept in E3 medium

(containing only 5 mM of NaCl) at 28.5°C, we tested salt and temperature tolerance of zebrafish embryos. No gross morphological differences or mortality were observed when zebrafish embryos were incubated at 37°C for up to 24 hours. To address the concern of decreased ILY activity with decreasing salt concentrations, we performed salt tolerance testing in zebrafish embryos. We found that zebrafish embryos can tolerate up to 95 mM NaCl (90 mM supplemented + 5 mM in E3 medium) without exhibiting any morphological defects or mortality. As this exceeds the 50 mM concentration required for ILY activity, we elected to perform all experiments with E3 medium supplemented with 90 mM NaCl for a final concentration of 95 mM NaCl.

ILY has previously shown to be potently hemolytic on human erythrocytes but not to nine other animal species tested including mouse, rat, chicken, rabbit, dog, cat, horse, cow and sheep (Nagamune et al., 1996). Since human CD59 receptor is more closely related to the rodent orthologue than the zebrafish, we hypothesized that ILY would not bind to zebrafish CD59 (Sun et al., 2013) and induce lysis. However, to our surprise, we found that ILY induces death at a concentration above 4 ng/μl in zebrafish embryos. It is likely that other components present in the ILY could be contributing to cell death in a non-specific manner but in a dose-dependent way. Performing mass spectrometry would help identify any toxic components present in ILY which might be contributing to death in ILY treated zebrafish embryos. Given the toxic nature of ILY at doses higher that 4 ng/μl, we performed all our immersion experiments at 4 ng/μl concentration. Embryos transiently expressing WT hCD59 began to die 1 hour after ILY immersion leading up to 100% mortality after one day. However, embryos which

transiently expressed the mutant form of hCD59 survived and did not exhibit any morphological defects suggesting that ILY is specific to hCD59 at lower concentrations where potential toxic components are diluted.

To further test the specificity of the hCD59/ILY system in zebrafish and to overcome some of the limitations of mRNA injection including the variation in expression levels of hCD59, we generated stable transgenic line expressing ZsGreen/hCD59 in branchiomotor neurons. Primary cells cultured from this transgenic line were rapidly (within 5 minutes) lysed by ILY treatment further validating the system. Ongoing studies aim to validate the hCD59-ILY system in intact transgenic embryos.

6.6 FIGURES AND LEGENDS

Figure 6.1: Assessment of high salt and ILY-induced mortality

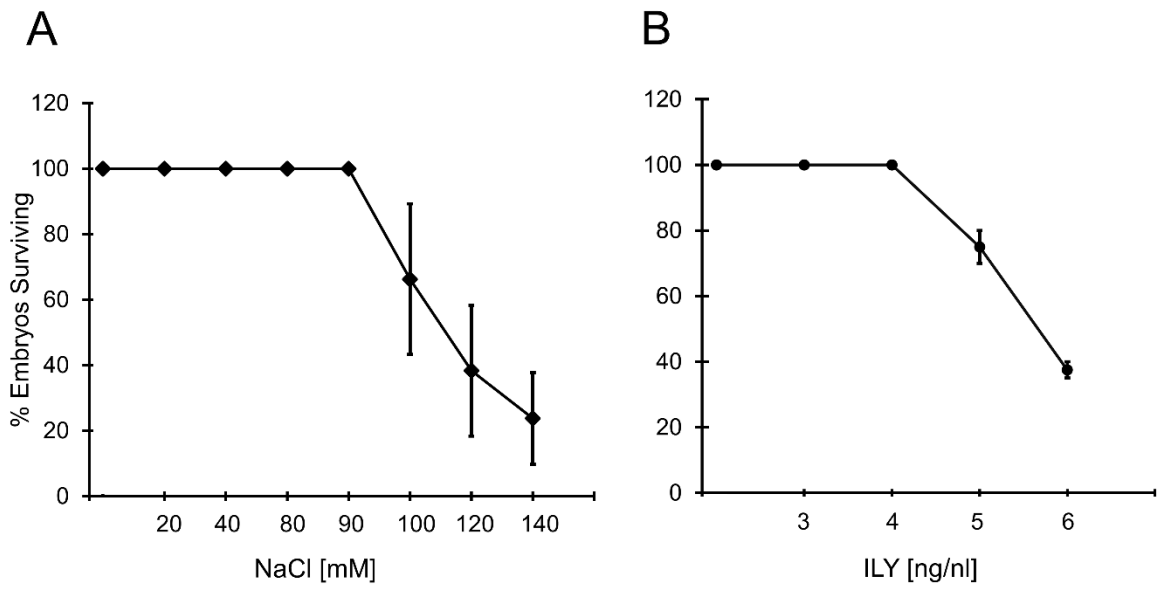

Figure 6.1 Assessment of high salt and ILY-induced mortality

(A) Wildtype (nontransgenic) embryos were treated with indicated concentrations of NaCl starting at 10 hpf. The number of the viable embryo was counted after overnight (14 hours) incubation at room temperature. Data are averages from two trails; n=40; error bars are SEM. **(B)** Wildtype (nontransgenic) embryos were treated with indicated concentrations of ILY at 24 hpf. The number of the viable embryo was counted after 1 hour incubation at 37 ºC. Data are averages from two trails; n=40; error bars are SEM.

Figure 6.2: Mortality upon exposure of mRNA injected embryos to ILY

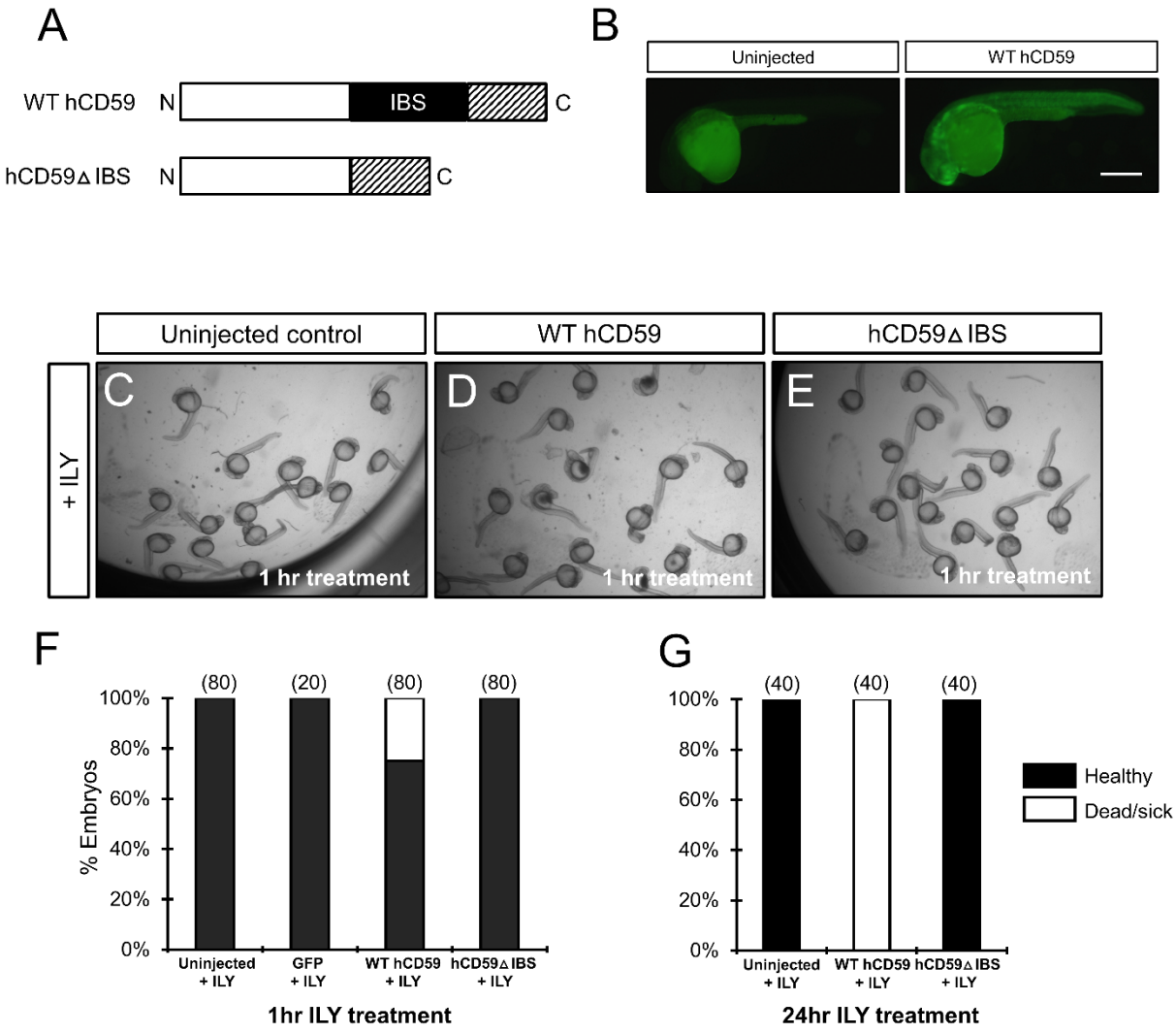

Figure 6.2: Mortality upon exposure of mRNA injected embryos to ILY

Construct used to get an expression of wildtype (WT) hCD59 and mutant hCD59 (hCD59ΔIBS) into embryos. Mutant hCD59 lacks ILY-binding domain. **(B)** Embryos injected with *hCD59* mRNA were positive for ZsGreen expression. Autofluorescence from yolk and yolk extension can be seen in both uninjected control as well as *hCD59* mRNA injected embryo. Lateral views of the embryo with anterior to the left. **(C-E)** Embryos were injected at the one-cell stage with WT *hCD59* mRNA, *hCD59Δ**IBS*** mRNA or control *GFP* mRNA. Uninjected embryos received no mRNA. Uninjected as well *hCD59Δ**IBS*** mRNA injected embryos looked morphologically normal (C, E). However, mortality was observed in WT *hCD59* mRNA injected embryos post ILY treatment (D). **(F, G)** Quantification of mortality data after 1-hour (F) and 24 hours (G) ILY immersion. The number in parenthesis denotes the number of embryos. Data are from 2-4 experiments. Scalebar in B is 400 μm.

Figure 6.3: Cell lysis upon treatment of WT hCD59-expressing embryos with ILY.

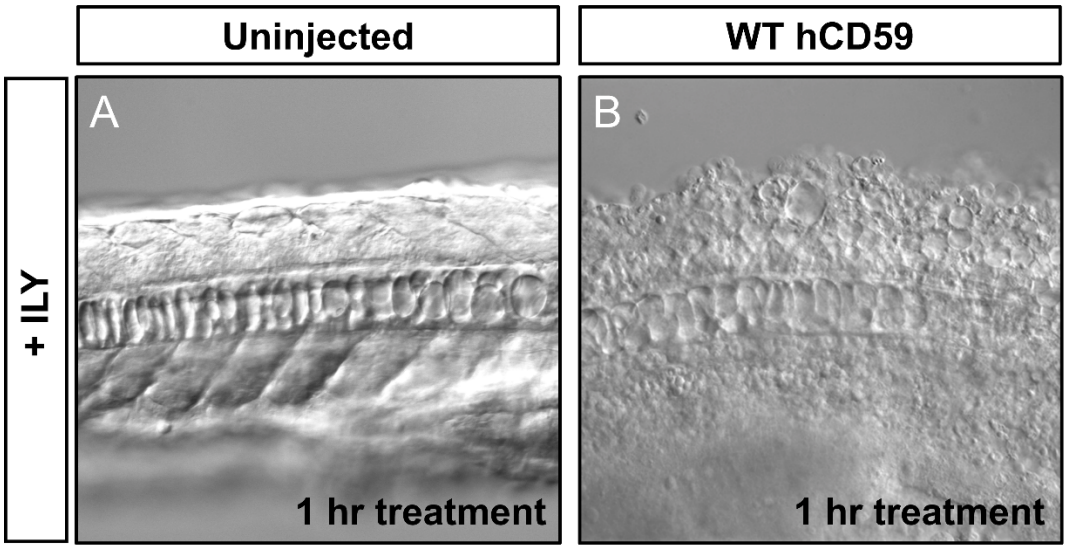

Figure 6.3: Cell lysis upon treatment of WT hCD59-expressing embryos with ILY. Lateral view of the trunk with anterior to the left. Clear somite boundaries can be seen in uninjected embryo after ILY treatment (A), however, vacuolation likely indicating lysis was observed in embryo injected with WT *hCD59* mRNA after ILY treatment (B).

Figure 6.4: Generation of transgenic line employed in this study

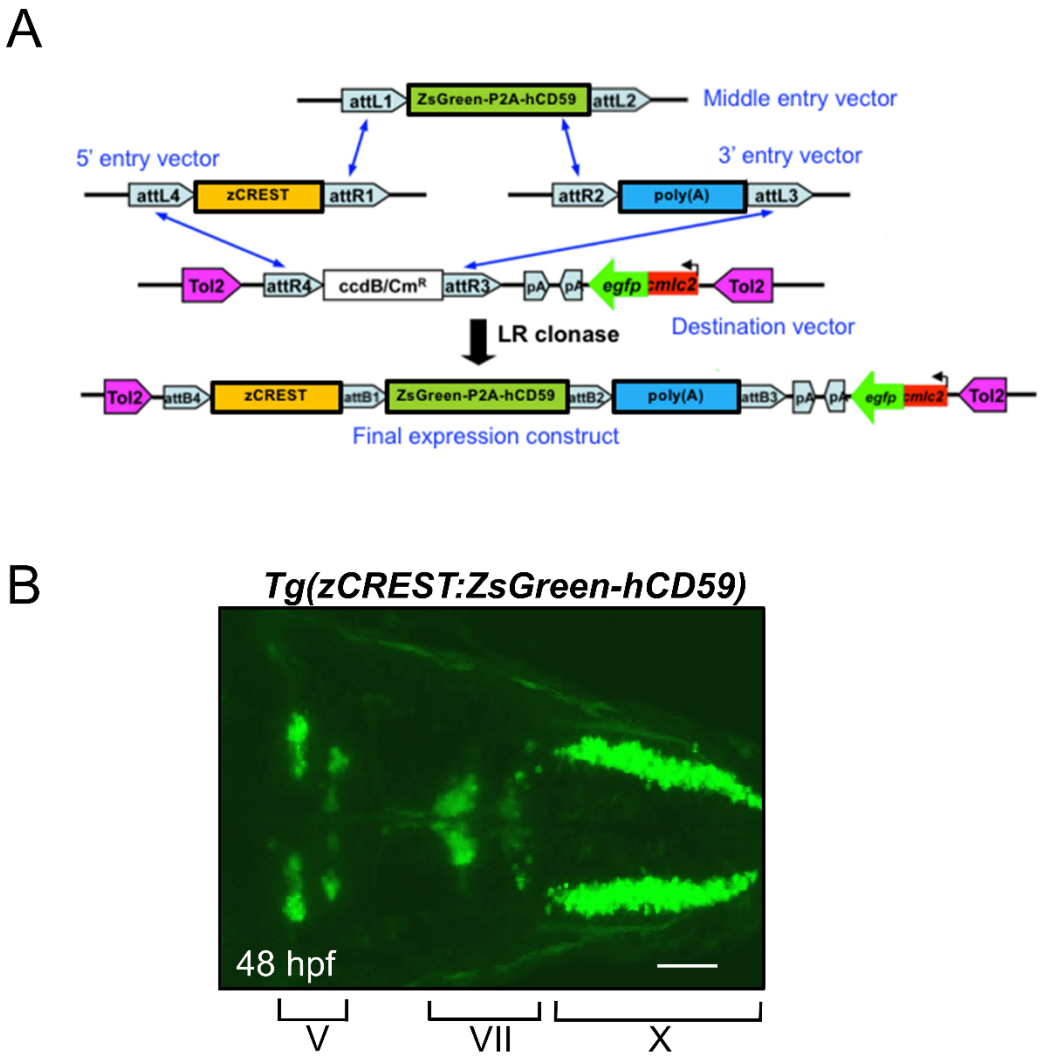

Figure 6.4: Generation of transgenic line employed in this study

(A) Schematic outlining the Gateway cloning strategy for generating a Tol2 vector to generate a stable transgenic line. The construct contains the *ZsGreen-P2A-hCD59* sequence flanked by *tol2* sequences. **(B)** Confocal *z*-stack of 48 hpf *Tg(zCREST:ZsGreen-hCD59)* embryo that was lightly fixed for 15 minutes at room temperature and mounted on PBS. ZsGreen expression can be seen in anterior and posterior clusters of trigeminal neurons (V), facial branchiomotor neurons (VII), and vagus neurons (X). Dorsal view of the hindbrain with anterior to the left.

Figure 6.5: ILY treatment in transgenic embryos

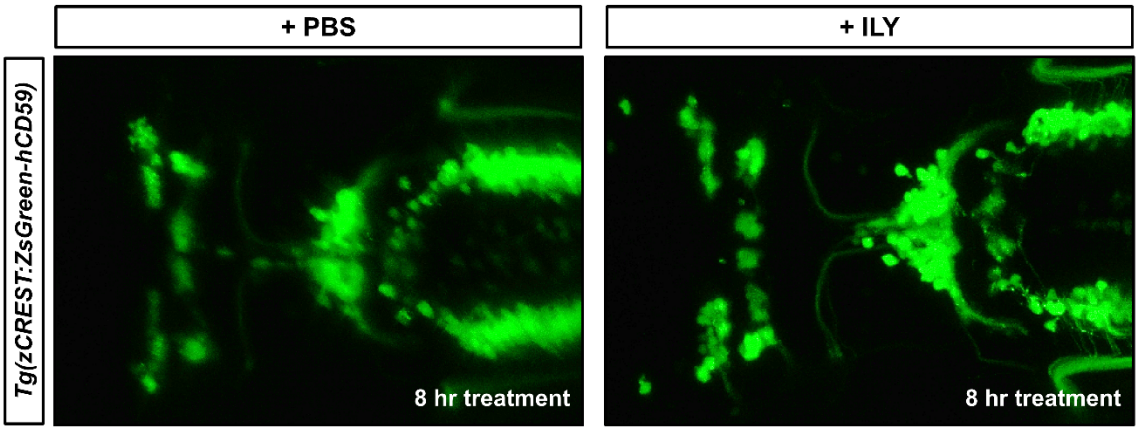

Figure 6.5: ILY treatment in transgenic embryos

Transgenic *Tg(zCREST:ZsGreen-hCD59)* embryos expressing ZsGreen-hCD59 were treated with PBS (control) or ILY(4 ng/µl) at 48 hpf and incubated at 37 ºC. No ablation was observed in both PBS treated (A) and ILY (B) treated embryos. Dorsal view with anterior to the left.

Figure 6.6: ILY induces rapid ablation of hCD59-expressing cultured neurons

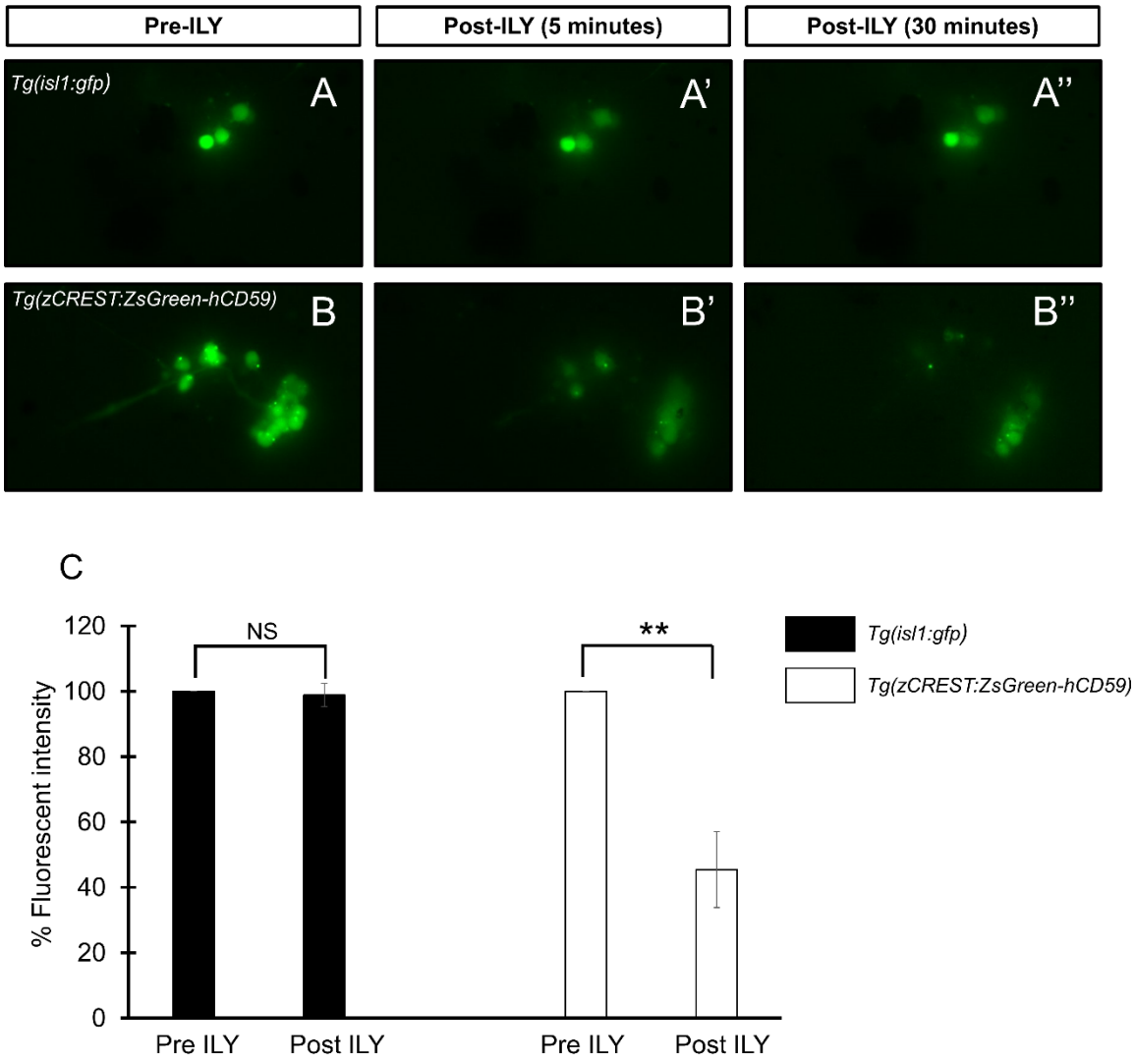

Figure 6.6: ILY induces rapid ablation of hCD59-expressing cultured neurons

Primary cells were cultured from 3 dpf *Tg(islet1:gfp)* (A) and *Tg(zCREST:ZsGreen-hcd59)* (B) embryos and plated on poly-L-lysine coated plates. Fluorescence intensity was reduced in the majority of cells from *Tg(zCREST:ZsGreen-hCD59)* embryos (B' and B'') post ILY treatment. However, no such reduction in fluorescence intensity was seen in cells from *Tg(islet1:gfp)* embryos post ILY treatment (A' and A''). C) Quantification of fluorescent intensity pre and post ILY treatment (30 minutes). **Student t-test, $p<0.001$; NS; not significant. Data are from 3 experiments.

REFERENCES

1. Amsterdam, A., Varshney, G.K., Burgess, S.M., 2011. Retroviral-mediated Insertional Mutagenesis in Zebrafish. Methods Cell Biol 104, 59-82.

2. Andersen, E.F., Asuri, N.S., Halloran, M.C., 2011. In vivo imaging of cell behaviors and F-actin reveals LIM-HD transcription factor regulation of peripheral versus central sensory axon development. Neural development 6, 27.

3. Ariga, J., Walker, S.L., Mumm, J.S., 2010. Multicolor time-lapse imaging of transgenic zebrafish: visualizing retinal stem cells activated by targeted neuronal cell ablation. Journal of visualized experiments : JoVE.

4. Arnaout, M.A., Goodman, S.L., Xiong, J.P., 2007. Structure and mechanics of integrin-based cell adhesion. Curr Opin Cell Biol 19, 495-507.

5. Arvanitis, D., Davy, A., 2008. Eph/ephrin signaling: networks. Genes Dev 22, 416-429.

6. Avci, H.X., Zelina, P., Thelen, K., Pollerberg, G.E., 2004. Role of cell adhesion molecule DM-GRASP in growth and orientation of retinal ganglion cell axons. Developmental biology 271, 291-305.

7. Barresi, M.J., Burton, S., Dipietrantonio, K., Amsterdam, A., Hopkins, N., Karlstrom, R.O., 2010. Essential genes for astroglial development and axon pathfinding during zebrafish embryogenesis. Developmental dynamics : an official publication of the American Association of Anatomists 239, 2603-2618.

8. Bastakis, G.G., Savvaki, M., Stamatakis, A., Vidaki, M., Karagogeos, D., 2015. Tag1 deficiency results in olfactory dysfunction through impaired migration of mitral cells. Development 142, 4318-4328.

9. Bernhardt, R.R., Chitnis, A.B., Lindamer, L., Kuwada, J.Y., 1990. Identification of spinal neurons in the embryonic and larval zebrafish. J Comp Neurol 302, 603-616.

10. Bill, B.R., Petzold, A.M., Clark, K.J., Schimmenti, L.A., Ekker, S.C., 2009. A primer for morpholino use in zebrafish. Zebrafish 6, 69-77.

11. Bilotta, J., 2000. Effects of abnormal lighting on the development of zebrafish visual behavior. Behavioural brain research 116, 81-87.

12. Bingham, S., Higashijima, S., Okamoto, H., Chandrasekhar, A., 2002. The Zebrafish trilobite gene is essential for tangential migration of branchiomotor neurons. Developmental biology 242, 149-160.

13. Bingham, S.M., Toussaint, G., Chandrasekhar, A., 2005. Neuronal development and migration in zebrafish hindbrain explants. Journal of neuroscience methods 149, 42-49.

14. Bomont, P., Cavalier, L., Blondeau, F., Ben Hamida, C., Belal, S., Tazir, M., Demir, E., Topaloglu, H., Korinthenberg, R., Tuysuz, B., Landrieu, P., Hentati, F., Koenig, M., 2000. The gene encoding gigaxonin, a new member of the cytoskeletal BTB/kelch repeat family, is mutated in giant axonal neuropathy. Nature genetics 26, 370-374.

15. Borovina, A., Superina, S., Voskas, D., Ciruna, B., 2010. Vangl2 directs the posterior tilting and asymmetric localization of motile primary cilia. Nature cell biology 12, 407-412.

16. Brand, M., Heisenberg, C.P., Warga, R.M., Pelegri, F., Karlstrom, R.O., Beuchle, D., Picker, A., Jiang, Y.J., Furutani-Seiki, M., van Eeden, F.J., Granato, M., Haffter, P., Hammerschmidt, M., Kane, D.A., Kelsh, R.N., Mullins, M.C., Odenthal, J., Nusslein-Volhard, C., 1996. Mutations affecting development of the midline and general body shape during zebrafish embryogenesis. Development 123, 129-142.

17. Brittis, P.A., Lemmon, V., Rutishauser, U., Silver, J., 1995. Unique changes of ganglion cell growth cone behavior following cell adhesion molecule perturbations: a time-lapse study of the living retina. Molecular and cellular neurosciences 6, 433-449.

18. Brose, K., Bland, K.S., Wang, K.H., Arnott, D., Henzel, W., Goodman, C.S., Tessier-Lavigne, M., Kidd, T., 1999. Slit proteins bind Robo receptors and have an evolutionarily conserved role in repulsive axon guidance. Cell 96, 795-806.

19. Brummendorf, T., Rathjen, F.G., 1996. Structure/function relationships of axon-associated adhesion receptors of the immunoglobulin superfamily. Current opinion in neurobiology 6, 584-593.

20. Bruno, C., Bertini, E., Federico, A., Tonoli, E., Lispi, M.L., Cassandrini, D., Pedemonte, M., Santorelli, F.M., Filocamo, M., Dotti, M.T., Schenone, A., Malandrini, A., Minetti, C., 2004. Clinical and molecular findings in patients with giant axonal neuropathy (GAN). Neurology 62, 13-16.

21. Buch, T., Heppner, F.L., Tertilt, C., Heinen, T.J., Kremer, M., Wunderlich, F.T., Jung, S., Waisman, A., 2005. A Cre-inducible diphtheria toxin receptor mediates cell lineage ablation after toxin administration. Nat Methods 2, 419-426.

22. Buchstaller, A., Kunz, S., Berger, P., Kunz, B., Ziegler, U., Rader, C., Sonderegger, P., 1996. Cell adhesion molecules NgCAM and axonin-1 form heterodimers in the neuronal membrane and cooperate in neurite outgrowth promotion. The Journal of cell biology 135, 1593-1607.

23. Caddy, J., Wilanowski, T., Darido, C., Dworkin, S., Ting, S.B., Zhao, Q., Rank, G., Auden, A., Srivastava, S., Papenfuss, T.A., Murdoch, J.N., Humbert, P.O., Parekh, V., Boulos, N., Weber, T., Zuo, J., Cunningham, J.M., Jane, S.M., 2010. Epidermal wound repair is regulated by the planar cell polarity signaling pathway. Developmental cell 19, 138-147.

24. Campbell, K., Gotz, M., 2002. Radial glia: multi-purpose cells for vertebrate brain development. Trends in neurosciences 25, 235-238.

25. Cantrell, V.A., Jessen, J.R., 2010. The planar cell polarity protein Van Gogh-Like 2 regulates tumor cell migration and matrix metalloproteinase-dependent invasion. Cancer letters 287, 54-61.

26. Carmean, V., Ribera, A.B., 2010. Genetic Analysis of the Touch Response in Zebrafish (). Int J Comp Psychol 23, 91.

27. Carreira-Barbosa, F., Concha, M.L., Takeuchi, M., Ueno, N., Wilson, S.W., Tada, M., 2003. Prickle 1 regulates cell movements during gastrulation and neuronal migration in zebrafish. Development 130, 4037-4046.

28. Chandrasekhar, A., 2004. Turning heads: development of vertebrate branchiomotor neurons. Developmental dynamics : an official publication of the American Association of Anatomists 229, 143-161.

29. Chandrasekhar, A., Moens, C.B., Warren, J.T., Jr., Kimmel, C.B., Kuwada, J.Y., 1997. Development of branchiomotor neurons in zebrafish. Development 124, 2633-2644.

30. Chandrasekhar, A., Schauerte, H.E., Haffter, P., Kuwada, J.Y., 1999. The zebrafish detour gene is essential for cranial but not spinal motor neuron induction. Development 126, 2727-2737.

31. Chang, Y.F., Imam, J.S., Wilkinson, M.F., 2007. The nonsense-mediated decay RNA surveillance pathway. Annu Rev Biochem 76, 51-74.

32. Chao, D.L., Ma, L., Shen, K., 2009. Transient cell-cell interactions in neural circuit formation. Nature reviews. Neuroscience 10, 262-271.

33. Chatzopoulou, E., Miguez, A., Savvaki, M., Levasseur, G., Muzerelle, A., Muriel, M.P., Goureau, O., Watanabe, K., Goutebroze, L., Gaspar, P., Zalc, B., Karagogeos, D., Thomas, J.L., 2008. Structural requirement of TAG-1 for retinal ganglion cell axons and myelin in the mouse optic nerve. The Journal of neuroscience : the official journal of the Society for Neuroscience 28, 7624-7636.

34. Chen, C.F., Chu, C.Y., Chen, T.H., Lee, S.J., Shen, C.N., Hsiao, C.D., 2011. Establishment of a transgenic zebrafish line for superficial skin ablation and functional validation of apoptosis modulators in vivo. PLoS One 6, e20654.

35. Chen, J.H., Wu, W., Li, H.S., Fagaly, T., Zhou, L., Wu, J.Y., Rao, Y., 2000. Embryonic expression and extracellular secretion of Xenopus slit. Neuroscience 96, 231-236.

36. Chin-Sang, I.D., George, S.E., Ding, M., Moseley, S.L., Lynch, A.S., Chisholm, A.D., 1999. The ephrin VAB-2/EFN-1 functions in neuronal signaling to regulate epidermal morphogenesis in C. elegans. Cell 99, 781-790.

37. Chitnis, A.B., Kuwada, J.Y., 1990. Axonogenesis in the brain of zebrafish embryos. The Journal of neuroscience : the official journal of the Society for Neuroscience 10, 1892-1905.

38. Ciruna, B., Jenny, A., Lee, D., Mlodzik, M., Schier, A.F., 2006. Planar cell polarity signalling couples cell division and morphogenesis during neurulation. Nature 439, 220-224.

39. Cloutier, J.F., Sahay, A., Chang, E.C., Tessier-Lavigne, M., Dulac, C., Kolodkin, A.L., Ginty, D.D., 2004. Differential requirements for semaphorin 3F and Slit-1 in axonal targeting, fasciculation, and segregation of olfactory sensory neuron projections. The Journal of neuroscience : the official journal of the Society for Neuroscience 24, 9087-9096.

40. Cooper, K.L., Armstrong, J., Moens, C.B., 2005. Zebrafish foggy/spt 5 is required for migration of facial branchiomotor neurons but not for their survival. Developmental dynamics : an official publication of the American Association of Anatomists 234, 651-658.

41. Cubedo, N., Cerdan, E., Sapede, D., Rossel, M., 2009. CXCR4 and CXCR7 cooperate during tangential migration of facial motoneurons. Molecular and cellular neurosciences 40, 474-484.

42. Culotti, J.G., Merz, D.C., 1998. DCC and netrins. Curr Opin Cell Biol 10, 609-613.

43. Cunningham, B.A., Hemperly, J.J., Murray, B.A., Prediger, E.A., Brackenbury, R., Edelman, G.M., 1987. Neural cell adhesion molecule: structure, immunoglobulin-like domains, cell surface modulation, and alternative RNA splicing. Science 236, 799-806.

44. Curado, S., Anderson, R.M., Jungblut, B., Mumm, J., Schroeter, E., Stainier, D.Y., 2007. Conditional targeted cell ablation in zebrafish: a new tool for regeneration studies. Developmental dynamics : an official publication of the American Association of Anatomists 236, 1025-1035.

45. Curado, S., Stainier, D.Y., Anderson, R.M., 2008. Nitroreductase-mediated cell/tissue ablation in zebrafish: a spatially and temporally controlled ablation method with applications in developmental and regeneration studies. Nature protocols 3, 948-954.

46. Darken, R.S., Scola, A.M., Rakeman, A.S., Das, G., Mlodzik, M., Wilson, P.A., 2002. The planar polarity gene strabismus regulates convergent extension movements in Xenopus. The EMBO journal 21, 976-985.

47. Davey, C.F., Mathewson, A.W., Moens, C.B., 2016. PCP Signaling between Migrating Neurons and their Planar-Polarized Neuroepithelial Environment Controls Filopodial Dynamics and Directional Migration. PLoS Genet 12, e1005934.

48. Davies, A., Simmons, D.L., Hale, G., Harrison, R.A., Tighe, H., Lachmann, P.J., Waldmann, H., 1989. CD59, an LY-6-like protein expressed in human lymphoid cells,

regulates the action of the complement membrane attack complex on homologous cells. J Exp Med 170, 637-654.

49. de la Rosa, E.J., Kayyem, J.F., Roman, J.M., Stierhof, Y.D., Dreyer, W.J., Schwarz, U., 1990. Topologically restricted appearance in the developing chick retinotectal system of Bravo, a neural surface protein: experimental modulation by environmental cues. The Journal of cell biology 111, 3087-3096.

50. Deiner, M.S., Kennedy, T.E., Fazeli, A., Serafini, T., Tessier-Lavigne, M., Sretavan, D.W., 1997. Netrin-1 and DCC mediate axon guidance locally at the optic disc: loss of function leads to optic nerve hypoplasia. Neuron 19, 575-589.

51. Dodd, J., Morton, S.B., Karagogeos, D., Yamamoto, M., Jessell, T.M., 1988. Spatial regulation of axonal glycoprotein expression on subsets of embryonic spinal neurons. Neuron 1, 105-116.

52. Dornfest, B.S., Bush, M.E., Lapin, D.M., Adu, S., Fulop, A., Naughton, B.A., 1990. Phenylhydrazine is a mitogen and activator of lymphoid cells. Annals of clinical and laboratory science 20, 353-370.

53. Eisen, J.S., Smith, J.C., 2008. Controlling morpholino experiments: don't stop making antisense. Development 135, 1735-1743.

54. Elsen, G.E., Choi, L.Y., Prince, V.E., Ho, R.K., 2009. The autism susceptibility gene met regulates zebrafish cerebellar development and facial motor neuron migration. Developmental biology 335, 78-92.

55. Engle, E.C., 2010. Human genetic disorders of axon guidance. Cold Spring Harb Perspect Biol 2, a001784.

56. Essner, J.J., Branford, W.W., Zhang, J., Yost, H.J., 2000. Mesendoderm and left-right brain, heart and gut development are differentially regulated by pitx2 isoforms. Development 127, 1081-1093.

57. Falk, J., Bechara, A., Fiore, R., Nawabi, H., Zhou, H., Hoyo-Becerra, C., Bozon, M., Rougon, G., Grumet, M., Puschel, A.W., Sanes, J.R., Castellani, V., 2005. Dual functional activity of semaphorin 3B is required for positioning the anterior commissure. Neuron 48, 63-75.

58. Falk, J., Bonnon, C., Girault, J.A., Faivre-Sarrailh, C., 2002. F3/contactin, a neuronal cell adhesion molecule implicated in axogenesis and myelination. Biology of the cell 94, 327-334.

59. Feng, D., Dai, S., Liu, F., Ohtake, Y., Zhou, Z., Wang, H., Zhang, Y., Kearns, A., Peng, X., Zhu, F., Hayat, U., Li, M., He, Y., Xu, M., Zhao, C., Cheng, M., Zhang, L., Wang, H., Yang, X., Ju, C., Bryda, E.C., Gordon, J., Khalili, K., Hu, W., Li, S., Qin, X., Gao, B., 2016. Cre-inducible human CD59 mediates rapid cell ablation after intermedilysin administration. The Journal of clinical investigation 126, 2321-2333.

60. Fitzli, D., Stoeckli, E.T., Kunz, S., Siribour, K., Rader, C., Kunz, B., Kozlov, S.V., Buchstaller, A., Lane, R.P., Suter, D.M., Dreyer, W.J., Sonderegger, P., 2000. A direct interaction of axonin-1 with NgCAM-related cell adhesion molecule (NrCAM) results in guidance, but not growth of commissural axons. The Journal of cell biology 149, 951-968.

61. Francks, C., Maegawa, S., Lauren, J., Abrahams, B.S., Velayos-Baeza, A., Medland, S.E., Colella, S., Groszer, M., McAuley, E.Z., Caffrey, T.M., Timmusk, T., Pruunsild, P., Koppel, I., Lind, P.A., Matsumoto-Itaba, N., Nicod, J., Xiong, L., Joober, R., Enard, W., Krinsky, B., Nanba, E., Richardson, A.J., Riley, B.P., Martin, N.G., Strittmatter, S.M., Moller, H.J., Rujescu, D., St Clair, D., Muglia, P., Roos, J.L., Fisher, S.E., Wade-Martins, R., Rouleau, G.A., Stein, J.F., Karayiorgou, M., Geschwind, D.H., Ragoussis, J., Kendler, K.S., Airaksinen, M.S., Oshimura, M., DeLisi, L.E., Monaco, A.P., 2007. LRRTM1 on chromosome 2p12 is a maternally suppressed gene that is associated paternally with handedness and schizophrenia. Molecular psychiatry 12, 1129-1139, 1057.

62. Furley, A.J., Morton, S.B., Manalo, D., Karagogeos, D., Dodd, J., Jessell, T.M., 1990. The axonal glycoprotein TAG-1 is an immunoglobulin superfamily member with neurite outgrowth-promoting activity. Cell 61, 157-170.

63. Gahtan, E., Baier, H., 2004. Of lasers, mutants, and see-through brains: functional neuroanatomy in zebrafish. Journal of neurobiology 59, 147-161.

64. Gahtan, E., Tanger, P., Baier, H., 2005. Visual prey capture in larval zebrafish is controlled by identified reticulospinal neurons downstream of the tectum. The Journal of neuroscience : the official journal of the Society for Neuroscience 25, 9294-9303.

65. Garel, S., Garcia-Dominguez, M., Charnay, P., 2000. Control of the migratory pathway of facial branchiomotor neurones. Development 127, 5297-5307.

66. Gennarini, G., Bizzoca, A., Picocci, S., Puzzo, D., Corsi, P., Furley, A.J., 2016. The role of Gpi-anchored axonal glycoproteins in neural development and neurological disorders. Molecular and cellular neurosciences.

67. George, S.E., Simokat, K., Hardin, J., Chisholm, A.D., 1998. The VAB-1 Eph receptor tyrosine kinase functions in neural and epithelial morphogenesis in C. elegans. Cell 92, 633-643.

68. Giddings, K.S., Johnson, A.E., Tweten, R.K., 2003. Redefining cholesterol's role in the mechanism of the cholesterol-dependent cytolysins. Proceedings of the National Academy of Sciences of the United States of America 100, 11315-11320.

69. Giddings, K.S., Zhao, J., Sims, P.J., Tweten, R.K., 2004. Human CD59 is a receptor for the cholesterol-dependent cytolysin intermedilysin. Nature structural & molecular biology 11, 1173-1178.

70. Gilland, E., Baker, R., 2005. Evolutionary patterns of cranial nerve efferent nuclei in vertebrates. Brain, behavior and evolution 66, 234-254.

71. Glasco, D.M., Sittaramane, V., Bryant, W., Fritzsch, B., Sawant, A., Paudyal, A., Stewart, M., Andre, P., Cadete Vilhais-Neto, G., Yang, Y., Song, M.R., Murdoch, J.N., Chandrasekhar, A., 2012. The mouse Wnt/PCP protein Vangl2 is necessary for migration of facial branchiomotor neurons, and functions independently of Dishevelled. Developmental biology 369, 211-222.

72. Golling, G., Amsterdam, A., Sun, Z., Antonelli, M., Maldonado, E., Chen, W., Burgess, S., Haldi, M., Artzt, K., Farrington, S., Lin, S.Y., Nissen, R.M., Hopkins, N., 2002. Insertional mutagenesis in zebrafish rapidly identifies genes essential for early vertebrate development. Nature genetics 31, 135-140.

73. Granato, M., van Eeden, F.J., Schach, U., Trowe, T., Brand, M., Furutani-Seiki, M., Haffter, P., Hammerschmidt, M., Heisenberg, C.P., Jiang, Y.J., Kane, D.A., Kelsh, R.N., Mullins, M.C., Odenthal, J., Nusslein-Volhard, C., 1996. Genes controlling and mediating locomotion behavior of the zebrafish embryo and larva. Development 123, 399-413.

74. Grant, P.K., Moens, C.B., 2010. The neuroepithelial basement membrane serves as a boundary and a substrate for neuron migration in the zebrafish hindbrain. Neural development 5, 9.

75. Gray, R.S., Roszko, I., Solnica-Krezel, L., 2011. Planar cell polarity: coordinating morphogenetic cell behaviors with embryonic polarity. Developmental cell 21, 120-133.

76. Grohmann, M., Paulmann, N., Fleischhauer, S., Vowinckel, J., Priller, J., Walther, D.J., 2009. A mammalianized synthetic nitroreductase gene for high-level expression. BMC cancer 9, 301.

77. Hamlin, J.A., Fang, H., Schwob, J.E., 2004. Differential expression of the mammalian homologue of fasciclin II during olfactory development in vivo and in vitro. J Comp Neurol 474, 438-452.

78. Hammerschmidt, M., Pelegri, F., Mullins, M.C., Kane, D.A., Brand, M., van Eeden, F.J., Furutani-Seiki, M., Granato, M., Haffter, P., Heisenberg, C.P., Jiang, Y.J., Kelsh, R.N., Odenthal, J., Warga, R.M., Nusslein-Volhard, C., 1996. Mutations affecting morphogenesis during gastrulation and tail formation in the zebrafish, Danio rerio. Development 123, 143-151.

79. Hao, J.C., Yu, T.W., Fujisawa, K., Culotti, J.G., Gengyo-Ando, K., Mitani, S., Moulder, G., Barstead, R., Tessier-Lavigne, M., Bargmann, C.I., 2001. C. elegans slit acts in midline, dorsal-ventral, and anterior-posterior guidance via the SAX-3/Robo receptor. Neuron 32, 25-38.

80. Hatten, M.E., 1999. Central nervous system neuronal migration. Annual review of neuroscience 22, 511-539.

81. Hatten, M.E., 2002. New directions in neuronal migration. Science 297, 1660-1663.

82. Hedgecock, E.M., Culotti, J.G., Hall, D.H., 1990. The unc-5, unc-6, and unc-40 genes guide circumferential migrations of pioneer axons and mesodermal cells on the epidermis in C. elegans. Neuron 4, 61-85.

83. Higashijima, S., Hotta, Y., Okamoto, H., 2000. Visualization of cranial motor neurons in live transgenic zebrafish expressing green fluorescent protein under the control of the islet-1 promoter/enhancer. The Journal of neuroscience : the official journal of the Society for Neuroscience 20, 206-218.

84. Hjorth, J., Key, B., 2002. Development of axon pathways in the zebrafish central nervous system. The International journal of developmental biology 46, 609-619.

85. Hoffman, E.J., Turner, K.J., Fernandez, J.M., Cifuentes, D., Ghosh, M., Ijaz, S., Jain, R.A., Kubo, F., Bill, B.R., Baier, H., Granato, M., Barresi, M.J., Wilson, S.W., Rihel, J., State, M.W., Giraldez, A.J., 2016. Estrogens Suppress a Behavioral Phenotype in Zebrafish Mutants of the Autism Risk Gene, CNTNAP2. Neuron 89, 725-733.

86. Holmes, G., Niswander, L., 2001. Expression of slit-2 and slit-3 during chick development. Developmental dynamics : an official publication of the American Association of Anatomists 222, 301-307.

87. Hong, E., Brewster, R., 2006. N-cadherin is required for the polarized cell behaviors that drive neurulation in the zebrafish. Development 133, 3895-3905.

88. Hong, K., Hinck, L., Nishiyama, M., Poo, M.M., Tessier-Lavigne, M., Stein, E., 1999. A ligand-gated association between cytoplasmic domains of UNC5 and DCC family receptors converts netrin-induced growth cone attraction to repulsion. Cell 97, 927-941.

89. Horwitz, A.R., Parsons, J.T., 1999. Cell migration--movin' on. Science 286, 1102-1103.

90. Hu, W., Ferris, S.P., Tweten, R.K., Wu, G., Radaeva, S., Gao, B., Bronson, R.T., Halperin, J.A., Qin, X., 2008. Rapid conditional targeted ablation of cells expressing human CD59 in transgenic mice by intermedilysin. Nature medicine 14, 98-103.

91. Huber, A.B., Kania, A., Tran, T.S., Gu, C., De Marco Garcia, N., Lieberam, I., Johnson, D., Jessell, T.M., Ginty, D.D., Kolodkin, A.L., 2005. Distinct roles for secreted semaphorin signaling in spinal motor axon guidance. Neuron 48, 949-964.

92. Huber, A.B., Kolodkin, A.L., Ginty, D.D., Cloutier, J.F., 2003. Signaling at the growth cone: ligand-receptor complexes and the control of axon growth and guidance. Annual review of neuroscience 26, 509-563.

93. Hughes, T.R., Ross, K.S., Cowan, G.J., Sivasankar, B., Harris, C.L., Mitchell, T.J., Morgan, B.P., 2009. Identification of the high affinity binding site in the Streptococcus

intermedius toxin intermedilysin for its membrane receptor, the human complement regulator CD59. Molecular immunology 46, 1561-1567.

94. Hummel, T., Schimmelpfeng, K., Klambt, C., 1999. Commissure formation in the embryonic CNS of Drosophila. Developmental biology 209, 381-398.

95. Hutson, L.D., Chien, C.B., 2002. Pathfinding and error correction by retinal axons: the role of astray/robo2. Neuron 33, 205-217.

96. Hwang, W.Y., Fu, Y., Reyon, D., Maeder, M.L., Tsai, S.Q., Sander, J.D., Peterson, R.T., Yeh, J.R., Joung, J.K., 2013. Efficient genome editing in zebrafish using a CRISPR-Cas system. Nature biotechnology 31, 227-229.

97. Hynes, R.O., 2002. Integrins: bidirectional, allosteric signaling machines. Cell 110, 673-687.

98. Ingold, E., Vom Berg-Maurer, C.M., Burckhardt, C.J., Lehnherr, A., Rieder, P., Keller, P.J., Stelzer, E.H., Greber, U.F., Neuhauss, S.C., Gesemann, M., 2015. Proper migration and axon outgrowth of zebrafish cranial motoneuron subpopulations require the cell adhesion molecule MDGA2A. Biol Open 4, 146-154.

99. Inoue, A., Takahashi, M., Hatta, K., Hotta, Y., Okamoto, H., 1994. Developmental regulation of islet-1 mRNA expression during neuronal differentiation in embryonic zebrafish. Developmental dynamics : an official publication of the American Association of Anatomists 199, 1-11.

100. Jao, L.E., Wente, S.R., Chen, W., 2013. Efficient multiplex biallelic zebrafish genome editing using a CRISPR nuclease system. Proceedings of the National Academy of Sciences of the United States of America 110, 13904-13909.

101. Jessell, T.M., 2000. Neuronal specification in the spinal cord: inductive signals and transcriptional codes. Nature reviews. Genetics 1, 20-29.

102. Jessen, J.R., Topczewski, J., Bingham, S., Sepich, D.S., Marlow, F., Chandrasekhar, A., Solnica-Krezel, L., 2002. Zebrafish trilobite identifies new roles for Strabismus in gastrulation and neuronal movements. Nature cell biology 4, 610-615.

103. Kaprielian, Z., Runko, E., Imondi, R., 2001. Axon guidance at the midline choice point. Developmental dynamics : an official publication of the American Association of Anatomists 221, 154-181.

104. Karlstrom, R.O., Trowe, T., Klostermann, S., Baier, H., Brand, M., Crawford, A.D., Grunewald, B., Haffter, P., Hoffmann, H., Meyer, S.U., Muller, B.K., Richter, S., van Eeden, F.J., Nusslein-Volhard, C., Bonhoeffer, F., 1996. Zebrafish mutations affecting retinotectal axon pathfinding. Development 123, 427-438.

105. Katoh, M., 2005. WNT/PCP signaling pathway and human cancer (review). Oncology reports 14, 1583-1588.

106. Kidd, T., Brose, K., Mitchell, K.J., Fetter, R.D., Tessier-Lavigne, M., Goodman, C.S., Tear, G., 1998. Roundabout controls axon crossing of the CNS midline and defines a novel subfamily of evolutionarily conserved guidance receptors. Cell 92, 205-215.

107. Kikuta, H., Kawakami, K., 2009. Transient and stable transgenesis using tol2 transposon vectors. Methods Mol Biol 546, 69-84.

108. Kimmel, C.B., Ballard, W.W., Kimmel, S.R., Ullmann, B., Schilling, T.F., 1995. Stages of embryonic development of the zebrafish. Developmental dynamics : an official publication of the American Association of Anatomists 203, 253-310.

109. Kimmel, C.B., Powell, S.L., Metcalfe, W.K., 1982. Brain neurons which project to the spinal cord in young larvae of the zebrafish. J Comp Neurol 205, 112-127.

110. Kitsukawa, T., Shimizu, M., Sanbo, M., Hirata, T., Taniguchi, M., Bekku, Y., Yagi, T., Fujisawa, H., 1997. Neuropilin-semaphorin III/D-mediated chemorepulsive signals play a crucial role in peripheral nerve projection in mice. Neuron 19, 995-1005.

111. Klinken, S.P., Holmes, K.L., Fredrickson, T.N., Erner, S.M., Morse, H.C., 3rd, 1987. Phenylhydrazine stimulates lymphopoiesis and accelerates Abelson murine leukemia virus-induced pre-B cell lymphomas. Journal of immunology 139, 3091-3098.

112. Knox, R.J., Friedlos, F., Jarman, M., Roberts, J.J., 1988. A new cytotoxic, DNA interstrand crosslinking agent, 5-(aziridin-1-yl)-4-hydroxylamino-2-nitrobenzamide, is formed from 5-(aziridin-1-yl)-2,4-dinitrobenzamide (CB 1954) by a nitroreductase enzyme in Walker carcinoma cells. Biochemical pharmacology 37, 4661-4669.

113. Kobe, B., Kajava, A.V., 2001. The leucine-rich repeat as a protein recognition motif. Current opinion in structural biology 11, 725-732.

114. Kok, F.O., Shin, M., Ni, C.W., Gupta, A., Grosse, A.S., van Impel, A., Kirchmaier, B.C., Peterson-Maduro, J., Kourkoulis, G., Male, I., DeSantis, D.F., Sheppard-Tindell, S., Ebarasi, L., Betsholtz, C., Schulte-Merker, S., Wolfe, S.A., Lawson, N.D., 2015. Reverse genetic screening reveals poor correlation between morpholino-induced and mutant phenotypes in zebrafish. Developmental cell 32, 97-108.

115. Koshkaryev, A., Barshtein, G., Nyska, A., Ezov, N., Levin-Harrus, T., Shabat, S., Nyska, M., Redlich, M., Tsipis, F., Yedgar, S., 2003. 2-Butoxyethanol enhances the adherence of red blood cells. Arch Toxicol 77, 465-469.

116. Kuhn, T.B., Stoeckli, E.T., Condrau, M.A., Rathjen, F.G., Sonderegger, P., 1991. Neurite outgrowth on immobilized axonin-1 is mediated by a heterophilic interaction with L1(G4). The Journal of cell biology 115, 1113-1126.

117. Kunz, B., Lierheimer, R., Rader, C., Spirig, M., Ziegler, U., Sonderegger, P., 2002. Axonin-1/TAG-1 mediates cell-cell adhesion by a cis-assisted trans-interaction. The Journal of biological chemistry 277, 4551-4557.

118. Kunz, S., Spirig, M., Ginsburg, C., Buchstaller, A., Berger, P., Lanz, R., Rader, C., Vogt, L., Kunz, B., Sonderegger, P., 1998. Neurite fasciculation mediated by complexes of axonin-1 and Ng cell adhesion molecule. The Journal of cell biology 143, 1673-1690.

119. Kurita, R., Sagara, H., Aoki, Y., Link, B.A., Arai, K., Watanabe, S., 2003. Suppression of lens growth by alphaA-crystallin promoter-driven expression of diphtheria toxin results in disruption of retinal cell organization in zebrafish. Developmental biology 255, 113-127.

120. Kwan, K.M., Fujimoto, E., Grabher, C., Mangum, B.D., Hardy, M.E., Campbell, D.S., Parant, J.M., Yost, H.J., Kanki, J.P., Chien, C.B., 2007. The Tol2kit: a multisite gateway-based construction kit for Tol2 transposon transgenesis constructs. Developmental dynamics : an official publication of the American Association of Anatomists 236, 3088-3099.

121. Lahl, K., Loddenkemper, C., Drouin, C., Freyer, J., Arnason, J., Eberl, G., Hamann, A., Wagner, H., Huehn, J., Sparwasser, T., 2007. Selective depletion of Foxp3+ regulatory T cells induces a scurfy-like disease. J Exp Med 204, 57-63.

122. Lang, D.M., Warren, J.T., Jr., Klisa, C., Stuermer, C.A., 2001. Topographic restriction of TAG-1 expression in the developing retinotectal pathway and target dependent reexpression during axon regeneration. Molecular and cellular neurosciences 17, 398-414.

123. Law, C.O., Kirby, R.J., Aghamohammadzadeh, S., Furley, A.J., 2008. The neural adhesion molecule TAG-1 modulates responses of sensory axons to diffusible guidance signals. Development 135, 2361-2371.

124. Lebedeva, S., de Jesus Domingues, A.M., Butter, F., Ketting, R.F., 2017. Characterization of genetic loss-of-function of Fus in zebrafish. RNA Biol 14, 29-35.

125. Lee, B., Lam, D.T., Baek, K., Yoon, J., Jeong, Y., 2015. Conditional cell ablation via diphtheria toxin reveals distinct requirements for the basal plate in the regional identity of diencephalic subpopulations. Genesis (New York, N.Y. : 2000) 53, 356-365.

126. Lele, Z., Folchert, A., Concha, M., Rauch, G.J., Geisler, R., Rosa, F., Wilson, S.W., Hammerschmidt, M., Bally-Cuif, L., 2002. parachute/n-cadherin is required for morphogenesis and maintained integrity of the zebrafish neural tube. Development 129, 3281-3294.

127. Lewandoski, M., 2001. Conditional control of gene expression in the mouse. Nature reviews. Genetics 2, 743-755.

128. Li, X., Roszko, I., Sepich, D.S., Ni, M., Hamm, H.E., Marlow, F.L., Solnica-Krezel, L., 2013. Gpr125 modulates Dishevelled distribution and planar cell polarity signaling. Development 140, 3028-3039.

129. Linhoff, M.W., Lauren, J., Cassidy, R.M., Dobie, F.A., Takahashi, H., Nygaard, H.B., Airaksinen, M.S., Strittmatter, S.M., Craig, A.M., 2009. An unbiased expression screen for synaptogenic proteins identifies the LRRTM protein family as synaptic organizers. Neuron 61, 734-749.

130. Lisabeth, E.M., Falivelli, G., Pasquale, E.B., 2013. Eph receptor signaling and ephrins. Cold Spring Harb Perspect Biol 5.

131. Liu, Y., Halloran, M.C., 2005. Central and peripheral axon branches from one neuron are guided differentially by Semaphorin3D and transient axonal glycoprotein-1. The Journal of neuroscience : the official journal of the Society for Neuroscience 25, 10556-10563.

132. Logan, C.Y., Nusse, R., 2004. The Wnt signaling pathway in development and disease. Annual review of cell and developmental biology 20, 781-810.

133. Lois, C., Garcia-Verdugo, J.M., Alvarez-Buylla, A., 1996. Chain migration of neuronal precursors. Science 271, 978-981.

134. Long, H., Sabatier, C., Ma, L., Plump, A., Yuan, W., Ornitz, D.M., Tamada, A., Murakami, F., Goodman, C.S., Tessier-Lavigne, M., 2004. Conserved roles for Slit and Robo proteins in midline commissural axon guidance. Neuron 42, 213-223.

135. Love, C.E., Prince, V.E., 2015. Rest represses maturation within migrating facial branchiomotor neurons. Developmental biology 401, 220-235.

136. Lumsden, A., Keynes, R., 1989. Segmental patterns of neuronal development in the chick hindbrain. Nature 337, 424-428.

137. Luquet, S., Perez, F.A., Hnasko, T.S., Palmiter, R.D., 2005. NPY/AgRP neurons are essential for feeding in adult mice but can be ablated in neonates. Science 310, 683-685.

138. Maness, P.F., Schachner, M., 2007. Neural recognition molecules of the immunoglobulin superfamily: signaling transducers of axon guidance and neuronal migration. Nat Neurosci 10, 19-26.

139. Mapp, O.M., Walsh, G.S., Moens, C.B., Tada, M., Prince, V.E., 2011. Zebrafish Prickle1b mediates facial branchiomotor neuron migration via a farnesylation-dependent nuclear activity. Development 138, 2121-2132.

140. Marin, O., Rubenstein, J.L., 2003. Cell migration in the forebrain. Annual review of neuroscience 26, 441-483.

141. Marin, O., Valiente, M., Ge, X., Tsai, L.H., 2010. Guiding neuronal cell migrations. Cold Spring Harb Perspect Biol 2, a001834.

142. Marlow, F., Zwartkruis, F., Malicki, J., Neuhauss, S.C., Abbas, L., Weaver, M., Driever, W., Solnica-Krezel, L., 1998. Functional interactions of genes mediating convergent extension, knypek and trilobite, during the partitioning of the eye primordium in zebrafish. Dev Biol 203, 382-399.

143. Mathias, J.R., Zhang, Z., Saxena, M.T., Mumm, J.S., 2014. Enhanced cell-specific ablation in zebrafish using a triple mutant of Escherichia coli nitroreductase. Zebrafish 11, 85-97.

144. May-Simera, H.L., Kai, M., Hernandez, V., Osborn, D.P., Tada, M., Beales, P.L., 2010. Bbs8, together with the planar cell polarity protein Vangl2, is required to establish left-right asymmetry in zebrafish. Developmental biology 345, 215-225.

145. McGuire, S.E., Roman, G., Davis, R.L., 2004. Gene expression systems in Drosophila: a synthesis of time and space. Trends in genetics : TIG 20, 384-391.

146. McManus, M.F., Golden, J.A., 2005. Neuronal migration in developmental disorders. J Child Neurol 20, 280-286.

147. Meeker, N.D., Hutchinson, S.A., Ho, L., Trede, N.S., 2007. Method for isolation of PCR-ready genomic DNA from zebrafish tissues. Biotechniques 43, 610, 612, 614.

148. Metcalfe, W.K., Myers, P.Z., Trevarrow, B., Bass, M.B., Kimmel, C.B., 1990. Primary neurons that express the L2/HNK-1 carbohydrate during early development in the zebrafish. Development 110, 491-504.

149. Miyashita, T., Yeo, S.Y., Hirate, Y., Segawa, H., Wada, H., Little, M.H., Yamada, T., Takahashi, N., Okamoto, H., 2004. PlexinA4 is necessary as a downstream target of Islet2 to mediate Slit signaling for promotion of sensory axon branching. Development 131, 3705-3715.

150. Montcouquiol, M., Rachel, R.A., Lanford, P.J., Copeland, N.G., Jenkins, N.A., Kelley, M.W., 2003. Identification of Vangl2 and Scrb1 as planar polarity genes in mammals. Nature 423, 173-177.

151. Moore, J.C., Mulligan, T.S., Torres Yordan, N., Castranova, D., Pham, V.N., Tang, Q., Lobbardi, R., Anselmo, A., Liwski, R.S., Berman, J.N., Sadreyev, R.I., Weinstein, B.M., Langenau, D.M., 2016. T cell immune deficiency in zap70 mutant zebrafish. Mol Cell Biol.

152. Muller, M., Jabs, N., Lorke, D.E., Fritzsch, B., Sander, M., 2003. Nkx6.1 controls migration and axon pathfinding of cranial branchio-motoneurons. Development 130, 5815-5826.

153. Murdoch, J.N., Damrau, C., Paudyal, A., Bogani, D., Wells, S., Greene, N.D., Stanier, P., Copp, A.J., 2014. Genetic interactions between planar cell polarity genes cause diverse neural tube defects in mice. Dis Model Mech 7, 1153-1163.

154. Nagamune, H., Ohnishi, C., Katsuura, A., Fushitani, K., Whiley, R.A., Tsuji, A., Matsuda, Y., 1996. Intermedilysin, a novel cytotoxin specific for human cells secreted by Streptococcus intermedius UNS46 isolated from a human liver abscess. Infection and immunity 64, 3093-3100.

155. Nakamura, F., Kalb, R.G., Strittmatter, S.M., 2000. Molecular basis of semaphorin-mediated axon guidance. Journal of neurobiology 44, 219-229.

156. Nambiar, R.M., Ignatius, M.S., Henion, P.D., 2007. Zebrafish colgate/hdac1 functions in the non-canonical Wnt pathway during axial extension and in Wnt-independent branchiomotor neuron migration. Mechanisms of development 124, 682-698.

157. Neuhauss, S.C., Biehlmaier, O., Seeliger, M.W., Das, T., Kohler, K., Harris, W.A., Baier, H., 1999. Genetic disorders of vision revealed by a behavioral screen of 400 essential loci in zebrafish. The Journal of neuroscience : the official journal of the Society for Neuroscience 19, 8603-8615.

158. Niculescu, C., Ganguli-Indra, G., Pfister, V., Dupe, V., Messaddeq, N., De Arcangelis, A., Georges-Labouesse, E., 2011. Conditional ablation of integrin alpha-6 in mouse epidermis leads to skin fragility and inflammation. European journal of cell biology 90, 270-277.

159. Noden, D.M., 1983. The role of the neural crest in patterning of avian cranial skeletal, connective, and muscle tissues. Developmental biology 96, 144-165.

160. Nusslein-Volhard, C., Wieschaus, E., Kluding, H., 1984. Mutations affecting the pattern of the larval cuticle inDrosophila melanogaster : I. Zygotic loci on the second chromosome. Wilehm Roux Arch Dev Biol 193, 267-282.

161. Odenthal, J., Haffter, P., Vogelsang, E., Brand, M., van Eeden, F.J., Furutani-Seiki, M., Granato, M., Hammerschmidt, M., Heisenberg, C.P., Jiang, Y.J., Kane, D.A., Kelsh, R.N., Mullins, M.C., Warga, R.M., Allende, M.L., Weinberg, E.S., Nusslein-Volhard, C., 1996. Mutations affecting the formation of the notochord in the zebrafish, Danio rerio. Development 123, 103-115.

162. Ohkura, K., Kawaguchi, Y., Tabata, A., Yamamoto, A., Shinohara, Y., Nagamune, H., Hori, H., 2012. Molecular profiles of cholesterol-dependent cytolysin family-derived 11mer regions. Anticancer research 32, 2343-2346.

163. Orger, M.B., Smear, M.C., Anstis, S.M., Baier, H., 2000. Perception of Fourier and non-Fourier motion by larval zebrafish. Nature neuroscience 3, 1128-1133.

164. Pan, X., Sittaramane, V., Gurung, S., Chandrasekhar, A., 2014. Structural and temporal requirements of Wnt/PCP protein Vangl2 function for convergence and extension movements and facial branchiomotor neuron migration in zebrafish. Mechanisms of development 131, 1-14.

165. Park, M., Moon, R.T., 2002. The planar cell-polarity gene stbm regulates cell behaviour and cell fate in vertebrate embryos. Nature cell biology 4, 20-25.

166. Parnavelas, J.G., Alifragis, P., Nadarajah, B., 2002. The origin and migration of cortical neurons. Progress in brain research 136, 73-80.

167. Parsons, M.J., Pollard, S.M., Saude, L., Feldman, B., Coutinho, P., Hirst, E.M., Stemple, D.L., 2002. Zebrafish mutants identify an essential role for laminins in notochord formation. Development 129, 3137-3146.

168. Paulus, J.D., Halloran, M.C., 2006. Zebrafish bashful/laminin-alpha 1 mutants exhibit multiple axon guidance defects. Developmental dynamics : an official publication of the American Association of Anatomists 235, 213-224.

169. Pavlou, O., Theodorakis, K., Falk, J., Kutsche, M., Schachner, M., Faivre-Sarrailh, C., Karagogeos, D., 2002. Analysis of interactions of the adhesion molecule TAG-1 and its domains with other immunoglobulin superfamily members. Molecular and cellular neurosciences 20, 367-381.

170. Pearlman, A.L., Faust, P.L., Hatten, M.E., Brunstrom, J.E., 1998. New directions for neuronal migration. Current opinion in neurobiology 8, 45-54.

171. Phillips, J.B., Blanco-Sanchez, B., Lentz, J.J., Tallafuss, A., Khanobdee, K., Sampath, S., Jacobs, Z.G., Han, P.F., Mishra, M., Titus, T.A., Williams, D.S., Keats, B.J., Washbourne, P., Westerfield, M., 2011. Harmonin (Ush1c) is required in zebrafish Muller glial cells for photoreceptor synaptic development and function. Dis Model Mech 4, 786-800.

172. Pisharath, H., Parsons, M.J., 2009. Nitroreductase-mediated cell ablation in transgenic zebrafish embryos. Methods in molecular biology (Clifton, N.J.) 546, 133-143.

173. Pocock, R., Mione, M., Hussain, S., Maxwell, S., Pontecorvi, M., Aslam, S., Gerrelli, D., Sowden, J.C., Woollard, A., 2008. Neuronal function of Tbx20 conserved from nematodes to vertebrates. Developmental biology 317, 671-685.

174. Pogoda, H.M., Sternheim, N., Lyons, D.A., Diamond, B., Hawkins, T.A., Woods, I.G., Bhatt, D.H., Franzini-Armstrong, C., Dominguez, C., Arana, N., Jacobs, J., Nix, R., Fetcho, J.R., Talbot, W.S., 2006. A genetic screen identifies genes essential for development of myelinated axons in zebrafish. Developmental biology 298, 118-131.

175. Portugues, R., Engert, F., 2009. The neural basis of visual behaviors in the larval zebrafish. Current opinion in neurobiology 19, 644-647.

176. Powell, S.K., Kleinman, H.K., 1997. Neuronal laminins and their cellular receptors. The international journal of biochemistry & cell biology 29, 401-414.

177. Qu, Y., Glasco, D.M., Zhou, L., Sawant, A., Ravni, A., Fritzsch, B., Damrau, C., Murdoch, J.N., Evans, S., Pfaff, S.L., Formstone, C., Goffinet, A.M., Chandrasekhar,

A., Tissir, F., 2010. Atypical cadherins Celsr1-3 differentially regulate migration of facial branchiomotor neurons in mice. The Journal of neuroscience : the official journal of the Society for Neuroscience 30, 9392-9401.

178. Rakic, P., 1974. Neurons in rhesus monkey visual cortex: systematic relation between time of origin and eventual disposition. Science 183, 425-427.

179. Raper, J.A., 2000. Semaphorins and their receptors in vertebrates and invertebrates. Current opinion in neurobiology 10, 88-94.

180. Rebman, J.K., Kirchoff, K.E., Walsh, G.S., 2016. Cadherin-2 Is Required Cell Autonomously for Collective Migration of Facial Branchiomotor Neurons. PLoS One 11, e0164433.

181. Reyes, R., Haendel, M., Grant, D., Melancon, E., Eisen, J.S., 2004. Slow degeneration of zebrafish Rohon-Beard neurons during programmed cell death. Developmental dynamics : an official publication of the American Association of Anatomists 229, 30-41.

182. Ribera, A.B., Nusslein-Volhard, C., 1998. Zebrafish touch-insensitive mutants reveal an essential role for the developmental regulation of sodium current. The Journal of neuroscience : the official journal of the Society for Neuroscience 18, 9181-9191.

183. Rivas, R.J., Hatten, M.E., 1995. Motility and cytoskeletal organization of migrating cerebellar granule neurons. The Journal of neuroscience : the official journal of the Society for Neuroscience 15, 981-989.

184. Rohrschneider, M.R., Elsen, G.E., Prince, V.E., 2007. Zebrafish Hoxb1a regulates multiple downstream genes including prickle1b. Developmental biology 309, 358-372.

185. Ross, L.S., Parrett, T., Easter, S.S., Jr., 1992. Axonogenesis and morphogenesis in the embryonic zebrafish brain. The Journal of neuroscience : the official journal of the Society for Neuroscience 12, 467-482.

186. Rossi, A., Kontarakis, Z., Gerri, C., Nolte, H., Holper, S., Kruger, M., Stainier, D.Y., 2015. Genetic compensation induced by deleterious mutations but not gene knockdowns. Nature 524, 230-233.

187. Roszko, I., Sawada, A., Solnica-Krezel, L., 2009. Regulation of convergence and extension movements during vertebrate gastrulation by the Wnt/PCP pathway. Seminars in cell & developmental biology 20, 986-997.

188. Saito, M., Iwawaki, T., Taya, C., Yonekawa, H., Noda, M., Inui, Y., Mekada, E., Kimata, Y., Tsuru, A., Kohno, K., 2001. Diphtheria toxin receptor-mediated conditional and targeted cell ablation in transgenic mice. Nature biotechnology 19, 746-750.

189. Sakai, J.A., Halloran, M.C., 2006. Semaphorin 3d guides laterality of retinal ganglion cell projections in zebrafish. Development 133, 1035-1044.

190. Sankrithi, N.S., O'Malley, D.M., 2010. Activation of a multisensory, multifunctional nucleus in the zebrafish midbrain during diverse locomotor behaviors. Neuroscience 166, 970-993.

191. Sassen, W.A., Lehne, F., Russo, G., Wargenau, S., Dubel, S., Koster, R.W., 2017. Embryonic zebrafish primary cell culture for transfection and live cellular and subcellular imaging. Developmental biology 430, 18-31.

192. Savvaki, M., Panagiotaropoulos, T., Stamatakis, A., Sargiannidou, I., Karatzioula, P., Watanabe, K., Stylianopoulou, F., Karagogeos, D., Kleopa, K.A., 2008. Impairment of learning and memory in TAG-1 deficient mice associated with shorter CNS internodes and disrupted juxtaparanodes. Molecular and cellular neurosciences 39, 478-490.

193. Schlatter, M.C., Buhusi, M., Wright, A.G., Maness, P.F., 2008. CHL1 promotes Sema3A-induced growth cone collapse and neurite elaboration through a motif required for recruitment of ERM proteins to the plasma membrane. Journal of neurochemistry 104, 731-744.

194. Serafini, T., Colamarino, S.A., Leonardo, E.D., Wang, H., Beddington, R., Skarnes, W.C., Tessier-Lavigne, M., 1996. Netrin-1 is required for commissural axon guidance in the developing vertebrate nervous system. Cell 87, 1001-1014.

195. Serafini, T., Kennedy, T.E., Galko, M.J., Mirzayan, C., Jessell, T.M., Tessier-Lavigne, M., 1994. The netrins define a family of axon outgrowth-promoting proteins homologous to C. elegans UNC-6. Cell 78, 409-424.

196. Severi, K.E., Portugues, R., Marques, J.C., O'Malley, D.M., Orger, M.B., Engert, F., 2014. Neural control and modulation of swimming speed in the larval zebrafish. Neuron 83, 692-707.

197. Sharma, A., Gokulchandran, N., Chopra, G., Kulkarni, P., Lohia, M., Badhe, P., Jacob, V.C., 2012. Administration of autologous bone marrow-derived mononuclear cells in children with incurable neurological disorders and injury is safe and improves their quality of life. Cell transplantation 21 Suppl 1, S79-90.

198. Sittaramane, V., Pan, X., Glasco, D.M., Huang, P., Gurung, S., Bock, A., Li, S., Wang, H., Kawakami, K., Matise, M.P., Chandrasekhar, A., 2013. The PCP protein Vangl2 regulates migration of hindbrain motor neurons by acting in floor plate cells, and independently of cilia function. Developmental biology 382, 400-412.

199. Sittaramane, V., Sawant, A., Wolman, M.A., Maves, L., Halloran, M.C., Chandrasekhar, A., 2009. The cell adhesion molecule Tag1, transmembrane protein Stbm/Vangl2, and Lamininalpha1 exhibit genetic interactions during migration of facial branchiomotor neurons in zebrafish. Developmental biology 325, 363-373.

200. Smith, A., Robinson, V., Patel, K., Wilkinson, D.G., 1997. The EphA4 and EphB1 receptor tyrosine kinases and ephrin-B2 ligand regulate targeted migration of branchial neural crest cells. Current biology : CB 7, 561-570.

201. Solecki, D.J., Govek, E.E., Tomoda, T., Hatten, M.E., 2006. Neuronal polarity in CNS development. Genes Dev 20, 2639-2647.

202. Solnica-Krezel, L., Stemple, D.L., Mountcastle-Shah, E., Rangini, Z., Neuhauss, S.C., Malicki, J., Schier, A.F., Stainier, D.Y., Zwartkruis, F., Abdelilah, S., Driever, W., 1996. Mutations affecting cell fates and cellular rearrangements during gastrulation in zebrafish. Development 123, 67-80.

203. Soltani, C.E., Hotze, E.M., Johnson, A.E., Tweten, R.K., 2007. Specific protein-membrane contacts are required for prepore and pore assembly by a cholesterol-dependent cytolysin. The Journal of biological chemistry 282, 15709-15716.

204. Song, H., Hu, J., Chen, W., Elliott, G., Andre, P., Gao, B., Yang, Y., 2010. Planar cell polarity breaks bilateral symmetry by controlling ciliary positioning. Nature 466, 378-382.

205. Song, M.R., 2007. Moving cell bodies: understanding the migratory mechanism of facial motor neurons. Archives of pharmacal research 30, 1273-1282.

206. Stainier, D.Y.R., Raz, E., Lawson, N.D., Ekker, S.C., Burdine, R.D., Eisen, J.S., Ingham, P.W., Schulte-Merker, S., Yelon, D., Weinstein, B.M., Mullins, M.C., Wilson, S.W., Ramakrishnan, L., Amacher, S.L., Neuhauss, S.C.F., Meng, A., Mochizuki, N., Panula, P., Moens, C.B., 2017. Guidelines for morpholino use in zebrafish. PLoS Genet 13, e1007000.

207. Stockinger, P., Maitre, J.L., Heisenberg, C.P., 2011. Defective neuroepithelial cell cohesion affects tangential branchiomotor neuron migration in the zebrafish neural tube. Development 138, 4673-4683.

208. Stoeckli, E.T., 2004. Ig superfamily cell adhesion molecules in the brain. Handb Exp Pharmacol, 373-401.

209. Stoeckli, E.T., Landmesser, L.T., 1995. Axonin-1, Nr-CAM, and Ng-CAM play different roles in the in vivo guidance of chick commissural neurons. Neuron 14, 1165-1179.

210. Sun, C., Wu, J., Liu, S., Li, H., Zhang, S., 2013. Zebrafish CD59 has both bacterial-binding and inhibiting activities. Developmental and comparative immunology 41, 178-188.

211. Suter, D.M., Pollerberg, G.E., Buchstaller, A., Giger, R.J., Dreyer, W.J., Sonderegger, P., 1995. Binding between the neural cell adhesion molecules axonin-1 and Nr-CAM/Bravo is involved in neuron-glia interaction. The Journal of cell biology 131, 1067-1081.

212. Suzuki, S.C., Takeichi, M., 2008. Cadherins in neuronal morphogenesis and function. Development, growth & differentiation 50 Suppl 1, S119-130.

213. Tabata, A., Ohkura, K., Ohkubo, Y., Tomoyasu, T., Ohkuni, H., Whiley, R.A., Nagamune, H., 2014. The diversity of receptor recognition in cholesterol-dependent cytolysins. Microbiology and immunology 58, 155-171.

214. Taniguchi, M., Yuasa, S., Fujisawa, H., Naruse, I., Saga, S., Mishina, M., Yagi, T., 1997. Disruption of semaphorin III/D gene causes severe abnormality in peripheral nerve projection. Neuron 19, 519-530.

215. Tazir, M., Nouioua, S., Magy, L., Huehne, K., Assami, S., Urtizberea, A., Grid, D., Hamadouche, T., Rautenstrauss, B., Vallat, J.M., 2009. Phenotypic variability in giant axonal neuropathy. Neuromuscul Disord 19, 270-274.

216. Tessier-Lavigne, M., Goodman, C.S., 1996. The molecular biology of axon guidance. Science 274, 1123-1133.

217. Thompson, H., Andrews, W., Parnavelas, J.G., Erskine, L., 2009. Robo2 is required for Slit-mediated intraretinal axon guidance. Developmental biology 335, 418-426.

218. Tongiorgi, E., Bernhardt, R.R., Schachner, M., 1995. Zebrafish neurons express two L1-related molecules during early axonogenesis. Journal of neuroscience research 42, 547-561.

219. Tzimourakas, A., Giasemi, S., Mouratidou, M., Karagogeos, D., 2007. Structure-function analysis of protein complexes involved in the molecular architecture of juxtaparanodal regions of myelinated fibers. Biotechnol J 2, 577-583.

220. Uemura, O., Okada, Y., Ando, H., Guedj, M., Higashijima, S., Shimazaki, T., Chino, N., Okano, H., Okamoto, H., 2005. Comparative functional genomics revealed conservation and diversification of three enhancers of the isl1 gene for motor and sensory neuron-specific expression. Developmental biology 278, 587-606.

221. Vajsar, J., Schachter, H., 2006. Walker-Warburg syndrome. Orphanet journal of rare diseases 1, 29.

222. Vanderlaan, G., Tyurina, O.V., Karlstrom, R.O., Chandrasekhar, A., 2005. Gli function is essential for motor neuron induction in zebrafish. Developmental biology 282, 550-570.

223. Veeman, M.T., Axelrod, J.D., Moon, R.T., 2003. A second canon. Functions and mechanisms of beta-catenin-independent Wnt signaling. Developmental cell 5, 367-377.

224. Vivancos, V., Chen, P., Spassky, N., Qian, D., Dabdoub, A., Kelley, M., Studer, M., Guthrie, S., 2009. Wnt activity guides facial branchiomotor neuron migration, and involves the PCP pathway and JNK and ROCK kinases. Neural development 4, 7.

225. Wada, H., Iwasaki, M., Sato, T., Masai, I., Nishiwaki, Y., Tanaka, H., Sato, A., Nojima, Y., Okamoto, H., 2005. Dual roles of zygotic and maternal Scribble1 in neural

migration and convergent extension movements in zebrafish embryos. Development 132, 2273-2285.

226. Wada, H., Tanaka, H., Nakayama, S., Iwasaki, M., Okamoto, H., 2006. Frizzled3a and Celsr2 function in the neuroepithelium to regulate migration of facial motor neurons in the developing zebrafish hindbrain. Development 133, 4749-4759.

227. Walsh, G.S., Grant, P.K., Morgan, J.A., Moens, C.B., 2011. Planar polarity pathway and Nance-Horan syndrome-like 1b have essential cell-autonomous functions in neuronal migration. Development 138, 3033-3042.

228. Wan, H., Korzh, S., Li, Z., Mudumana, S.P., Korzh, V., Jiang, Y.J., Lin, S., Gong, Z., 2006. Analyses of pancreas development by generation of gfp transgenic zebrafish using an exocrine pancreas-specific elastaseA gene promoter. Experimental cell research 312, 1526-1539.

229. Wanner, S.J., Prince, V.E., 2013. Axon tracts guide zebrafish facial branchiomotor neuron migration through the hindbrain. Development 140, 906-915.

230. Warren, J.T., Jr., Chandrasekhar, A., Kanki, J.P., Rangarajan, R., Furley, A.J., Kuwada, J.Y., 1999. Molecular cloning and developmental expression of a zebrafish axonal glycoprotein similar to TAG-1. Mechanisms of development 80, 197-201.

231. Westerfield, M., 1995. The Zebrafish Book.

232. Whitlock, K.E., Westerfield, M., 2000. The olfactory placodes of the zebrafish form by convergence of cellular fields at the edge of the neural plate. Development 127, 3645-3653.

233. Wickham, S.E., Hotze, E.M., Farrand, A.J., Polekhina, G., Nero, T.L., Tomlinson, S., Parker, M.W., Tweten, R.K., 2011. Mapping the intermedilysin-human CD59 receptor interface reveals a deep correspondence with the binding site on CD59 for complement binding proteins C8alpha and C9. The Journal of biological chemistry 286, 20952-20962.

234. Williams, J.A., Barrios, A., Gatchalian, C., Rubin, L., Wilson, S.W., Holder, N., 2000. Programmed cell death in zebrafish rohon beard neurons is influenced by TrkC1/NT-3 signaling. Developmental biology 226, 220-230.

235. Williams, S.E., Mann, F., Erskine, L., Sakurai, T., Wei, S., Rossi, D.J., Gale, N.W., Holt, C.E., Mason, C.A., Henkemeyer, M., 2003. Ephrin-B2 and EphB1 mediate retinal axon divergence at the optic chiasm. Neuron 39, 919-935.

236. Wolman, M.A., Liu, Y., Tawarayama, H., Shoji, W., Halloran, M.C., 2004. Repulsion and attraction of axons by semaphorin3D are mediated by different neuropilins in vivo. The Journal of neuroscience : the official journal of the Society for Neuroscience 24, 8428-8435.

237. Wolman, M.A., Regnery, A.M., Becker, T., Becker, C.G., Halloran, M.C., 2007. Semaphorin3D regulates axon axon interactions by modulating levels of L1 cell adhesion molecule. The Journal of neuroscience : the official journal of the Society for Neuroscience 27, 9653-9663.

238. Wolman, M.A., Sittaramane, V.K., Essner, J.J., Yost, H.J., Chandrasekhar, A., Halloran, M.C., 2008. Transient axonal glycoprotein-1 (TAG-1) and laminin-alpha1 regulate dynamic growth cone behaviors and initial axon direction in vivo. Neural development 3, 6.

239. Yamamoto, M., Boyer, A.M., Crandall, J.E., Edwards, M., Tanaka, H., 1986. Distribution of stage-specific neurite-associated proteins in the developing murine nervous system recognized by a monoclonal antibody. The Journal of neuroscience : the official journal of the Society for Neuroscience 6, 3576-3594.

240. Yang, C.T., Sengelmann, R.D., Johnson, S.L., 2004. Larval melanocyte regeneration following laser ablation in zebrafish. The Journal of investigative dermatology 123, 924-929.

241. Yokoyama, N., Romero, M.I., Cowan, C.A., Galvan, P., Helmbacher, F., Charnay, P., Parada, L.F., Henkemeyer, M., 2001. Forward signaling mediated by ephrin-B3 prevents contralateral corticospinal axons from recrossing the spinal cord midline. Neuron 29, 85-97.

242. Zhao, X.F., Ellingsen, S., Fjose, A., 2009. Labelling and targeted ablation of specific bipolar cell types in the zebrafish retina. BMC Neurosci 10, 107.

Vita

Suman Gurung was born May 20th, 1987 in Nepal to Krishna Raj and Goma Gurung. Suman came to the US in 2007 after completing his high school in his home country. He received his combined Bachelor's/Master's degree in Biotechnology from the College of Agriculture, Biotechnology, and Natural Resources at the University of Nevada, Reno and was awarded the Outstanding Graduate Student in Biotechnology. This work was completed under the guidance of Dr. Anand Chandrasekhar at the University of Missouri, Columbia. Suman will join the lab of Dr. Saulius Sumanas at the Cincinnati Children's Hospital Medical Center in June 2018.